SECTION BUILDER: A FINITE ELEMENT TOOL FOR ANALYSIS AND DESIGN OF COMPOSITE BEAM CROSS-SECTIONS

A Thesis
Presented to
The Academic Faculty

by

Uttam Kumar Chakravarty

In Partial Fulfillment
of the Requirements for the Degree
Doctor of Philosophy in the
School of Aerospace Engineering

Georgia Institute of Technology
April 2008

SECTION BUILDER: A FINITE ELEMENT TOOL FOR ANALYSIS AND DESIGN OF COMPOSITE BEAM CROSS-SECTIONS

Approved by:

Professor Olivier A. Bauchau, Advisor
School of Aerospace Engineering
Georgia Institute of Technology

Professor James I. Craig
School of Aerospace Engineering
Georgia Institute of Technology

Professor Dewey H. Hodges
School of Aerospace Engineering
Georgia Institute of Technology

Professor Vitali Volovoi
School of Aerospace Engineering
Georgia Institute of Technology

Professor Hassan Mahfuz
Professor of Ocean Engineering
Florida Atlantic University

Date Approved: March 27, 2008

To

Almighty God,

The memory of my father,

and

My mother

ACKNOWLEDGEMENTS

First and foremost, I would like to express my sincere thanks to my dissertation advisor, Professor Olivier A. Bauchau, for his continuous support and guidance throughout my doctoral study. This work would not have been possible without all the insightful discussions with him.

I thank my committee members, Professors James I. Craig, Dewey H. Hodges, Vitali Volovoi, and Hassan Mahfuz for their time, effort, and enlightening suggestions which were essential in improving the quality of this work. I also express my gratitude to Professor Hassan Mahfuz, who was my M.S. thesis advisor at Tuskegee University, for becoming my committee member coming from Florida Atlantic University.

I would like to thank Professor Jeff Jagoda, Associate Chair for Graduate Studies and Research in the School of Aerospace Engineering, for providing me financial support, guidance, and suggestion during my education at Georgia Institute of Technology.

I would also like to thank the sponsors of the NRTC/CRI project (WBS No. 2006-B-01-01.5-A1) for supporting me to finish this thesis.

I would like to thank all my lab mates for their constant help and stimulating discussion, specially Wei-En Li for providing me with VABS-ANSYS Toolset results for validating SectionBuilder results.

I would like to thank my family members for their love, support, and encouragement without which this endeavor would never have been completed.

Finally and above all, I would like to thank God for giving me the opportunity to be here, in this world.

TABLE OF CONTENTS

DEDICATION iii

ACKNOWLEDGEMENTS iv

LIST OF FIGURES vii

SUMMARY xii

I INTRODUCTION 1

II LITERATURE REVIEW 6

2.1 Mesh Generation 6

2.2 Beam Modeling 10

III CAPABILITIES OF SECTIONBUILDER 14

3.1 Introduction 14

3.1.1 Model definition phase 14

3.1.2 Computational phase 17

3.1.3 Post processing phase 21

3.2 Parametric Shape Section Configurations 22

3.2.1 Definition of airfoil sections 22

3.2.2 Definition of circular arcs 26

3.2.3 Definition of C-sections 28

3.2.4 Definition of circular cylinders 33

3.2.5 Definition of double boxes 34

3.2.6 Definition of I-sections 52

3.2.7 Definition of rectangular boxes 59

3.2.8 Definition of rectangular sections 62

3.2.9 Definition of circular tubes 63

3.2.10 Definition of triangular sections 77

3.2.11 Definition of T-sections 79

3.3 Builder 85

3.3.1 Definition of walls 85
3.3.2 Definition of Split-connector sections 88
3.3.3 Definition of T-connector sections 90
3.3.4 Definition of V-connector sections 94
3.3.5 Definition of core sections 95
IV RESULTS AND DISCUSSION 109
V CONCLUSIONS 133
VI RECOMMENDATIONS FOR FUTURE WORK 134
APPENDIX A CONVEX HULL 135
APPENDIX B DELAUNAY TRIANGULATION 137
REFERENCES 141
VITA 149

LIST OF FIGURES

1	Overall beam cross-section analysis and design processes	2
2	Beam cross-section analysis phases	4
3	The three phases of beam cross-section analysis	15
4	Configuration of the C-section	16
5	Actual rotor blade cross-section with core material	16
6	Airfoil section construction	17
7	Cross-sections for incorporating core materials in the cavities	18
8	Nine noded quadrilateral element (top) and six noded triangular element (bottom) with orientation of nodes	19
9	Configuration of the airfoil section with no web	22
10	Configuration of the airfoil section with a single web	23
11	Configuration of the airfoil section with two webs	23
12	The three zones of the airfoil section	25
13	Example 1. Airfoil section	26
14	Example 2. Airfoil section with two webs	27
15	Configuration of the circular arc	28
16	Example 2. Circular arc section	29
17	Example 2. Circular arc section	30
18	Configuration of the C-section	31
19	The three zones of the C-section	37
20	Configuration of the L-section	38
21	The two zones of the L-section	39
22	Configuration of the reverse L-section	40
23	The two zones of the reverse L-section	41
24	Configuration of the strip section	42
25	The zone of the strip section	43
26	Example 1. C-section	44

27 Example 2. C-section 44
28 Example 3. Reverse L-section 45
29 Example 4. L-section 45
30 Example 5. Strip section 46
31 Configuration of the circular cylinder 47
32 Example 1. Cylinder 48
33 Configuration of the double box 49
34 The four zones of the double box 50
35 Example 1. Double box 51
36 Example 2. Double box 51
37 Configuration of the I-section 52
38 The four zones of the I-section 55
39 Configuration of the Z-section 56
40 The zones of the Z-section 57
41 Configuration of the T-section 58
42 The zones of the T-section 65
43 Example 1. I-section 66
44 Example 2. I-section 66
45 Example 3. Z-section 67
46 Example 4. Z-section 67
47 Example 5. T-section 68
48 Configuration of the rectangular box. The dimensions of the various elements of the section are indicated on the figure. The three shaded areas correspond to the three zones of the section 69
49 The three zones of the rectangular box 70
50 Example 1. Rectangular box 71
51 Example 2. Rectangular box 71
52 Configuration of the rectangular section 72
53 Solid zones of the rectangular section 73

54 Example 1. Rectangular section 73
55 Example 2. Rectangular section 74
56 Configuration of the circular tube 75
57 Example 1. Circular tube 76
58 Example 2. Circular tube 76
59 Configuration of the triangular section with open or closed section . . 77
60 The three zones of the triangular section 78
61 Example 1. Triangular section 79
62 Configuration of the T-section 80
63 The three zones of the T-section 83
64 Example 1. T-section 84
65 Example 2. T-section 84
66 General configuration of a wall 86
67 Definition of the stacking sequence and actual configuration of the wall 87
68 Connection of two walls 88
69 Example 1. Wall with arbitrary lay-ups 89
70 Example 2. Connection between two walls 90
71 Three walls can be connected as above with a Split-connector 91
72 Three walls and a Split-connector (in detail) 92
73 Example 1. Split-connector with three walls 93
74 Three walls can be connected as above with a T-connector 94
75 Three walls can be connected as above with a T-connector 95
76 Three walls and T-connector in upward direction (in detail) 96
77 Example 1. T-connector with three walls 97
78 Example 2. Two T-connectors with five walls 98
79 Example 3. Four T-connectors with eight walls 99
80 Two walls can be connected as above with a V-connector 102
81 Two walls and a V-connector (in detail) 103
82 Example 1. V-connector with two walls 103

83 Free mesh generation steps 104
84 Free mesh generation steps (continued) 105
85 Example 1. Free mesh generation 106
86 Example 2. Free mesh generation 107
87 Free mesh generation technique to integrate core material between two walls 108
88 Simple airfoil cross-section with mesh generation 109
89 Variation of axial stiffness with number of elements plot 110
90 Stiffnesses for simple airfoil section 110
91 Geometry and analysis results for airfoil cross-section with one web . 112
92 Stiffnesses and compliance matrices for airfoil section with one web . 113
93 Sectional mass matrix for airfoil section with one web 113
94 Geometry and analysis results for complex rotor blade cross-section . 115
95 Sectional properties of complex rotor blade section 116
96 Mesh generation of rectangular cross-section with two walls and core material 117
97 Variation of axial stiffness with the thickness of walls for the rectangular cross-section 118
98 Sectional properties of the rectangular cross-section with two walls and core material 119
99 Variation of torsional stiffness with DOF for mapped and free meshes 120
100 Variation of maximum shear stress with the thickness of walls for the rectangular cross-section 122
101 Variation of shear stress with number of DOF at the location, x2=0.5 m and x3=0.3 m 123
102 Variation of shear stress with number of DOF at the location, x2=0.6 m and x3=0.4 m 124
103 Variation of shear stresses, (τ_{12} and τ_{13}) across cross-section along paths A and B 125
104 Airfoil cross-section with core material 126
105 Sectional properties of airfoil cross-section with core material 127

106 Variation of axial stiffness with DOF for the airfoil cross-section with core material 128

107 Variation of shear stress with DOF for the airfoil cross-section with core material at the top of the upper skin and half chord location . . 128

108 Complex rotor blade cross-section with core material 130

109 Sectional properties of complex rotor blade cross-section with core material 131

110 Variation of axial stiffness with DOF for complex rotor blade cross-section with core material 132

111 Variation of shear stress with DOF for complex rotor blade cross-section with core material at the top of the upper skin and near quarter chord location 132

112 Convex and non-convex hulls 136

113 Delaunay triangles: the projection of three-dimensional convex hull in two-dimensional plane 140

SUMMARY

SectionBuilder is an innovative finite element based tool, developed for analysis and design of composite beam cross-sections. The tool can handle the cross-sections with parametric shapes and arbitrary configurations. It can also handle arbitrary lay-ups for predefined beam cross-section geometries in a consistent manner. The material properties for each layer of the cross-section can be defined on the basis of the design requirements. This tool is capable of dealing with multi-cell composite cross-sections with arbitrary lay-ups. It has also the benefit of handling the variation of thickness of skin and D-spars for beams such as rotor blades. A typical cross-section is considered as a collection of interconnected walls. Walls with arbitrary lay-ups based on predefined geometries and material properties are generated first. The complex composite beam cross-sections are developed by connecting the walls using various types of connectors. These connectors are compatible with the walls, i.e., the thickness of the layers of the walls must match with those of the connectors at the place of connection. Cross-sections are often reinforced by core material for constructing realistic rotor blade cross-sections. The tool has the ability to integrate core materials into the cross-sections. A mapped mesh is considered for meshing parametric shapes, walls and various connectors, whereas a free mesh is considered for meshing the core materials. A new algorithm based on the Delaunay refinement algorithm is developed for creating the best possible free mesh for core materials. After meshing the cross-section, the tool determines the sectional properties using finite element analysis. This tool computes sectional properties including stiffness matrix, compliance matrix, mass matrix, and principal axes. A visualization environment is integrated with the tool

for visualizing the stress and strain distributions over the cross-section.

CHAPTER I

INTRODUCTION

Composite materials have found increasing use in aerospace and civil engineering construction. One of the common areas of application is rotor blade construction where composite materials with complex lay-ups are used. The following properties can be improved when composite materials are used: specific strength, specific stiffness, weight, and fatigue life [59]. For example, composite blades have more than twice the fatigue life of standard metal blades now in service. Blades are integrated with titanium leading edge for erosion protection.

The overall composite beam cross-section analysis process proposed in this work is shown in fig. 1. The analysis processes can be broken into three steps: model definition, mesh generation, and finite element analysis. The geometry and material properties are defined in model definition phase. Meshes are generated at the mesh generation phase for finite element analysis of cross-sections. Finite element analysis is performed for computing the cross-sectional properties and stress distributions over the cross-section.

Industry does not use a detailed CAD representation of the beam cross-section for the purpose of cross-sectional analysis. CAD is used mainly to support the manufacturing process. Rather, simplified representations are used, and the cross-sectional properties are computed from these simplified models. Often, rather than dealing with individual composite plies, laminate properties are used that effectively smear individual ply properties. These simplified models present major advantages: the cross-section can be rapidly defined, design iterations are easily performed, and engineers and designers do not need lengthy and costly training required to use large

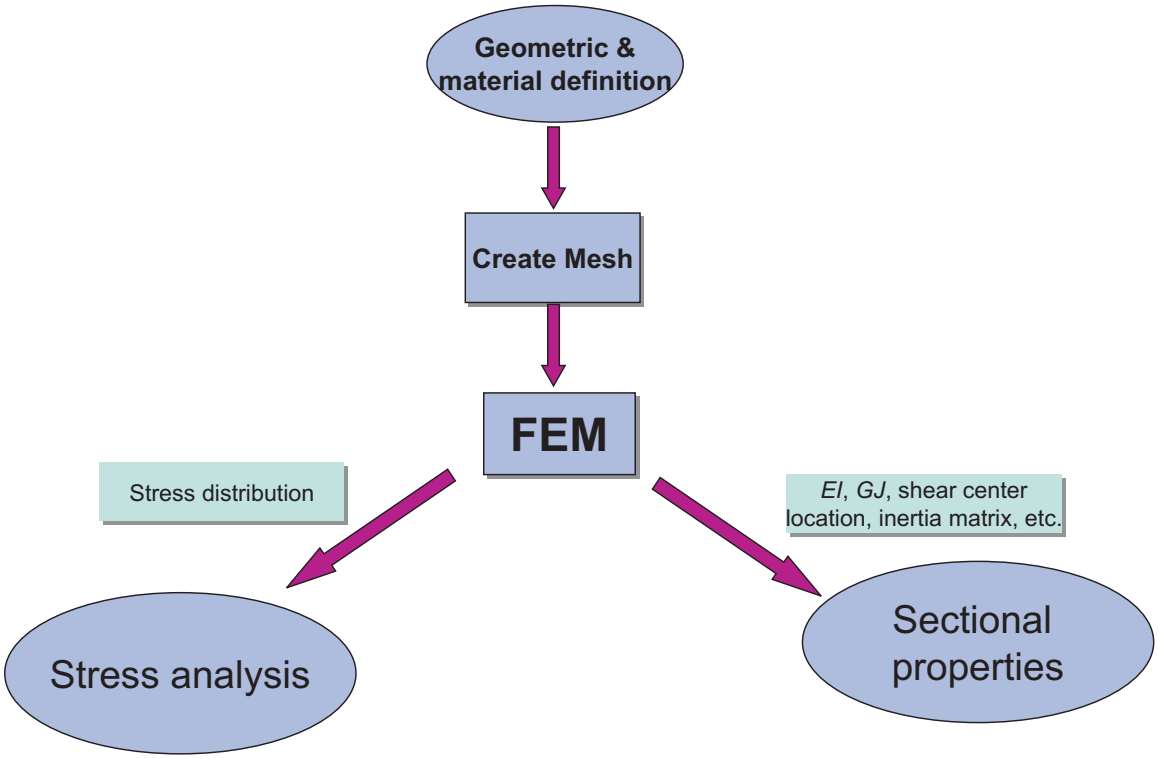

Figure 1: Overall beam cross-section analysis and design processes

commercial packages such as CATIA or ANSYS. However, it is unknown how accurate the simplified models are in relation to those constructed based on three-dimensional properties.

Advanced analytical tools facilitate the design and accurate analysis process of composite beam cross-sections and reduce the cost of design process. But it is an awkward and time-consuming process to define ply layout and stacking sequence with CAD tools. For this reason, tools to automate this process have been designed. But the geometric configurations that can be defined are often limited.

For example, VABS (Variational Asymptotic Beam Sectional Analysis) [28, 100, 99, 54] with ANSYS, known as VABS-ANSYS Toolset, is the best available tool for beam cross-sections design and analysis. Here beam cross-section geometry is defined in a CAD tool, CATIA where the cross-section is defined by areas with specified

laminate material properties, areas are bounded by reference curves that define material orientation, and geometry is exported to ANSYS. ANSYS is then used to create the analysis mesh and identify reference edges for all areas. Custom macros and a special-purpose C-language code are used to construct free meshes within each area, material orientation is computed at the centroid of each element, and results are exported along with material properties as a VABS input file. VABS is used for finite element analysis for computing cross-sectional properties and stress distributions over the cross-sections. VABS computes the cross-sectional stiffness matrix, principal axes, neutral axis, area centroid, mass centroid, and mass matrix. It also exports strain, stress, and warping recovery data. Finally, ANSYS is used for visualization: custom macros create a two-dimensional stress field in a cross-sectional layer (single element thick) to enable the user to visualize stress and strain over the cross-section for specified applied cross-sectional resultants. But it is still difficult and time consuming process to construct a realistic composite beam cross-section using ANSYS, CATIA, and other CAD tools. It might take several days work to design a realistic composite beam such as rotor blade cross-section and compute cross-sectional properties. Complex lay-ups and ply add/drops are very difficult to accommodate using these tools. As a result, a new tool is required to overcome these difficulties of the available tools.

SectionBuilder is an innovative finite element based tool, developed to overcome the lack of functionalities of the other available tools for analysis and design of beam cross-sections. This analysis can be conveniently broken into three separate phases: the model definition phase, the computational phase, and the post-processing phase, as shown in fig. 2 (where 3D defines three-dimensional.)

The heart of the problem, and the focus of the development task, is in the model definition phase. In this phase, the geometric characteristics of the cross-section must be described along with the physical properties of the constituent materials.

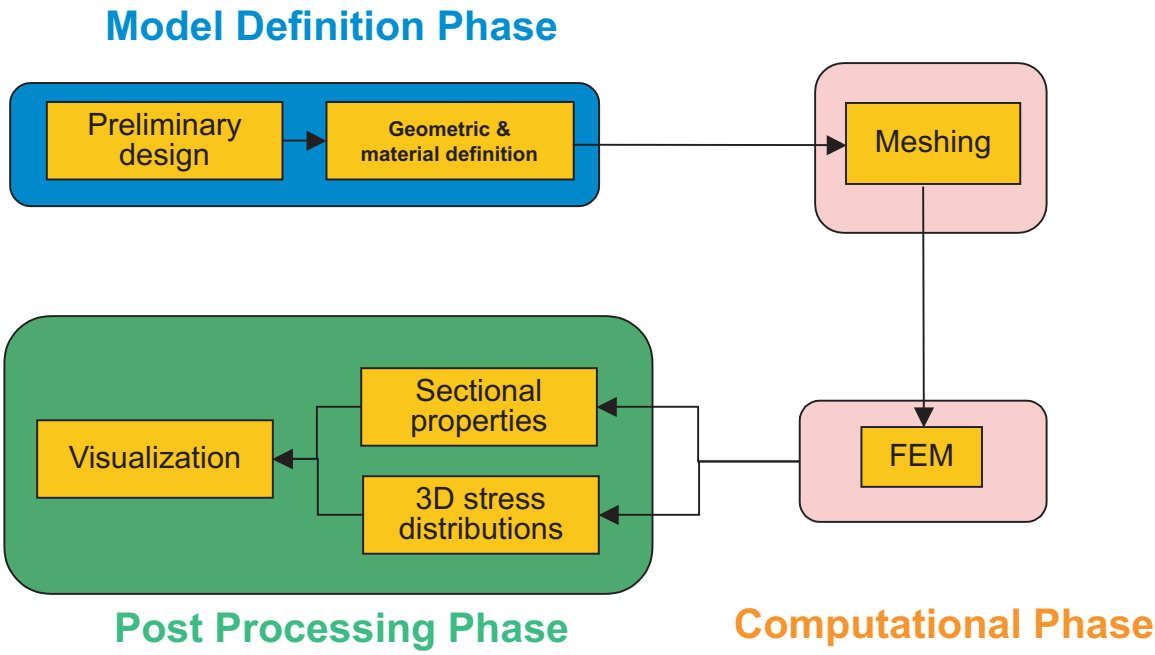

Figure 2: Beam cross-section analysis phases

The model definition is quite different at the preliminary and detailed design stages. Starting from the definition of a curve, the user defines layers of material that can be stacked on top of each other in an arbitrary fashion to define a realistic beam cross-section. The cross-section is formed by joining together a number of user defined walls, each defined by an arbitrary curve and material properties. This approach to the definition of the cross-sections enables very general geometries to be defined. For example, this tool can handle multiple cells with arbitrary lay-ups for beam cross-sections. SectionBuilder has been developed and tested with the ability to deal with general topologies and composite materials that are encountered in actual beam cross-sections configurations. The ability to handle configurations where more than two walls are connected together has been developed and tested; this situation is encountered in realistic beam such as rotor blade configurations, for instance at the intersection of the vertical shear web with the airfoil upper or lower flanges. Test cases are run for typical blade configurations involving a front D-spar connecting to

an aft fairing and multi-cell blade cross-sections. It has also the benefit to handle the variation of thickness of both skin and D-spars. Core materials are integrated into rotor blades for reinforcing the cross-sections and preventing shape changes during operation. A new algorithm based on the Delaunay refinement algorithm is proposed for creating the best possible free mesh of core materials for finite element analysis as explained in section 3.3.5. On the other hand, the computational phase uses the finite element analysis to compute cross-sectional properties and three-dimensional stress distributions based on a model of the cross-section described in the input file. The most efficient beam cross-sectional analysis tool, VABS [28, 100, 99, 54] is considered for finite element analysis for SectionBuilder. The final, post-processing phase provides the visualization of the computed stress and strain distributions for the SectionBuilder. The entire process is integrated into a design environment that includes the definition of the cross-section, the analysis, and the visualization of the results.

CHAPTER II

LITERATURE REVIEW

Beams are structures which have one dimension (length) much larger than the other two (the cross-section dimensions). SectionBuilder computes the sectional properties of beams in three phases: define the geometry, generate the mesh, and perform finite element analysis. Many algorithms are available for mesh generation of a section; many beam models are also available for finite element analysis. So the heart of this research is to find the appropriate mesh generation techniques and beam models for finite element analysis. The literature review on mesh generation and beam modeling is given below at two different sections.

2.1 Mesh Generation

In general, a mapped mesh [4, 34] is used for generating eight and nine noded quadrilateral elements over regular domains. On the other hand, for domains of complex shape, free meshes featuring three and six noded triangular elements are preferred. From the literature review, it is noted that Delaunay triangulation is the most popular technique for triangular free mesh generation. Although this is still a very active research area, there have been a lot of work in this area. Many algorithms are available for Delaunay triangulation of a set of points. The algorithms can be divided into five categories [16, 45, 48]: divide-and-conquer [38, 49], incremental [33, 47, 49, 48, 75], sweepline [44], gift wrapping [37, 71, 92], and site lifting [3].

The first $\mathcal{O}(n \log n)$ algorithm for two-dimensional Delaunay triangulation was a divide-and-conquer algorithm. Shamos and Hoey [91] developed an algorithm for the construction of a Voronoi diagram, which is considered equivalent to a Delaunay triangulation. In programming practice, Shamos and Hoey's algorithm is unnecessarily

complicated, because forming a Delaunay triangulation directly is much easier, and is in fact the easiest way to construct a Voronoi diagram. Lee and Schachter [70] were the first to publish a divide-and-conquer algorithm that directly constructs a Delaunay triangulation. The algorithm is nonetheless intricate, and Guibas and Stolfi [49] provide an important aid to programmers by filling out many implementation details. Dwyer [38] offers an interesting modification to divide-and-conquer Delaunay triangulation that achieves better asymptotic performance on some vertex sets, and offers improved speed in practice as well. Chew [30] also presented a $\mathcal{O}(n \log n)$ divide-and-conquer algorithm for constrained Delaunay triangulation.

The incremental technique can be a suitable way of constructing Delaunay triangles for a set of scattered points on a plane. In this technique, a large initial triangle surrounding all the points is considered. The points are incrementally inserted inside the triangle. The large triangle is divided into smaller triangles using the inserted points. The process is continued until all the points are inserted and a mesh is produced. There are two ways of implementing this technique. At first, the topology around the inserted point can be updated by the diagonal flipping operation to restore the Delaunay triangulation properties [68, 69]. Guibas, Knuth and Sharir [48] presented a diagonal flipping operation that can be implemented based on a randomized algorithm. In the second method, all triangles whose circumcircles contain the inserted point are removed and the resulting cavity is triangulated by linking the inserted point to all vertices of the cavity boundary [21, 97].

The $\mathcal{O}(n \log n)$, two-dimensional sweepline algorithm was developed by Fortune [44] for constructing Delaunay triangles. Fortune's algorithm builds the triangulation by sweeping a horizontal line vertically up on the plane. The growing triangulation accretes below the sweepline. The upper surface of the growing triangulation is called the front. When the sweepline collides with a vertex, a new edge is created that connects the vertex to the front. This algorithm ensures that there is no vertex inside the

circumcircle when the sweepline reaches at the top of the circumcircle of a Delaunay triangle and finally the triangle is created.

Another type of Delaunay triangulation technique constructs triangles by starting with a single Delaunay triangle and the incrementally discovering valid Delaunay triangles, one at a time. This technique is also known as gift wrapping algorithm. Each new triangle is constructed from an edge of a previously discovered triangle by finding the site that joins with the end vertices of that edge to form a new triangle whose circumcircle does not contain other sites [92]. From an initial edge, the triangulation grows until the convex hull of the point set is triangulated.

Fang and Piegl [41] presented a gift-wrapping algorithm of Delaunay triangulation of two-dimensional points using a uniform grid. This algorithm consists of three main steps: finding a starting point and the first edge, forming triangles, and putting all triangles together. They considered uniform grid structure for triangulation, finding boundary edges and nearest points. They create triangles by going around the mesh frontier in a consistent (clockwise or anti-clockwise) direction. This technique ensures the triangulation is correct and complete.

Brown [22] was the first to establish the connection between n-dimensional Voronoi diagrams and (n+1)-dimensional convex hulls. For example, a two-dimensional Delaunay triangulation of a point set is equivalent to the projection of the convex of a three-dimensional point set. Therefore, the three-dimensional mesh representing the convex hull can be constructed by lifting the two-dimensional triangulation into three-dimensional space. This is known as the site lifting approach.

Amenta et al. [1] proposed a Voronoi based surface construction algorithm that performs well in two and three dimensions. This technique is based on the three-dimensional Voronoi diagram and Delaunay triangulation [19]. This algorithm produces a set of triangles called the crust of the sample points. All vertices of the crust triangles are sample points. Amenta et al. [2] also improved this algorithm by a new

algorithm called power crust that improves the results for difficult cases including models with sharp corners, unevenly distributed point samples and cavities.

Edelsbrunner et al. [39, 40] proposed algorithm for parameterized construction associated with polyhedral shape with a set of scattered points on a plane. Hoppe [55] also presented an algorithm for constructing Delaunay triangulation for scattered points on a plane. Boissonat et al. [18] proposed an algorithm similar to Hoppe's algorithm. This algorithm is to construct smooth surfaces of arbitrary topology from scattered sample of points and normals of the surfaces. Curless and Levoy [35] proposed a volumetric method for integration range of images. This volumetric representation consists of a cumulative weighted signed distance function. The algorithm works with one range image at a time where it first scan the image and convert it to a distance. It then combines the result with the data already acquired using a simple additive scheme. Oblonsek et al. [74] also proposed a three phase surface based procedure for object reconstruction from three-dimensional scattered points. This algorithm can produce fine meshes for surfaces with sharp edges and corners. Morris and Kandle [73] also presented surface based procedure for Delaunay triangulation for free mesh generation.

Delaunay refinement algorithms, introduced by Chew [31, 32] and Ruppert [89] are very popular techniques for triangular free mesh generation. Delaunay refinement algorithms for mesh generation operate by maintaining a Delaunay triangulation, which is refined by inserting carefully placed vertices until the mesh meets constraints on element quality and size. These algorithms are successful because they exploit several favorable characteristics of Delaunay triangulation. One such characteristic is that a Delaunay triangulation maximizes the minimum angle among all possible triangulations of a point set. Another feature is that inserting a vertex is a local operation, and hence is inexpensive except in unusual cases. The act of inserting a vertex to improve poor quality elements in one part of a mesh will not unnecessarily

perturb a distant part of the mesh that has no bad elements. The central question of any Delaunay refinement algorithm is, "Where should the next vertex be inserted?" and a reasonable answer is, "As far from other vertices as possible." If a new vertex is inserted too close to another vertex, the resulting small edge will engender thin triangles. Because a Delaunay triangle has no vertices in its circumcircle, a Delaunay triangulation is an ideal search structure for finding points that are far from other vertices. (Its no coincidence that the circumcenter of each triangle of a Delaunay triangulation is a vertex of the corresponding Voronoi diagram.) Ruppert [89] proves that his algorithm produces nicely graded, size-optimal meshes with no angles smaller than about 20.7^0. There are also many researchers such as in Refs. [29, 67, 90, 88] who worked on improving the mesh quality and introduced many Delaunay refinement algorithms. The basic concept is same for all the refinement algorithms: insert vertices until the mesh meets constraints on element quality and size. Center of circumcircle, centroid, and middle of the largest edge of a triangle are considered for inserting a vertex for a triangular element for improving the mesh quality.

2.2 Beam Modeling

There are essentially three types of structures based on the relative sizes of their three dimensions: massive bodies, plates and shells, and beams. For massive bodies all three dimensions are comparable. Many structures have one dimension (thickness) very small comparing with other two (length and width) and are known as plates and shells. This type of structure can be considered as two-dimensional and the stress analysis is easier than three-dimensional analysis. Beams have one dimension (length) large compared to the other two dimensions. Stress analysis is much easier for beams as compared to three-dimensional or two-dimensional cases. Modeling of this kind of dimensionally reduced structures can be performed with less effort than for their three-dimensional counterparts. For composite materials, the analytical

solutions for beams are still very complex, and solutions are known for special cases only [77, 78, 87, 17, 58]. As a result, numerical techniques, such as finite element analysis [72, 7, 8, 9, 10, 62, 63, 64, 56, 65, 66, 11, 57, 5, 6] is considered for calculating the structural properties of beams. This thesis focuses on the sectional analysis of beams, so previous work mainly on beam modeling is reviewed here.

Hodges [50, 54] did a literature review on composite beam modeling. He classified the modeling into two approaches: "analytical approaches" and "finite element-based approaches." The warping function and stiffness properties are found from closed form calculation or from simple analytical approximations (in the geometry of the cross-section as well as for the form of the warping displacements). On the other hand, the finite-element-based approach offers "a versatility and modeling flexibility that no analytical method can match." It allows one to determine the warping function and elastic properties "for any general cross-section geometry that can be modeled with standard two-dimensional finite elements." The detail literature review on composite beam modeling can also be found in Refs. [24, 82, 95, 98, 99].

There is much literature available on beam modeling. Berdichevsky and his co-workers introduced VAM (Variational Asymptotic Method) [12, 13, 15, 13, 14] for three-dimensional beam modeling. They decoupled three-dimensional nonlinear elasticity problem into a two-dimensional linear cross-sectional analysis to provide the elastic constants and a one-dimensional nonlinear beam problem to calculate the global deformation. Borri et al. [46, 20] developed a technique based on the principle of virtual work for calculating the cross-sectional properties and the warping functions for prismatic composite beams. They also extended their work for initially curved and twisted composite beams [20]. But this formulation is not asymptotically correct for composite beam modeling. Petrov et al. [79, 80] developed a geometrically exact nonlinear formulation by considering the three-dimensional exact solution for a prismatic beam with the kinematic assumption. These models can be applied

to isotropic beams but they do not produce accurate enough results for composite beams. Taufik et al. [93] proposed a model for calculating stresses and stiffnesses from the longitudinal nodal warping and six constants representing the rigid displacement of the section considering assumptions on strains. But this technique is not accurate enough for composite beams modeling due to very restrictive strain assumptions. Kim and White [61] developed a model for box beam. In-plane deformation of the cross-section is neglected and transverse shear strains vary parabolically across the thickness is assumed here. Both warping and transverse shear effects are considered and can be modeled for both thin- and thick-walled beams. Jung, Nagaraj, and Chopra [60] also developed a composite beam model that can handle out-of-plane warping, warping restraint and transverse shear for both thin- and thick-walled beams. The authors assessed the model with several analytical and experimental results. Rand [86] found that not only out-of-plane warping but also in-plane warping plays a significant role for certain lay-ups angles for solid orthotropic beam under the action of bending moment for his model. Composite beam modeling is also treated in Refs. [94, 83, 84, 53, 51, 23, 85, 96].

But Hodges and his coworkers claimed that Variational Asymptotic Beam Sectional Analysis (VABS), a finite element based approach, developed by them [52, 25, 26, 27, 28, 83, 85, 99, 54], is the most efficient available model to design and analyze composite beam cross-sections. So VABS is considered for performing finite element analysis for SectionBuilder. The key features of VABS as stated in Ref. [99] are as follows:

1. The VAM (Variational Asymptotic Method) [12, 13, 15, 13] is used as the mathematical foundation of VABS to decouple a general three-dimensional nonlinear elasticity problem into a two-dimensional linear cross-sectional analysis to provide the elastic constants and a one-dimensional nonlinear beam problem to calculate the global deformation.

2. Asymptotically correct sectional analysis and geometrically exact beam analysis are derived from a common framework based on the concept of decomposition of the rotation tensor [36].

3. This theory is not problem specific but is general enough to accurately represent a nonhomogeneous anisotropic beam with arbitrary cross-sectional shape.

CHAPTER III

CAPABILITIES OF SECTIONBUILDER

3.1 Introduction

SectionBuilder is a finite element based cross-sectional analysis tool. The overall cross-sectional analysis process is shown in fig. 3 (where 3D defines three-dimensional.) The analysis processes can be broken into three phases: model definition phase, computational phase, and post processing phase. The geometry and material properties are defined in model definition phase. Computational phase has two steps: mesh generation and finite element analysis phases. Finite element analysis is performed for computing the sectional properties and stress distributions over the cross-section. The final, post processing phase provides the visualization of the computed stress fields. The entire process is integrated into a design environment that includes the definition of the cross-section, the analysis and the visualization of the results.

3.1.1 Model definition phase

In this phase, the geometric characteristics of the cross-section along with the physical properties of the constituent materials is described. SectionBuilder can create cross-sections of parametric shapes and arbitrary configuration as explained in the following sections.

3.1.1.1 Cross-sections of parametric shapes

These cross-sections have given geometric shapes that are parameterized. Parametric shapes can be airfoil sections, circular arcs, C-sections, L-sections, circular cylinders, double boxes, I-sections, rectangular, rectangular sections, circular tubes, triangular sections, T-sections, Z-sections, etc.

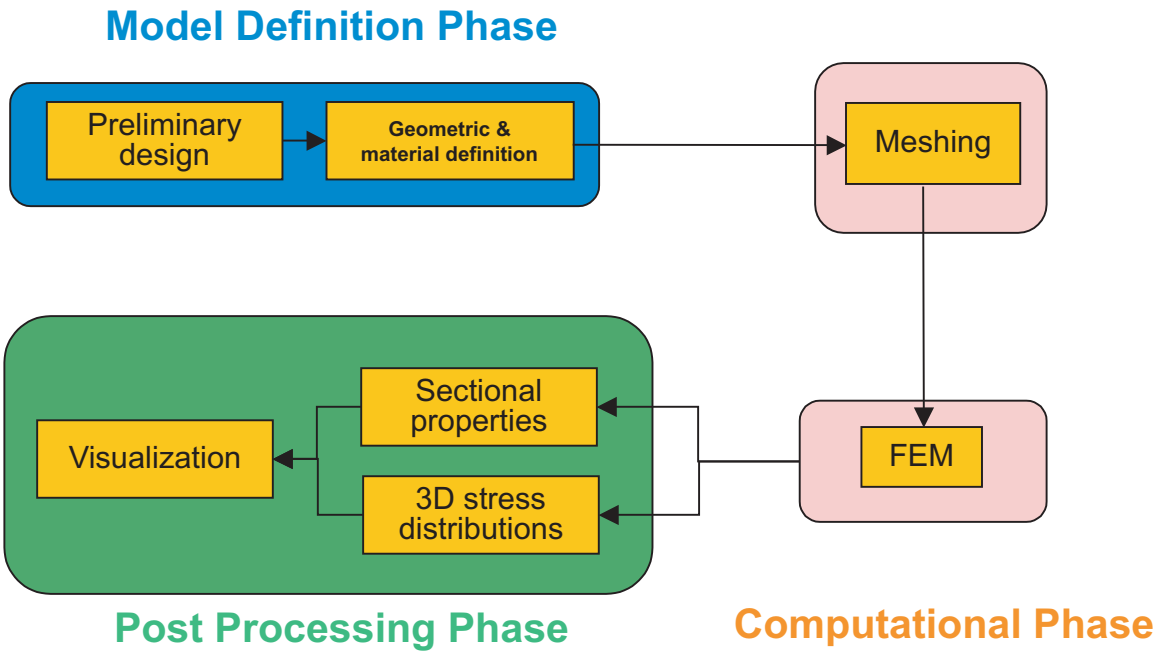

Figure 3: The three phases of beam cross-section analysis

For example, the parametric shape of a typical C-section is depicted in fig. 4. The dimensions such as height and thickness of web; widths, thicknesses, and skew angle of top and bottom flanges; thicknesses of top and bottom flange reinforcements (if present) need to be provided as input information for constructing the section. The section consists of several subsections to which independent material properties can be assigned.

This tool can create other parametric sections as explained in section 3.2.

3.1.1.2 Cross-sections of arbitrary configuration

SectionBuilder can create cross-sections with arbitrary configuration. For example, a realistic rotor blade cross-section is shown in fig. 5. This cross-section is airfoil shaped with one web, made of composite material plies. The cross-section is reinforced with core material at the aft portion of the section for keeping the proper shape during operation. Aluminum honeycomb is used as core material for this cross-section.

As shown in fig. 6, a typical beam (example: rotor blade) cross-section is viewed

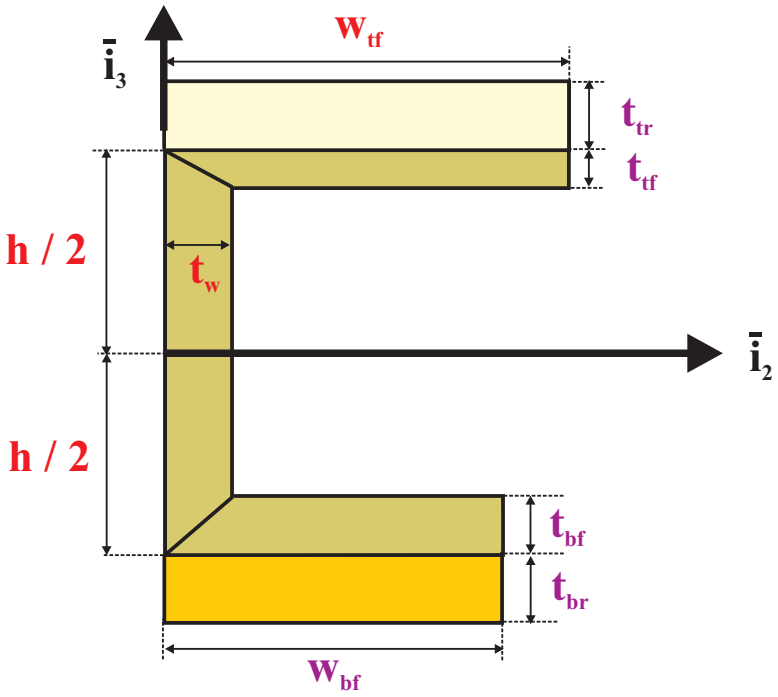

Figure 4: Configuration of the C-section

Figure 5: Actual rotor blade cross-section with core material

as a number of interconnected walls in SectionBuilder. Walls are constructed by stacking composite material plies on an user defined arbitrary base curve. Walls are constructed in this technique because realistic complex cross-sections are built by laying layers of composite materials in a mold of arbitrary shape. It is possible to connect several walls to create complex cross-section, as depicted in fig. 6. Split-connectors, T-connectors, and V-connectors are available for connecting walls for creating a realistic beam cross-section.

For example, a typical cross-section is created with five walls, shown in fig. 6. The upper flange of the profile consists of `Wall1`, and `Wall2`, whereas the lower flange

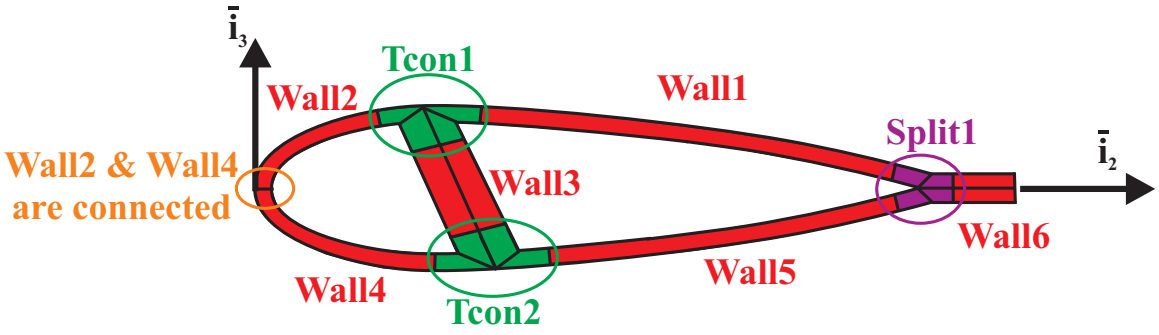

Figure 6: Airfoil section construction

consists of `Wall4`, and `Wall5`. The web consists of `Wall3`, and finally, the trailing edge tab consists of `Wall6`. The web, and flanges are connected together by T-connectors, labeled `Tcon1`, and `Tcon2`. The trailing edge tab splits into the upper, and lower flanges through a Split-connector, labeled `Split1`. Finally, two walls can be directly connected to each other, such as `Wall2`, and `Wall4` near the leading edge of the airfoil section.

In general, the cross-sections are reinforced with core materials for keeping the original shape during operation. SectionBuilder can integrate core materials into the rotor blade cross-sections. For example, the cavities of the cross-sections that are shown in fig. 7 could be filled with core materials for constructing realistic rotor blade cross-sections as shown in fig. 5.

At this point, closed Boundary curves, and corresponding points from the walls of cross-sections are available as input information shown in fig. 7 for defining the core materials. The mesh generation technique for core materials are explained in the section 3.1.2.1.

3.1.2 Computational phase

This phase has two steps: mesh generation and finite element analysis as explained in the following sections.

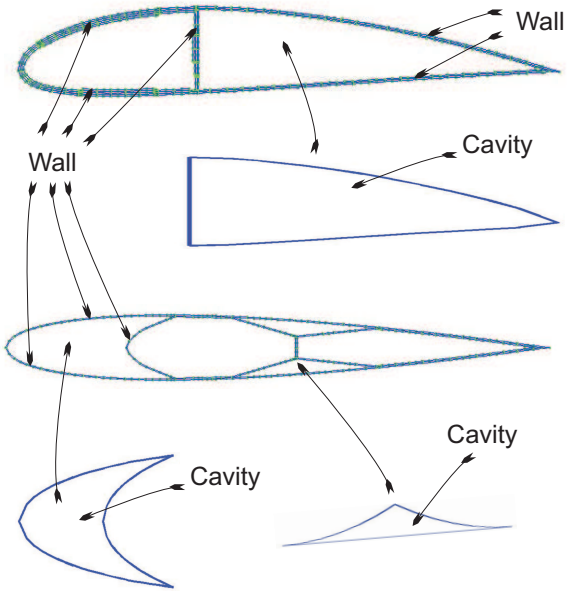

Figure 7: Cross-sections for incorporating core materials in the cavities

3.1.2.1 Mesh generation phase

For performing the finite element analysis, the meshes need to be generated after defining the geometries and material properties of the cross-sections properly. Mapped and/or free meshes are considered based on the nature of the cross-section. Mapped and free meshes are considered for generating the nine noded (27 degrees of freedom) quadrilateral and six noded (18 degrees of freedom) triangular elements respectively. Computational results are converged more rapidly for quadrilateral elements due to their higher number of degrees of freedom as compared to triangular elements. But mapped meshes are not considered everywhere because mapped meshes are suitable for creating meshes inside rectangular shaped closed boundaries only. These rectangular shaped closed boundaries are found for parametric shaped sections (such as C-sections,) walls, and connectors (such as T-connectors.) But free meshes can be generated inside any arbitrary closed boundary (such as triangular shapes.) As a result, free meshes are considered for generating meshes inside the arbitrary closed

boundaries which can be found when core materials are incorporated with in arbitrary shaped cross-sections. The mapped and free meshes generation techniques are explained in the following paragraphs.

Mapped mesh generation

For SectionBuilder, mapped meshes are considered for generating quadrilateral elements [4, 34] for all sections (i.e., parametric shapes, walls, connectors, etc) except for core materials. Nine noded quadrilateral elements are generated based on mapped meshes. These elements have four nodes at the four corners, four nodes at the middle of the four edges and one node at the center of the elements shown in fig. 8.

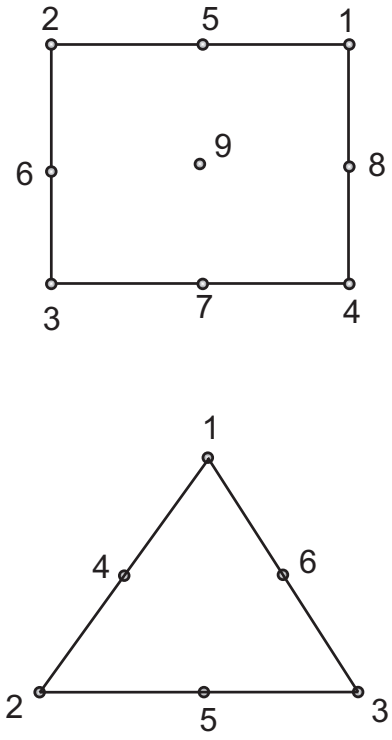

Figure 8: Nine noded quadrilateral element (top) and six noded triangular element (bottom) with orientation of nodes

Mesh density is considered as an important input parameter for creating mapped meshes. The longest dimension of a section is divided by the mesh density for calculating the characteristic length of finite elements for mapped meshes generation. The

size of the element is adjusted based on this characteristic length. If a certain dimension of a section is higher than the characteristic length but less than the one and half, the number of element is considered one. On the other hand, if the dimension of a section is higher than one and half times of the characteristic length but less than the double, the number of elements are considered two.

Free mesh generation

The free meshes generate six noded triangular elements for core materials. These triangular elements have three nodes at the three corners and other three nodes at the middle of the three edges as shown in fig. 8. Free meshes are considered for core materials which lie inside the cavities produced from the walls of the cross-sections. Delaunay triangulation [43, 76] is the most popular and efficient technique for free mesh generation for this kind of situation. Because this technique ensures the minimum angle of the triangles is equal or greater than that generated by any other techniques and produces the best possible meshes. As a result, the Delaunay triangulation technique is considered here for creating free meshes for core materials. The Delaunay triangulation technique is discussed in appendix B. The detail free mesh generation technique for core materials of cross-sections is explained in section 3.3.5.1.

3.1.2.2 Finite element analysis phase

After defining the cross-section, finite element analysis is performed for computing sectional properties and stress distributions over the cross-section. Hodges and his coworkers claimed that Variational Asymptotic Beam Sectional Analysis (VABS), developed by them [52, 25, 26, 27, 28, 83, 85, 99, 54], is the most efficient available tool for finite element analysis of beam cross-sections. So, VABS is considered here for finite element analysis. The key features of VABS as stated in Ref. [99] are as follows:

1. The VAM (Variational Asymptotic Method) [12, 13, 15, 13] is used as the

mathematical foundation of VABS to decouple a general three-dimensional nonlinear elasticity problem into a two-dimensional linear cross-sectional analysis to provide the elastic constants and a one-dimensional nonlinear beam problem to calculate the global deformation.

2. Asymptotically correct sectional analysis and geometrically exact beam analysis are derived from a common framework based on the concept of decomposition of the rotation tensor [36].

3. This theory is not problem specific but is general enough to accurately represent a nonhomogeneous anisotropic beam with arbitrary cross-sectional shape.

3.1.3 Post processing phase

This phase provides the visualization of the computed stress fields. The sectional properties are also found in the generated output file of SectionBuilder. The entire process is integrated into a design environment that includes the definition of the cross-section, the analysis and the visualization of the results.

3.2 Parametric Shape Section Configurations

SectionBuilder can create parametric shape section configurations. Parametric shapes can be airfoil sections, circular arcs, C-sections, L-sections, circular cylinders, double boxes, I-sections, rectangular, rectangular sections, circular tubes, triangular sections, T-sections, Z-sections, etc. The definition of these sections with few examples are discussed below.

3.2.1 Definition of airfoil sections

Airfoil sections are parametric configurations with no internal web, as depicted in fig. 9, or with one or two internal webs, as shown in fig. 10 and 11, respectively. Airfoil sections consist of top and bottom flanges with optional internal webs. The section consists of up to three zones to which independent material properties can be assigned.

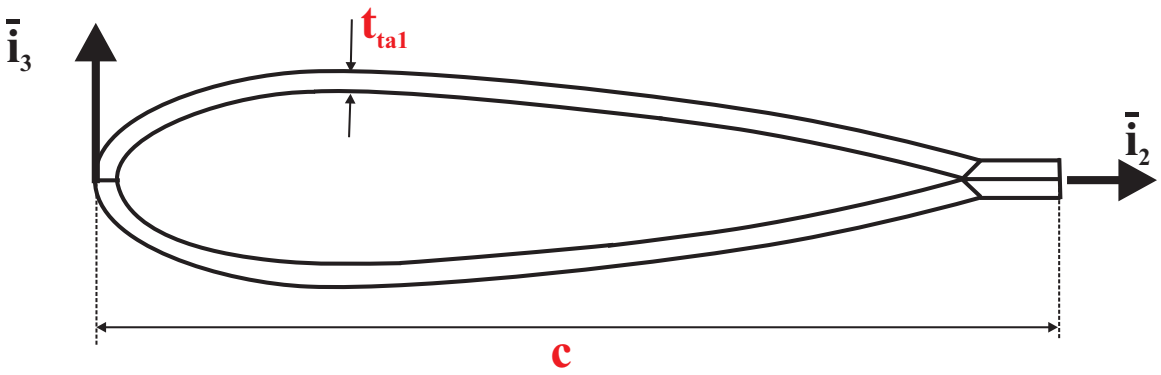

Figure 9: Configuration of the airfoil section with no web

The dimensions of the section are defined by the following parameters.

3.2.1.1 Airfoil Dimensions

1. The chord, c, of the airfoil section.

2. The thickness, t_{ta1}, of the section wall for the no web design. For the single or dual web design, this is the wall thickness for the front portion of the airfoil.

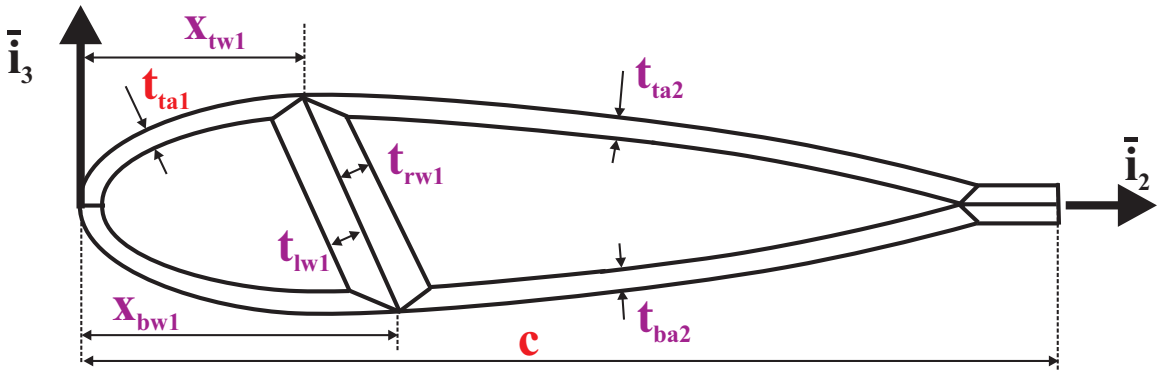

Figure 10: Configuration of the airfoil section with a single web

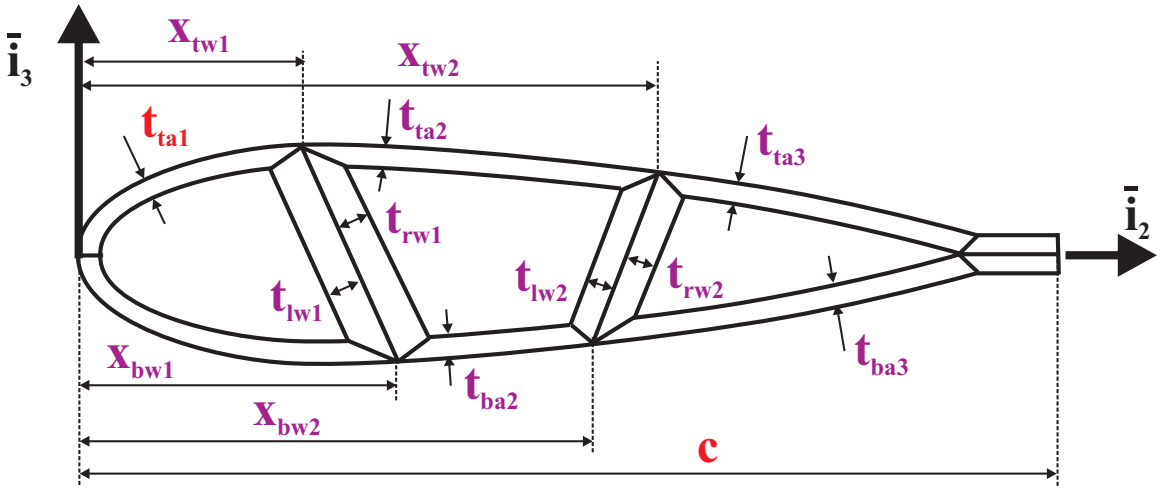

Figure 11: Configuration of the airfoil section with two webs

3.2.1.2 Airfoil Thickness

1. The top wall thickness, t_{ta2}, of the aft or middle portion of the airfoil for the single or dual web design, respectively (*default value:* $t_{\text{ta2}} = t_{\text{ta1}}$).

2. The bottom wall thickness, t_{ba2}, of the aft or middle portion of the airfoil for the single or dual web design, respectively (*default value:* $t_{\text{ba2}} = t_{\text{ta2}}$).

3. The top wall thickness, t_{ta3}, of the aft portion of the airfoil for the dual web design (*default value:* $t_{\text{ta3}} = t_{\text{ta2}}$).

4. The bottom wall thickness, t_{ba3}, of the aft portion of the airfoil for the dual web

design (*default value:* $t_{\mathrm{ba3}} = t_{\mathrm{ta2}}$).

3.2.1.3 Web 1 Dimensions

1. The location, x_{tw1}, of the intersection of the first web with the upper airfoil profile; this is a dimensional quantity (*default value:* $x_{\mathrm{tw1}} = 0$). This variable is also used as a flag for the presence of the first web: if $x_{\mathrm{tw1}} \neq 0$, at least one web is present.

2. The location, x_{bw1}, of the intersection of the first web with the lower airfoil profile; this is a dimensional quantity (*default value:* $x_{\mathrm{bw1}} = x_{\mathrm{tw1}}$).

3. The thickness, t_{lw1}, of the left portion of the first web (*default value:* $t_{\mathrm{lw1}} = t_{\mathrm{ta1}}$).

4. The thickness, t_{rw1}, of the right portion of the first web (*default value:* $t_{\mathrm{rw1}} = t_{\mathrm{ta2}}$).

3.2.1.4 Web 2 Dimensions

1. The location, x_{tw2}, of the intersection of the second web with the upper airfoil profile; this is a dimensional quantity (*default value:* $x_{\mathrm{tw2}} = 0$). This variable is also used as a flag for the presence of the second web: if $x_{\mathrm{tw2}} \neq 0$, two webs are present.

2. The location, x_{bw2}, of the intersection of the second web with the lower airfoil profile; this is a dimensional quantity (*default value:* $x_{\mathrm{bw2}} = x_{\mathrm{tw2}}$).

3. The thickness, t_{lw2}, of the left portion of the second web (*default value:* $t_{\mathrm{lw2}} = t_{\mathrm{ta1}}$).

4. The thickness, t_{rw2}, of the right portion of the second web (*default value:* $t_{\mathrm{rw2}} = t_{\mathrm{ta2}}$).

As shown in fig. 12, the section is divided into three zones.

1. The front portion of the airfoil consists of the components labeled **Flg1U**, **Flg1L**, and **LWeb1**.

2. The middle portion of the airfoil consists of the components labeled *RWeb1*, *Flg2U*, *Flg2L*, and *LWeb2*; these components are present in the single and dual web designs only.

3. The aft portion of the airfoil consists of the components labeled *RWeb2*, *Flg3U*, *Flg3L*, *TedU*, and *TedL*; these components are present for the dual web design only.

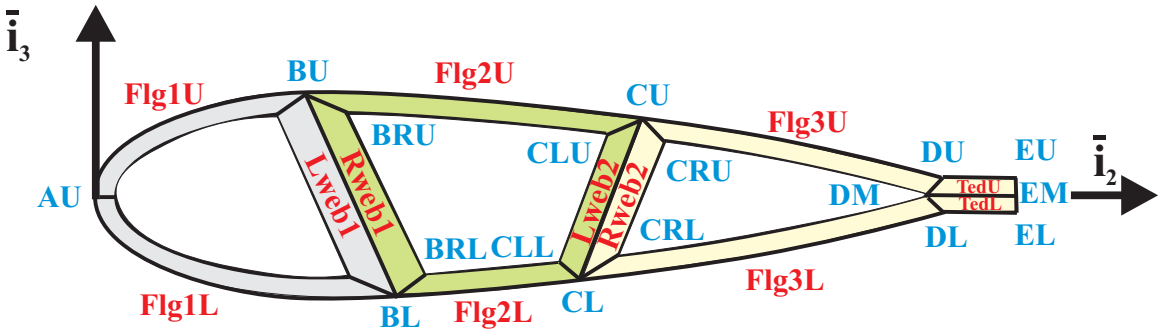

Figure 12: The three zones of the airfoil section

3.2.1.5 Examples

A few examples that describe the construction procedure of this type of section are shown below.

Example 1

This example shows a NACA four digit series airfoil section. The chord length, thickness, material properties, and mesh density are assigned here. This example also shows the principal centroidal axes of bending.

Example 2

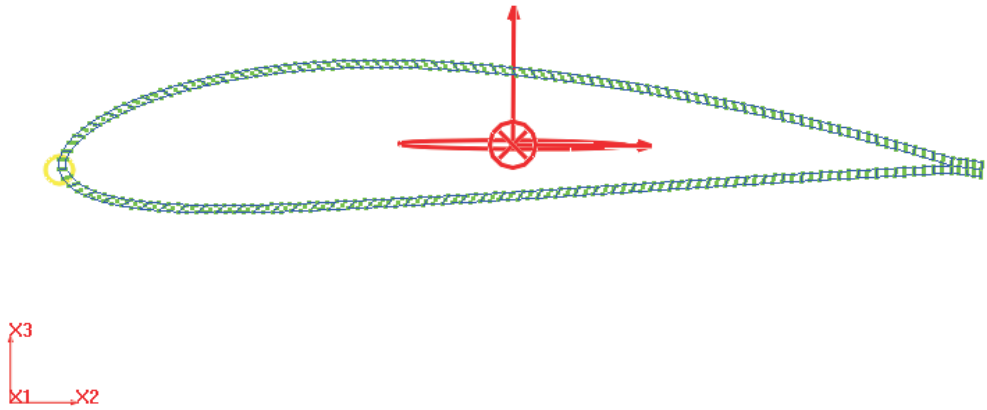

Figure 13: Example 1. Airfoil section

This example shows a NACA four digit series airfoil section. The section has two webs. The chord length, the location of the webs, thickness of the upper, lower section, and web, material properties, and mesh density are assigned here. This example also shows the principal axes of inertia at the mass center.

3.2.2 Definition of circular arcs

Circular arcs are predefined sections presenting the shape, shown in fig. 15. Circular arcs consist of an area included between two circular arcs spanned by a common angle. The section consists of a single zone to which material properties can be assigned. The circular arc is an **open circular tube**, as shown in fig. 15. **Closed circular tubes** can be defined with the help of the circular tube predefined section as described in section 3.2.9.

The dimensions of the section, shown in fig. 15, are defined by the following parameters.

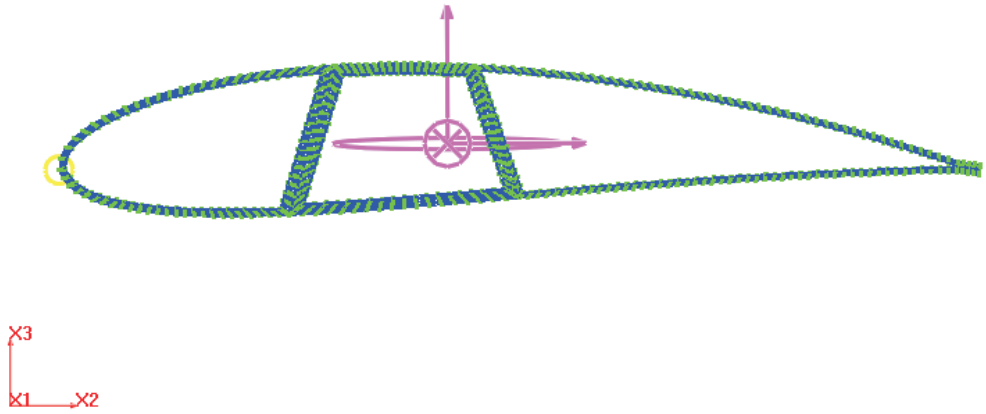

Figure 14: Example 2. Airfoil section with two webs

1. The outer radius, R_O, and inner radius, R_I, of the circular tube.

2. The initial angle, θ_I, and final angle, θ_F, of the circular arc, both measured in degrees. Note: $0 \leq \theta_I < 360$, $0 < \theta_F \leq 360$, and $\theta_I < \theta_F$. Even when $\theta_I = 0$ and $\theta_F = 360$, the circular arc is still an open circular tube.

The section is made of a single, homogeneous material.

3.2.2.1 Examples

A few examples that describe the construction procedure of this type of section are shown below.

Example 1

This example shows a circular arc. Here the inner and outer radii, initial (0^0) and final (180^0) angular positions of the arc, material, and mesh density are assigned for constructing this section. This example also shows the principal axes of shearing at

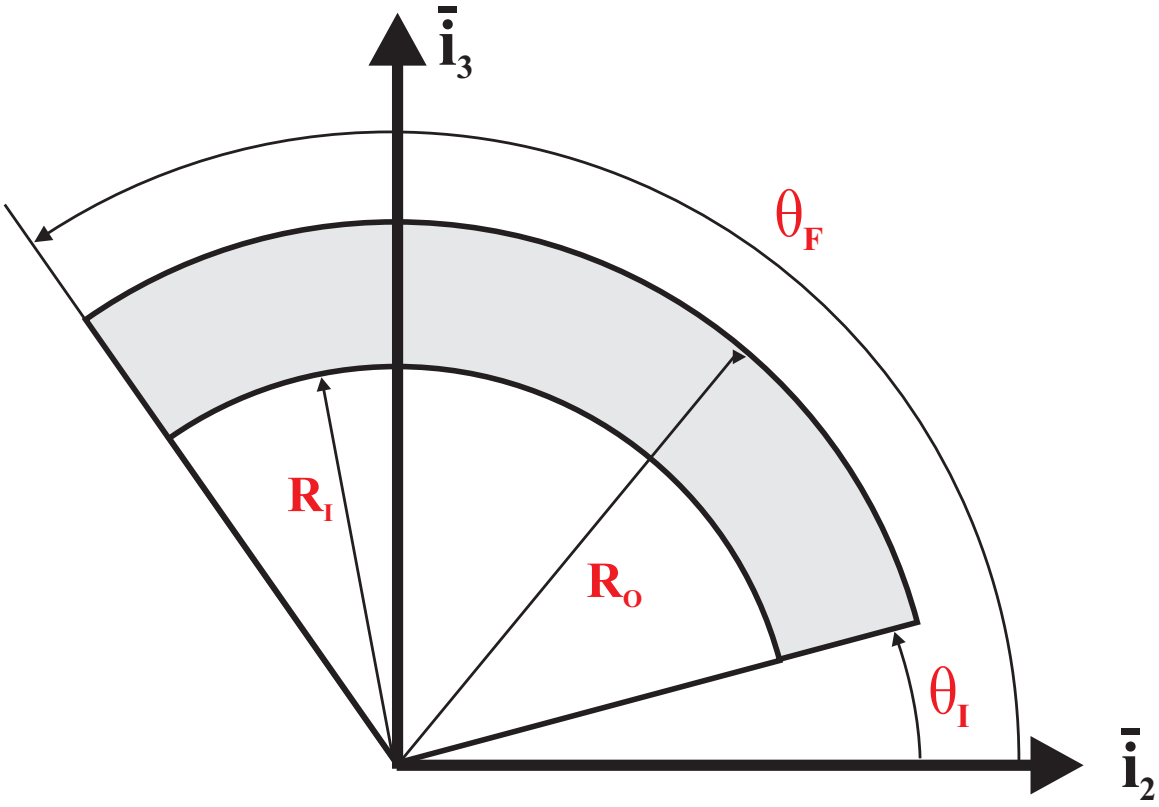

Figure 15: Configuration of the circular arc

the shear center.

Example 2

This example shows a circular arc. Here the inner and outer radii, initial and final angular positions of the arc, material, and mesh density are assigned for constructing this section. This example also shows the shear strain field over the cross-section under the applied sectional loads.

3.2.3 Definition of C-sections

C-sections are parametric configurations of the shape depicted in fig. 18. They consist of a C-section, possibly reinforced by top and/or bottom flanges. The section consists of up to three zones to which independent material properties can be assigned. Note that through the use of fixed frames, the C-section can be made to look like the

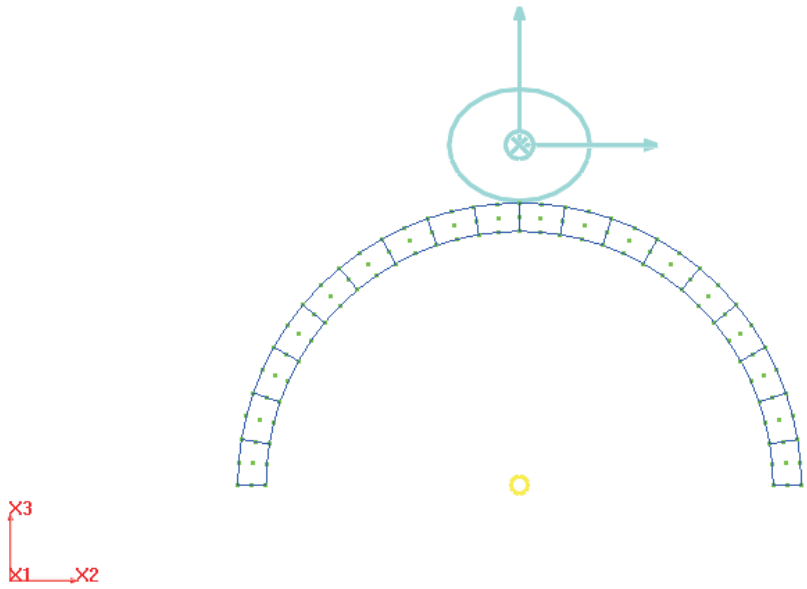

Figure 16: Example 2. Circular arc section

following shapes: ⊓, ⊔, ⊏, or ⊐.

The dimensions of the section, as depicted in fig. 18, are defined by the following parameters.

3.2.3.1 Web dimensions

1. The height, h, of the web.

2. The thickness, t_{w}, of the web.

3.2.3.2 Top flange dimensions

1. The width, w_{tf}, of the top flange.

2. The thickness, t_{tf}, of the top flange (*default value:* $t_{\mathrm{tf}} = t_{\mathrm{w}}$).

3. The skew angle, α_{tf}, of the top flange, positive up, measured in degrees (*default value:* $\alpha_{\mathrm{tf}} = 0$).

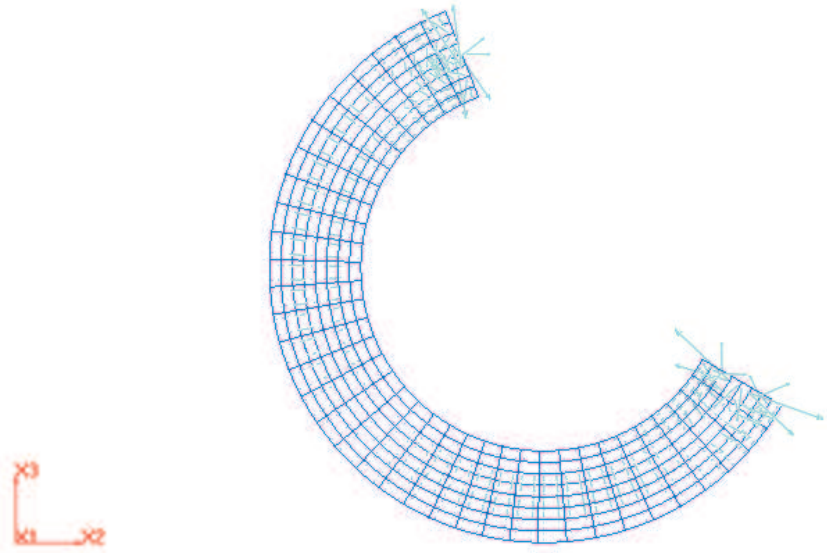

Figure 17: Example 2. Circular arc section

4. The thickness, t_{tr}, of the top reinforcement flange; this thickness applies to both left and right reinforcements, which cannot exist independently of each other (*default value:* $t_{\text{tr}} = 0$). This variable is also used as a flag for the presence of the top flange reinforcement: if $t_{\text{tr}} > 0$, this reinforcement is present.

3.2.3.3 Bottom flange dimensions

1. The width, w_{bf}, of the bottom flange(*default value:* $w_{\text{bf}} = w_{\text{tf}}$).

2. The thickness, t_{bf}, of the bottom flange (*default value:* $t_{\text{bf}} = t_{\text{tf}}$).

3. The skew angle, α_{bf}, of the top flange, positive down, measured in degrees (*default value:* $\alpha_{\text{bf}} = 0$).

4. The thickness, t_{br}, of the bottom reinforcement flange; this thickness applies to both left and right reinforcements, which cannot exist independently of each other (*default value:* $t_{\text{br}} = 0$). This variable is also used as a flag for the presence of the bottom flange reinforcement: if $t_{\text{br}} > 0$, this reinforcement is present.

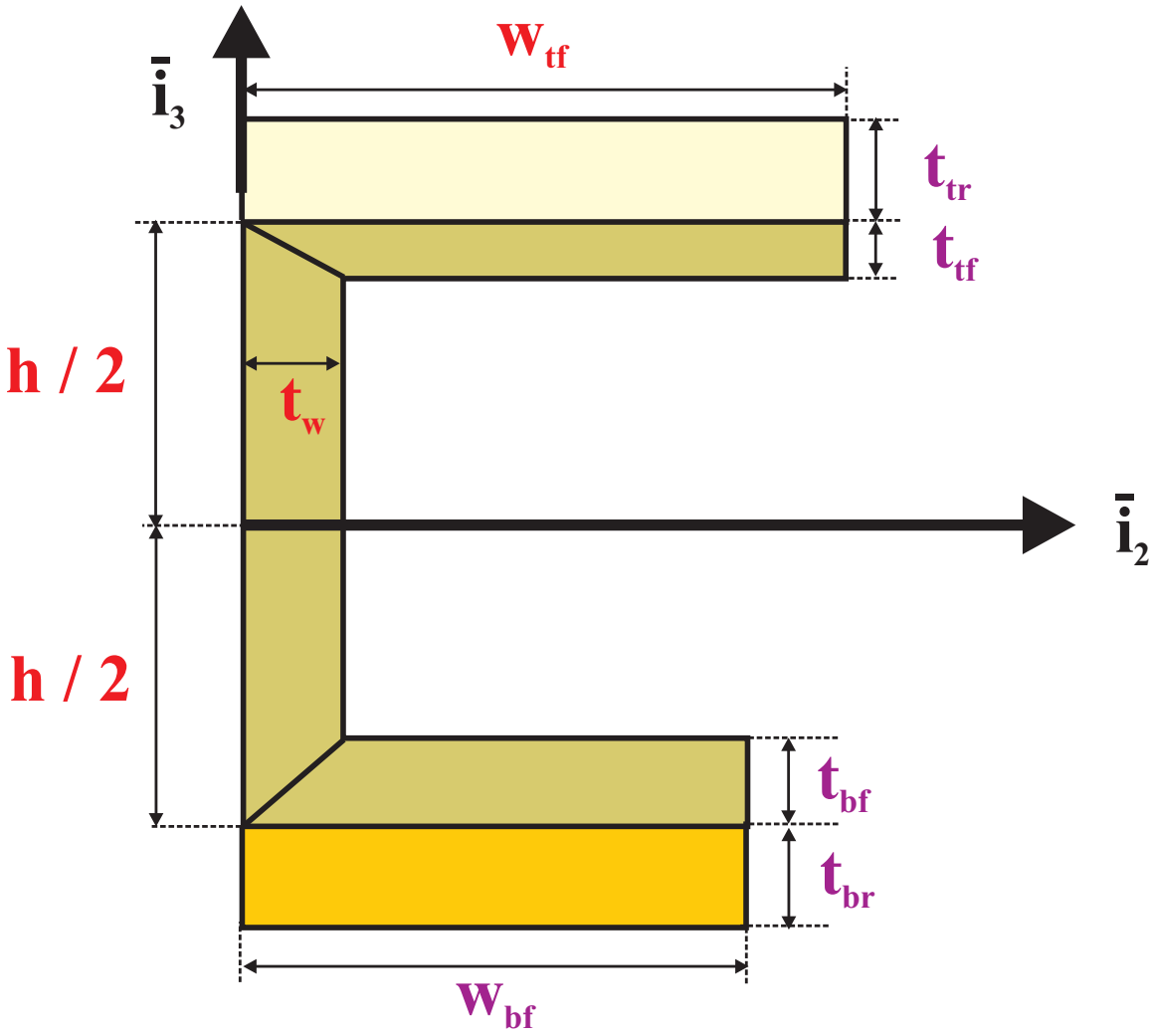

Figure 18: Configuration of the C-section

As shown in fig. 19, the section is divided into three zones.

1. The top reinforcement flange consists of a single solid labeled *TFlgR*.
2. The C-section it self consists of the solids labeled **TFlg**, **Web**, and **BFlg**.
3. The bottom reinforcement flange consists of a single solid labeled *BFlgR*.

3.2.3.4 Special Cases

1. If the width, $w_{\text{tf}} = 0$, the section looks like L-shape depicted in fig. 20. This L-shape section does not have TFlgR and TFlg solids, shown in fig. 21.

2. If the width, $w_{\text{bf}} = 0$, the section looks like reverse L-shape depicted in fig. 22. This reverse L-shape section does not have BFlgR and BFlg solids, shown in fig. 23.

3. If the widths, $w_{\text{tf}} = 0$ and $w_{\text{bf}} = 0$, the section looks like a strip depicted in fig. 24. This strip section does not have TFlgR, TFlg, BFlgR, and BFlg solids, shown in fig. 25. It only has Web.

3.2.3.5 Examples

A few examples that describe the construction procedure of this type of section are shown below.

Example 1

This example shows a C-section. Here web height, web thickness, top flange width, web material, and mesh density are assigned for constructing this section. This example also shows the shear strain field over the cross-section under the applied sectional loads.

Example 2

This example shows also a C-section with skewed top and bottom flanges. Here web height, web thickness, top flange width, top flange thickness, flange reinforce thicknesses, flange skew angles, materials, and mesh density are assigned for constructing this section. This example also shows the axial stress field over the cross-section under the applied sectional loads.

Example 3

This example shows a reverse L-section. Here web height, web thickness, top flange width, bottom flange width=0, web material, and mesh density are assigned for constructing this section. This example also shows principal centroidal axes of bending.

Example 4

This example shows a L-section. Here web height, web thickness, top flange width=0, bottom flange width, flange reinforce thickness, materials, and mesh density are assigned for constructing this section. This example also shows axial stress field over the cross-section under the applied sectional loads.

Example 5

This example shows a strip section. Here web height, web thickness, top flange width = 0, bottom flange width=0, web material, and mesh density are assigned for constructing this section. This example also shows principal axes of inertia at the mass center.

3.2.4 Definition of circular cylinders

Circular cylinders are predefined sections presenting the shape, shown in fig. 31. Circular cylinders consist of a solid circular cylinder. The section consists of a single zone to which material properties can be assigned. The circular cylinders are solid cylinders, as shown in fig. 31. Hollow circular cylinder, or circular tubes can be defined with the help of the circular tube predefined section as described in section 3.2.9.

The dimensions of the circular cylinder, shown in fig. 31, are defined by a single parameter, the radius (R) of the cylinder. The section is made of a single, homogeneous material.

3.2.4.1 Examples

An example that describes the construction procedure of this type of section is shown below.

Example 1

This example shows a Circular cylinder. Here radius, frame definition, material, and mesh density are assigned for constructing this section. This example also shows

the warping displacement of the cross-section under the applied sectional loads.

3.2.5 Definition of double boxes

Double boxes are parametric configurations of the shape depicted in fig. 33. They consist of an double box, possibly reinforced by top and/or bottom flanges. The section consists of up to four zones to which independent material properties can be assigned. Note that through the use of fixed frames, the double box can be made to look like the following shapes: H-sections.

The dimensions of the double box, shown in fig. 33, are defined by the following parameters.

3.2.5.1 Web dimensions

1. The height, h, of the section.
2. The thickness, t_{lw}, of the left part of the web.
3. The thickness, t_{rw}, of the right part of the web.

3.2.5.2 Top left flange dimensions

1. The width, w_{tlf}, of the top left flange.
2. The thickness, t_{tlf}, of the top left flange (*default value:* $t_{\mathrm{tlf}} = t_{\mathrm{lw}}$).
3. The skew angle, α_{tlf}, of the top left flange, positive up, measured in degrees (*default value:* $\alpha_{\mathrm{tlf}} = 0$).
4. The thickness, t_{tr}, of the top reinforcement flange; this thickness applies to both left and right reinforcements that cannot exist independently of each other (*default value:* $t_{\mathrm{tr}} = 0$). This variable is also used as a flag for the presence of the top flange reinforcement: if $t_{\mathrm{tr}} > 0$, this reinforcement is present.

3.2.5.3 Top right flange dimensions

1. The width, w_{trf}, of the top right flange (*default value:* $w_{\text{trf}} = w_{\text{tlf}}$).

2. The thickness, t_{trf}, of the top right flange (*default value:* $t_{\text{trf}} = t_{\text{rw}}$).

3. The skew angle, α_{trf}, of the top right flange, positive up, measured in degrees (*default value:* $\alpha_{\text{trf}} = 0$).

3.2.5.4 Bottom left flange dimensions

1. The width, w_{blf}, of the bottom left flange (*default value:* $w_{\text{blf}} = w_{\text{tlf}}$).

2. The thickness, t_{blf}, of the bottom left flange (*default value:* $t_{\text{blf}} = t_{\text{tlf}}$).

3. The skew angle, α_{blf}, of the bottom left flange, positive down, measured in degrees (*default value:* $\alpha_{\text{blf}} = 0$).

4. The thickness, t_{br}, of the bottom reinforcement flange; this thickness applied to both left and right reinforcements that cannot exist independently of each other (*default value:* $t_{\text{br}} = 0$). This variable is also used as a flag for the presence of the bottom flange reinforcement: if $t_{\text{br}} > 0$, this reinforcement is present.

3.2.5.5 Bottom right flange dimensions

1. The width, w_{brf}, of the bottom right flange (*default value:* $w_{\text{brf}} = w_{\text{trf}}$).

2. The thickness, t_{brf}, of the bottom right flange (*default value:* $t_{\text{brf}} = t_{\text{trf}}$).

3. The skew angle, α_{brf}, of the bottom right flange, positive down, measured in degrees (*default value:* $\alpha_{\text{brf}} = 0$).

As shown in fig. 34, the section is divided into four zones.

1. The top reinforcement flange consists of components labeled *TLFlgR* and *TRFlgR*

2. The left portion of the double box itself consists of components labeled **TLFlg**, **LWeb**, and **BLFlg**.

3. The right portion of the double box itself consists of components labeled **TRFlg**, **RWeb**, and **BRFlg**.

4. The top reinforcement flange consists of components labeled *BLFlgR* and *BRFlgR*.

3.2.5.6 Examples

A few examples that describe the construction procedure of this type of section are shown below.

Example 1

This example shows a double box. Here web height, web thicknesses, flange width, web materials, and mesh density are assigned for constructing this section. This example also shows the axial strain field over the cross-section under the applied sectional loads.

Example 2

This example shows a double box with skewed flanges. Here web height, web thicknesses, flange widths,flange thicknesses, flange reinforcement thickness, flange skew angles, materials, and mesh density are assigned for constructing this section. This example also shows the axial stress field over the cross-section under the applied sectional loads.

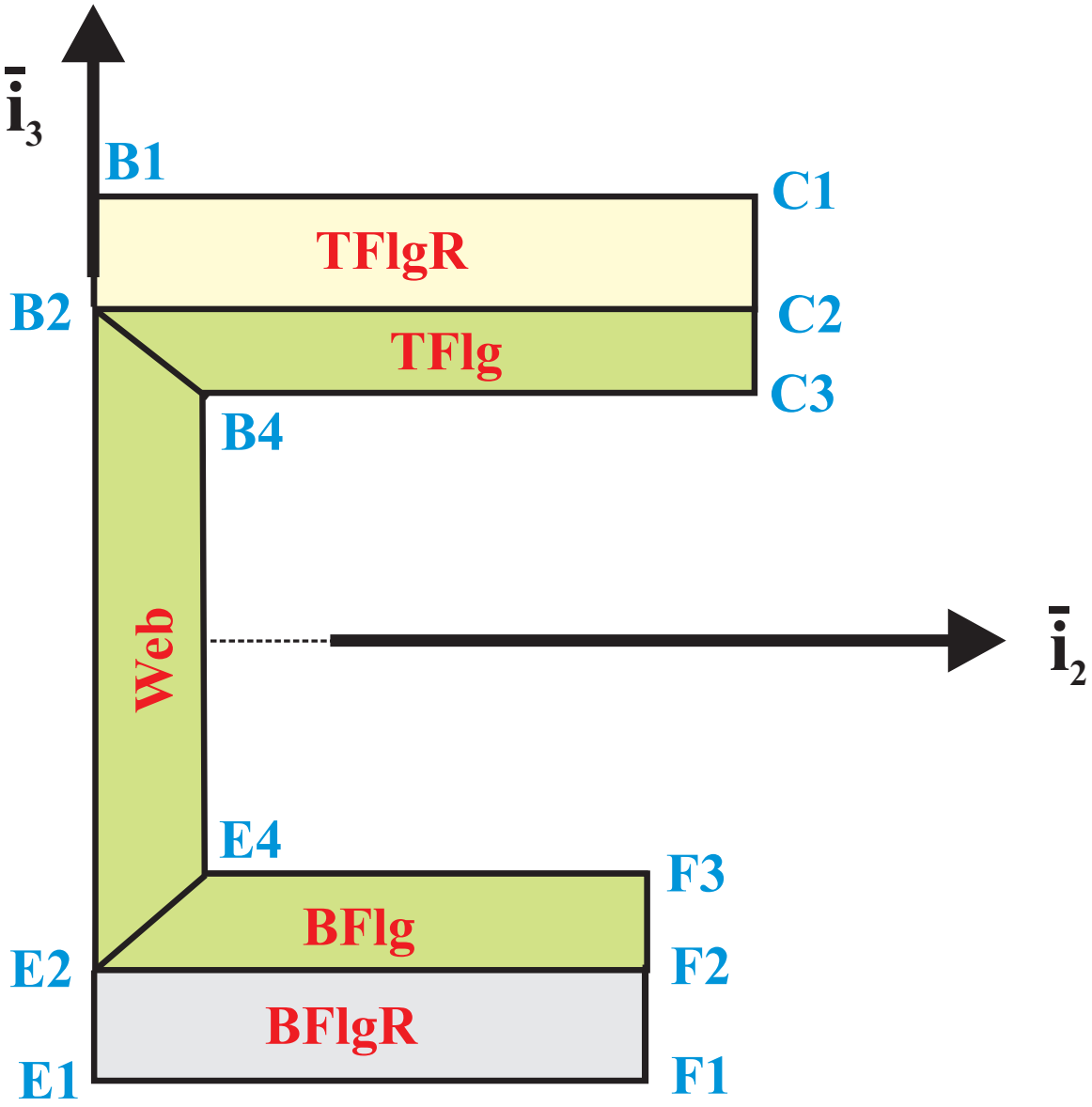

Figure 19: The three zones of the C-section

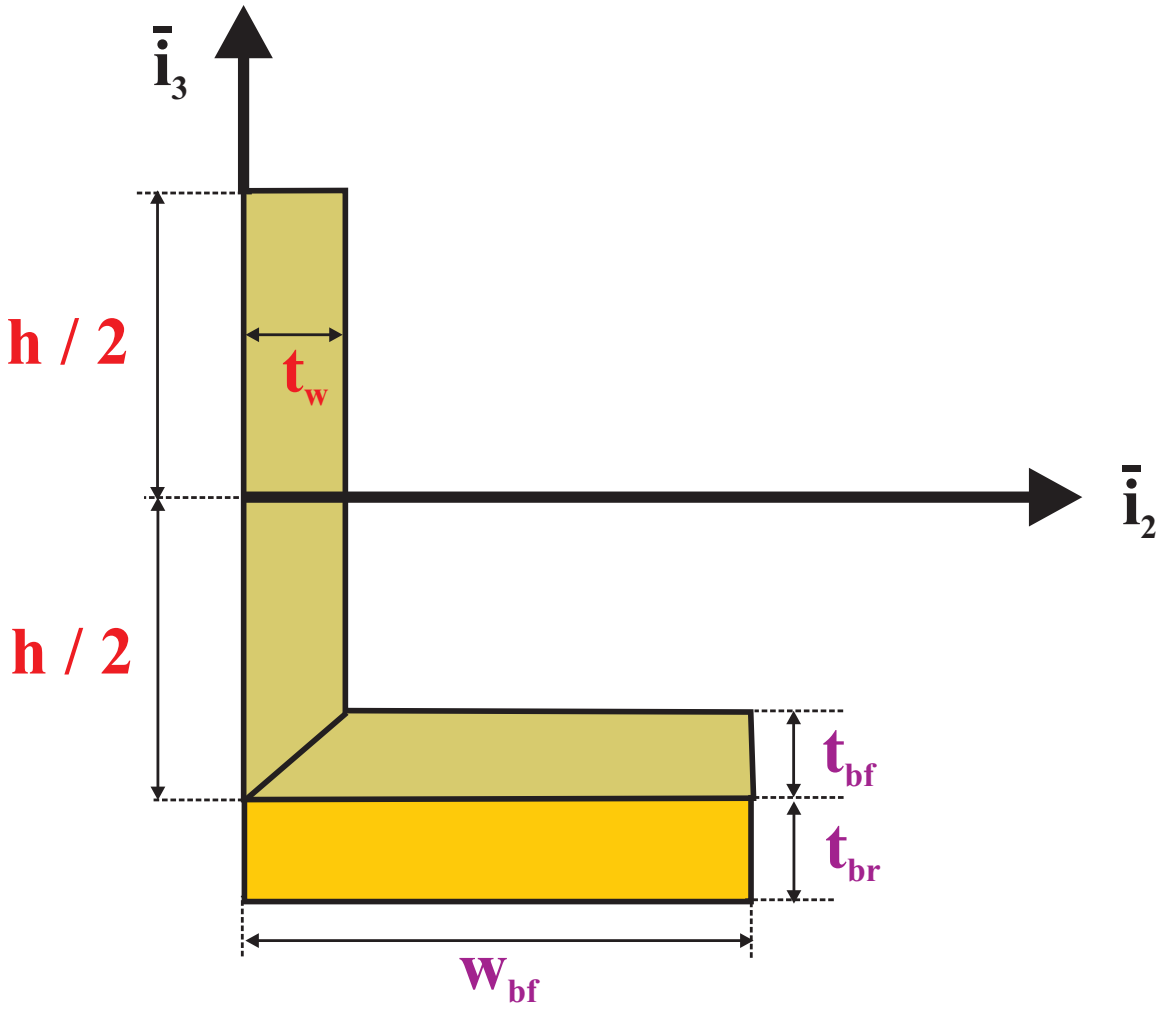

Figure 20: Configuration of the L-section

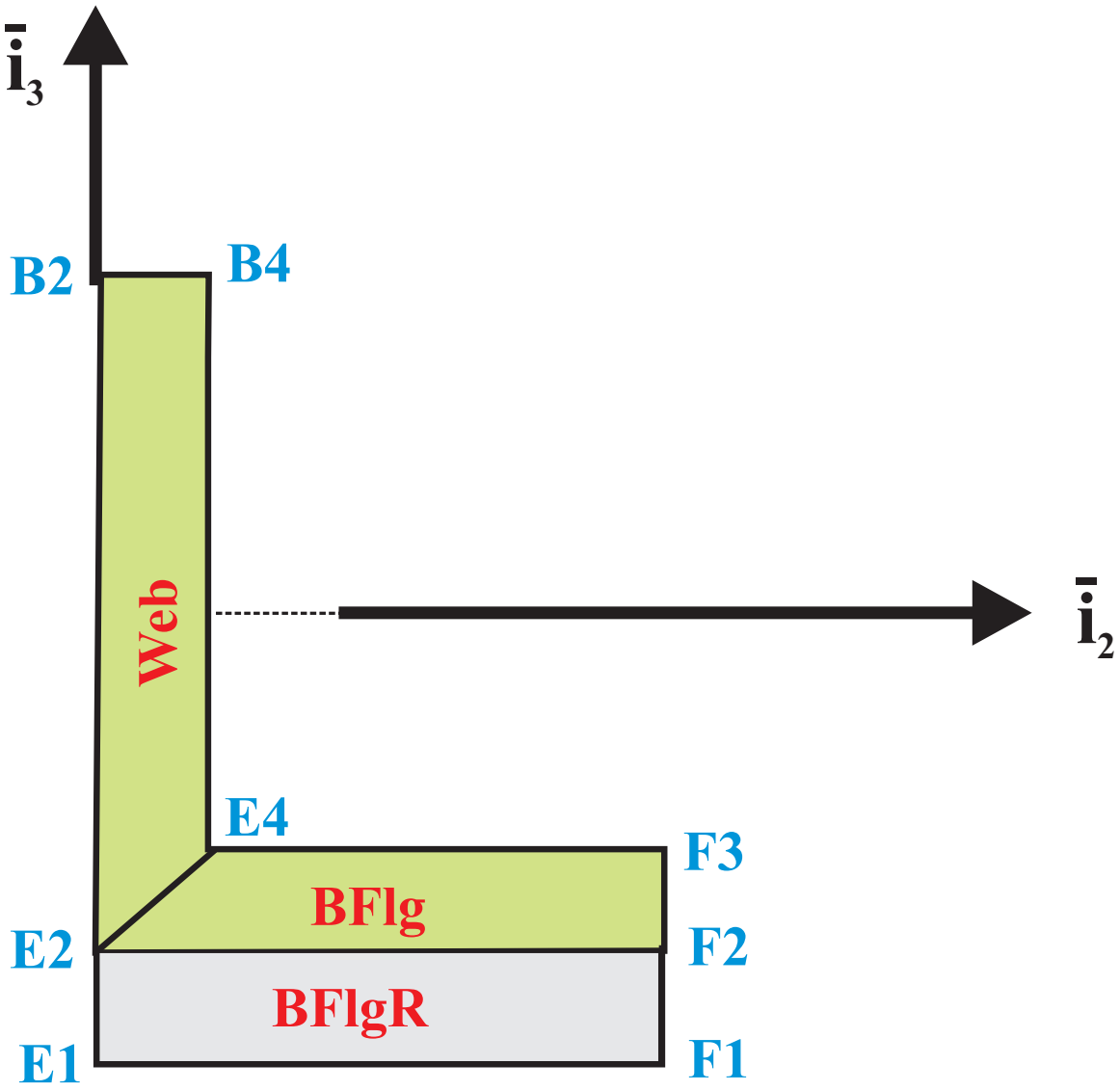

Figure 21: The two zones of the L-section

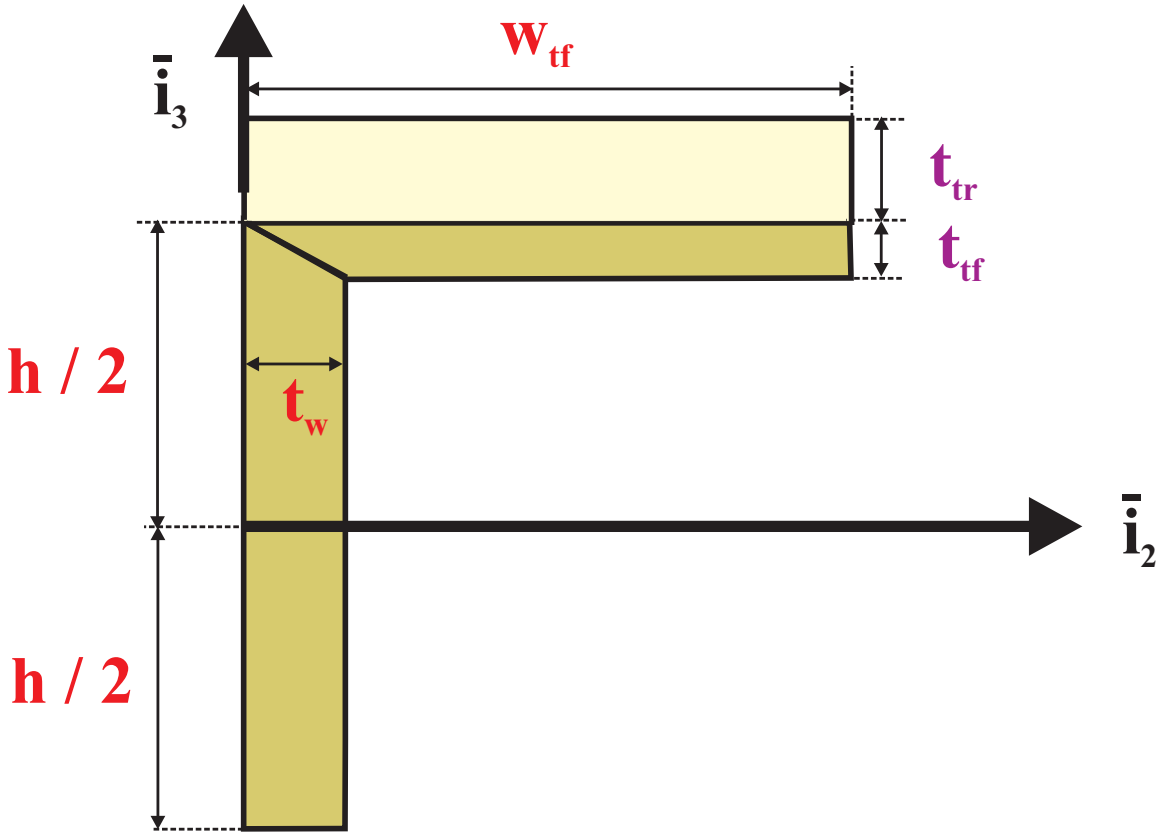

Figure 22: Configuration of the reverse L-section

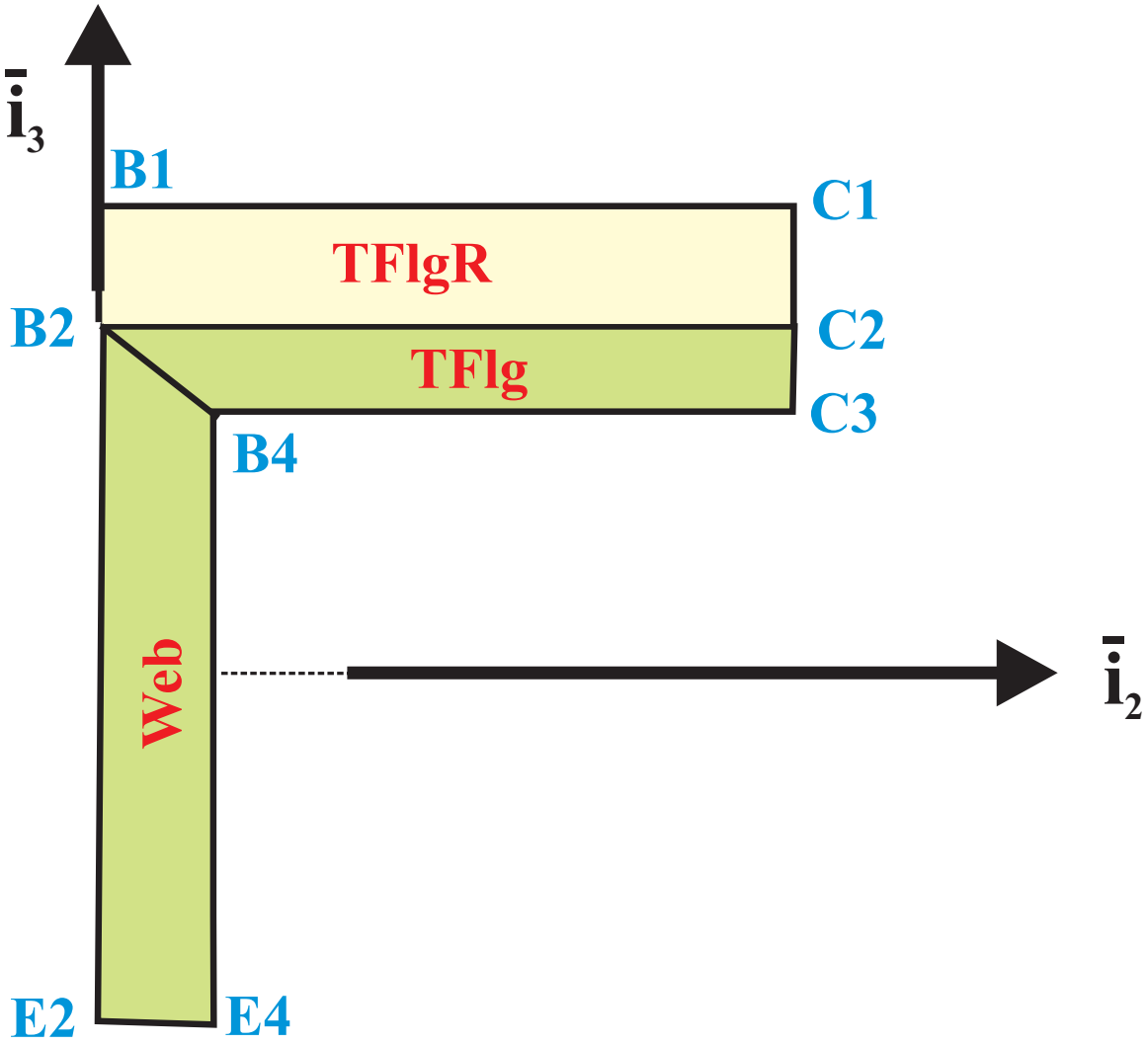

Figure 23: The two zones of the reverse L-section

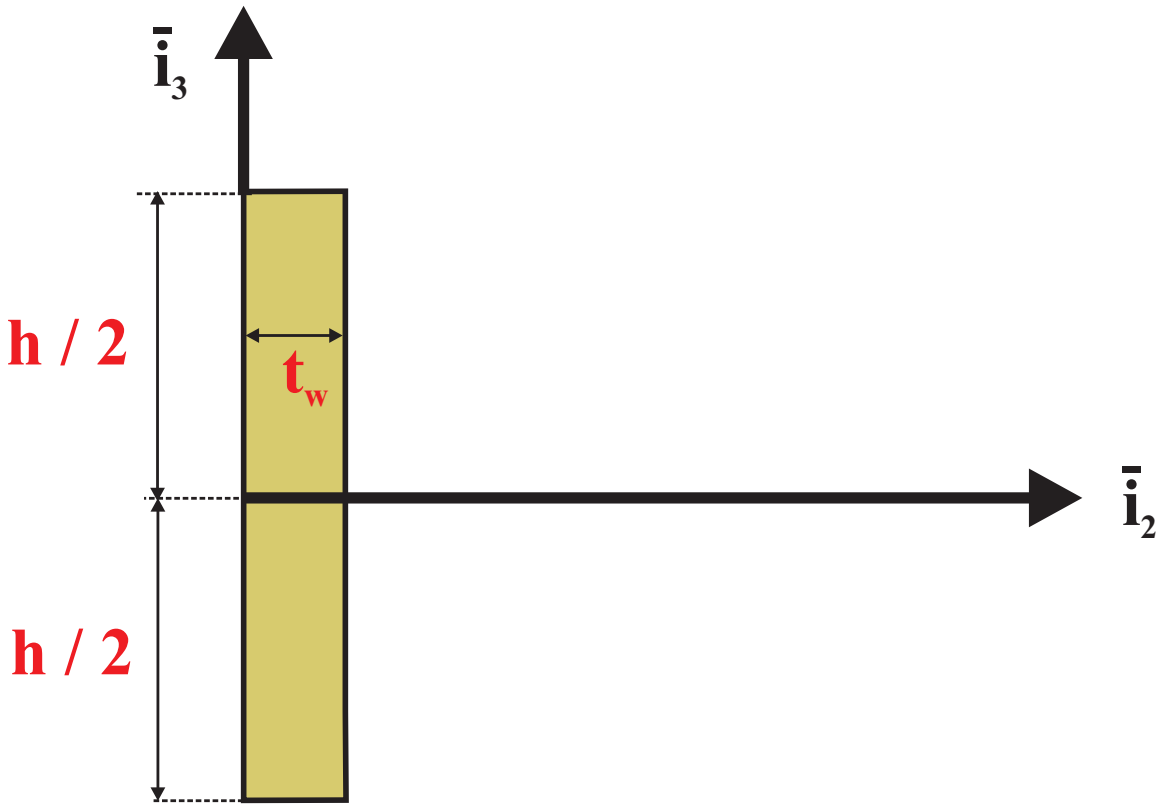

Figure 24: Configuration of the strip section

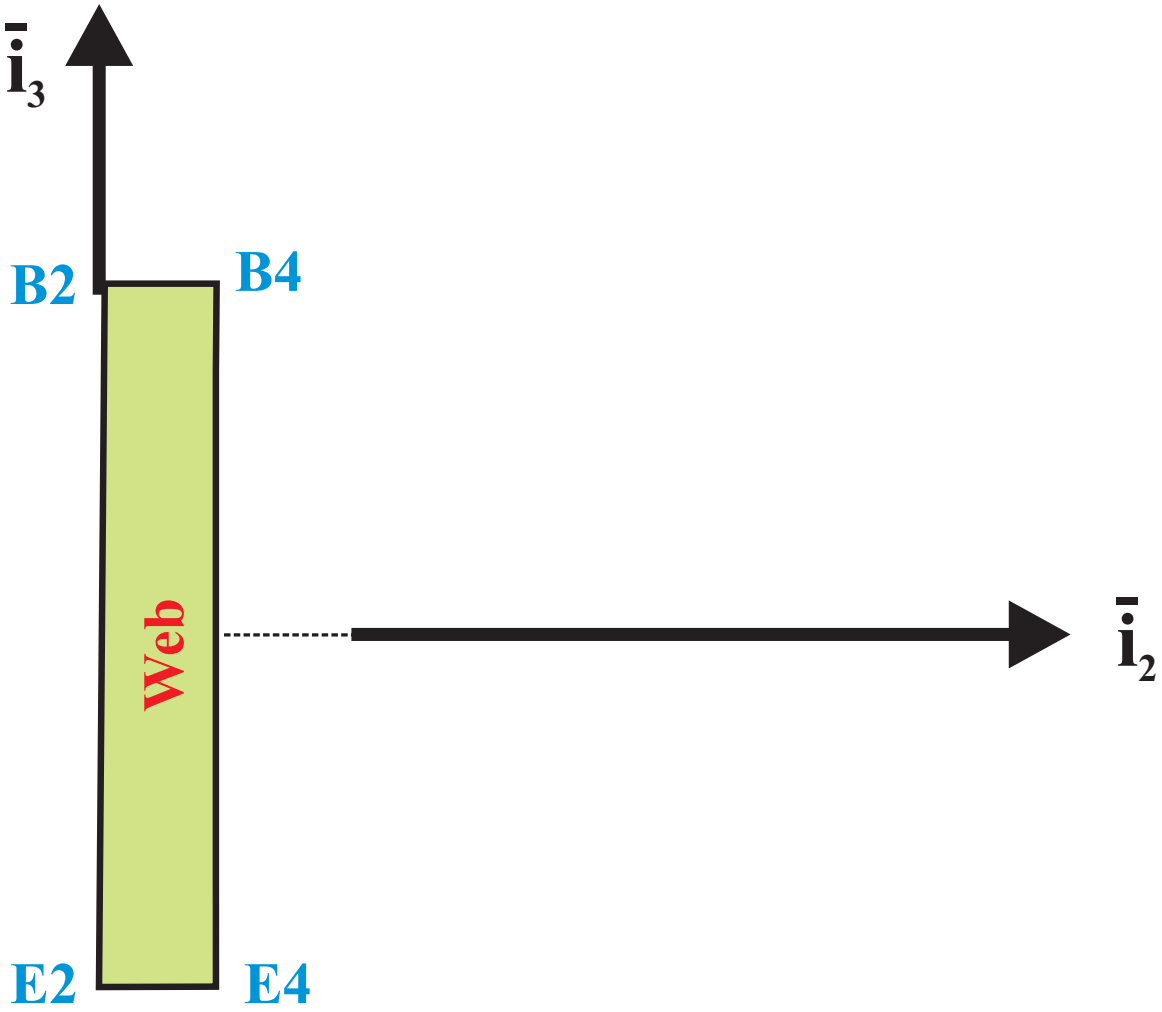

Figure 25: The zone of the strip section

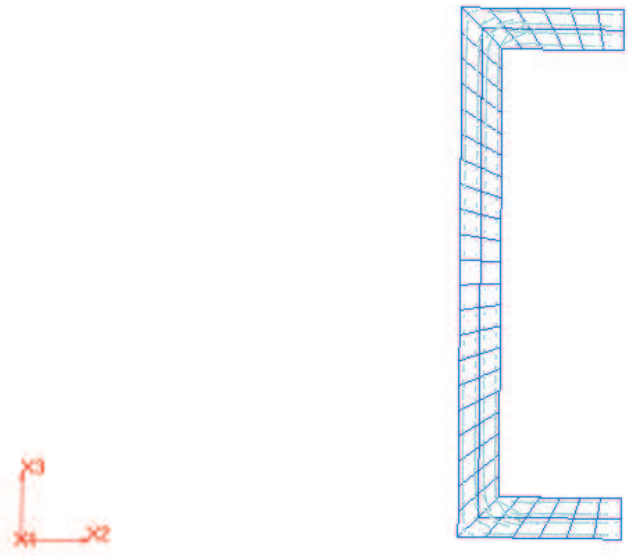

Figure 26: Example 1. C-section

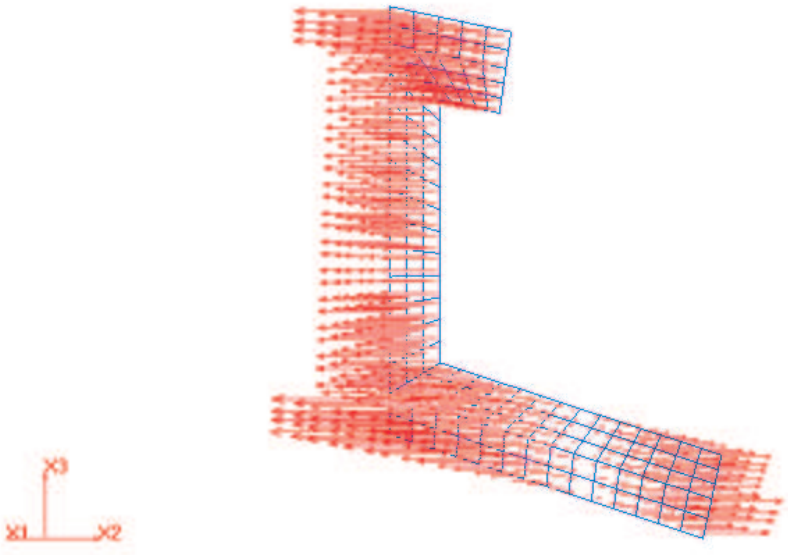

Figure 27: Example 2. C-section

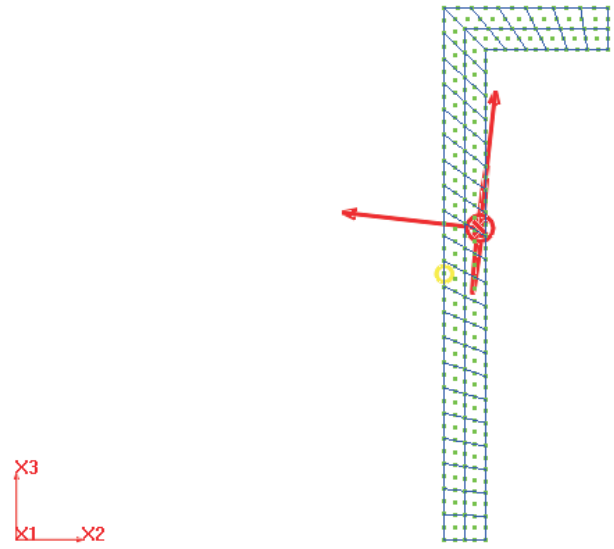

Figure 28: Example 3. Reverse L-section

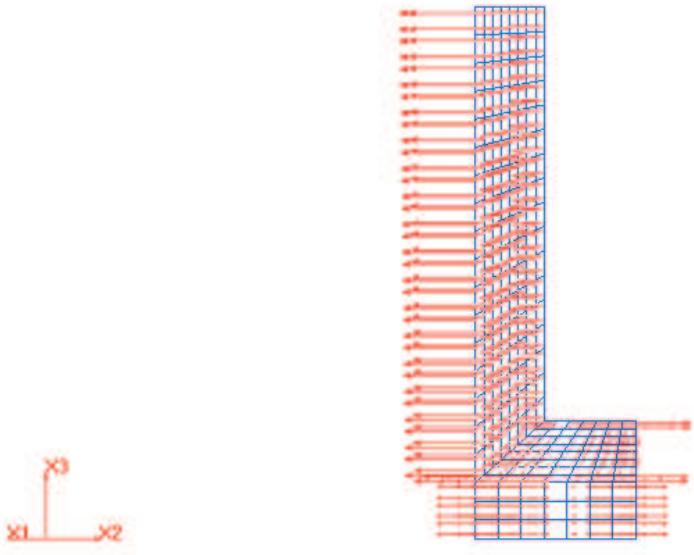

Figure 29: Example 4. L-section

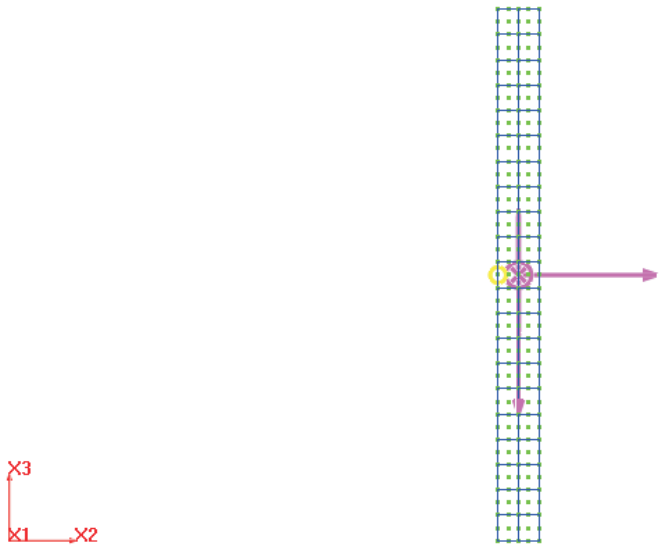

Figure 30: Example 5. Strip section

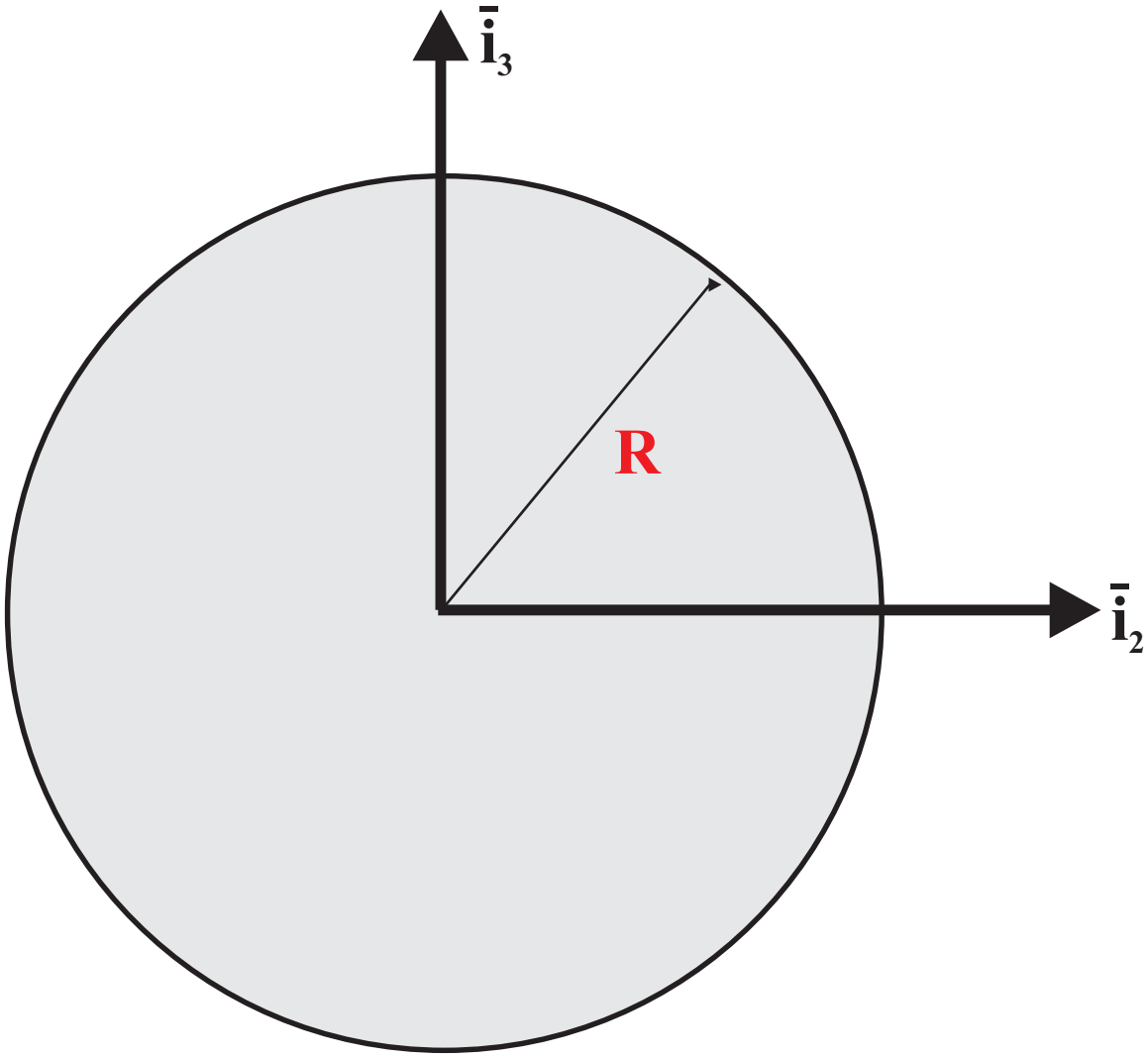

Figure 31: Configuration of the circular cylinder

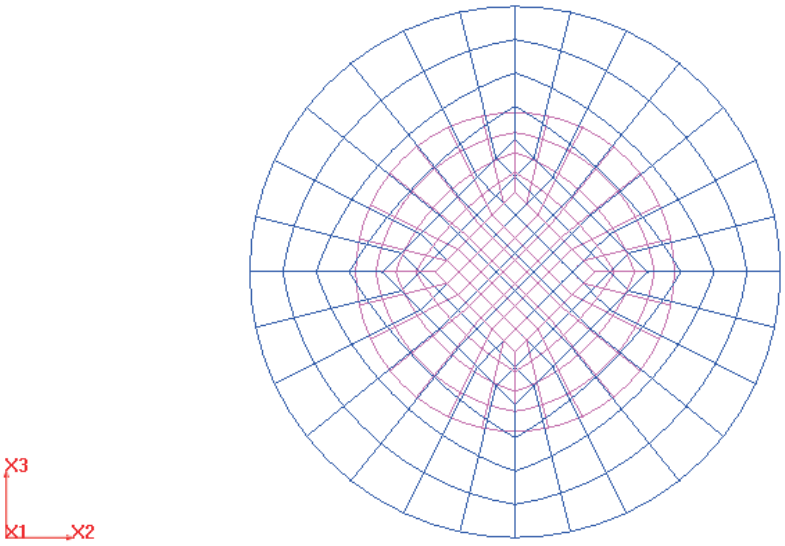

Figure 32: Example 1. Cylinder

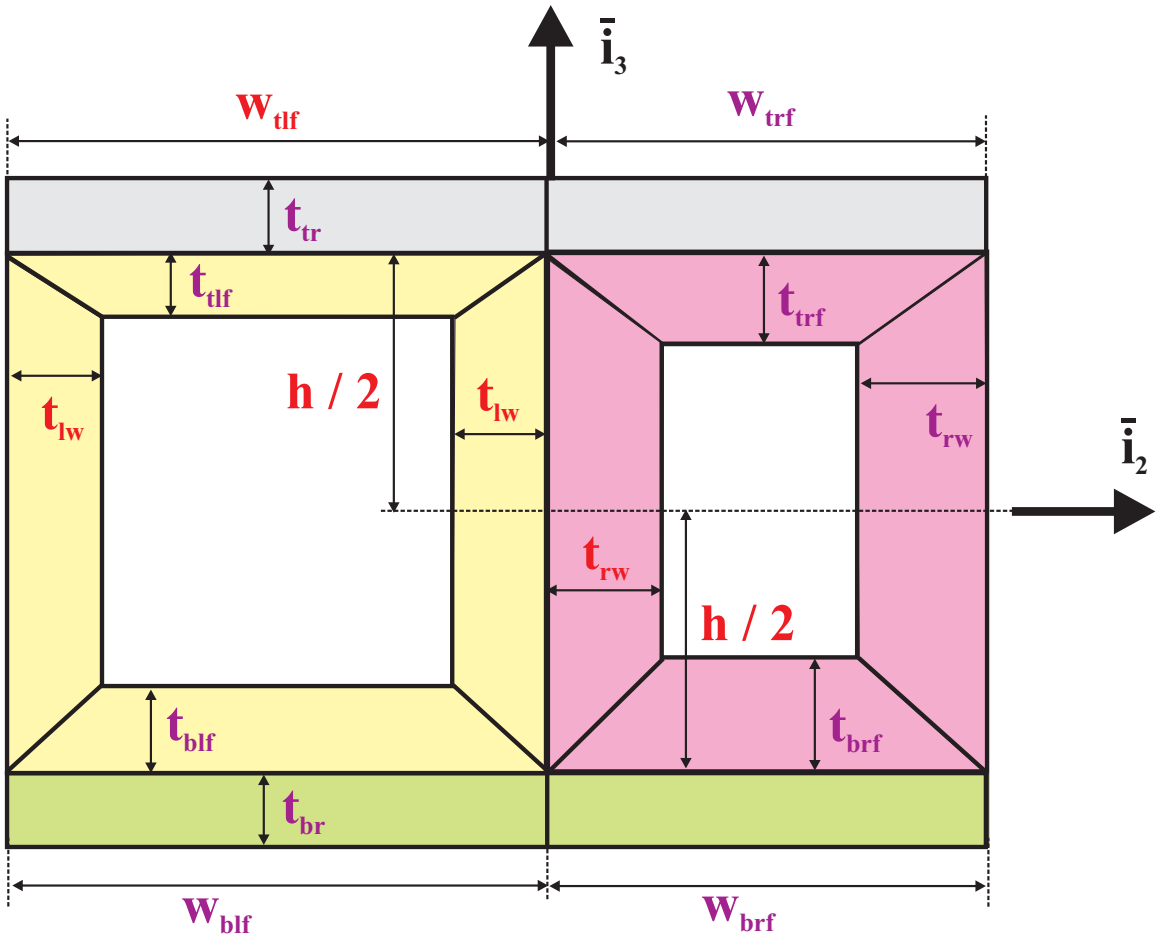

Figure 33: Configuration of the double box

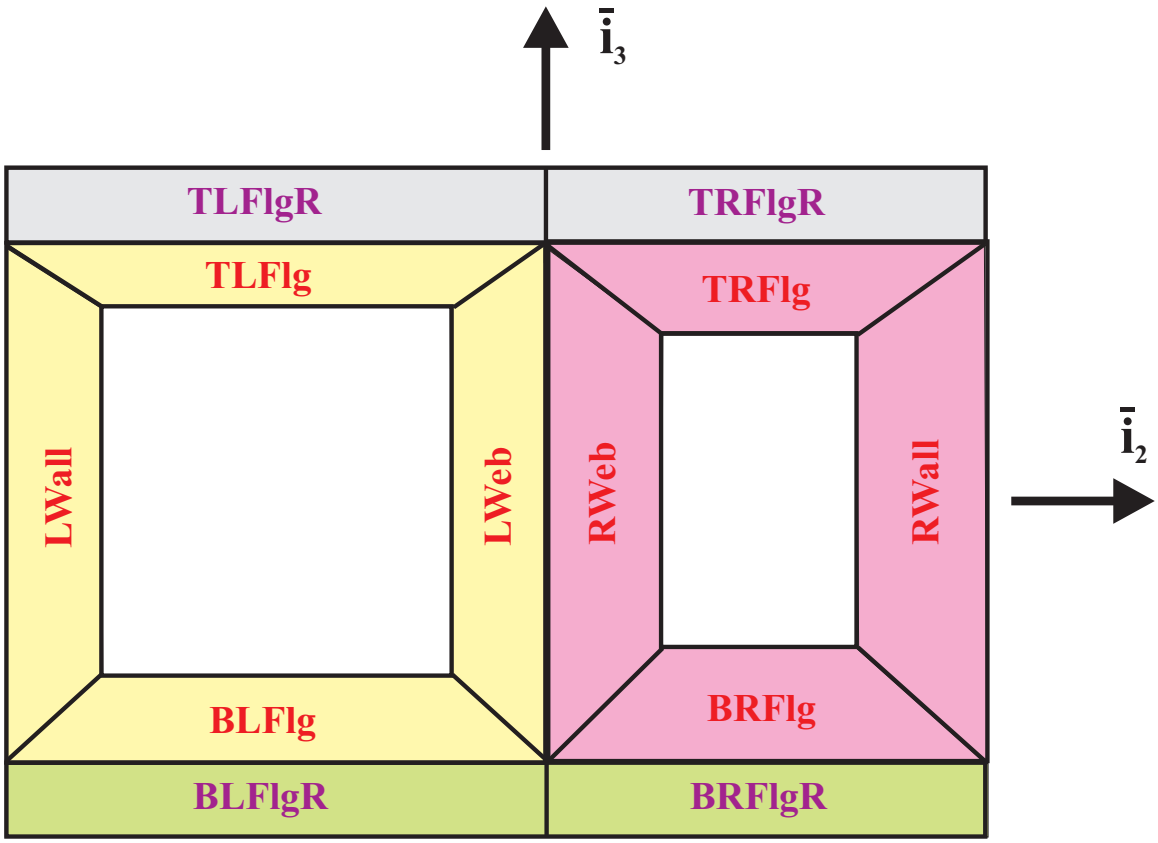

Figure 34: The four zones of the double box

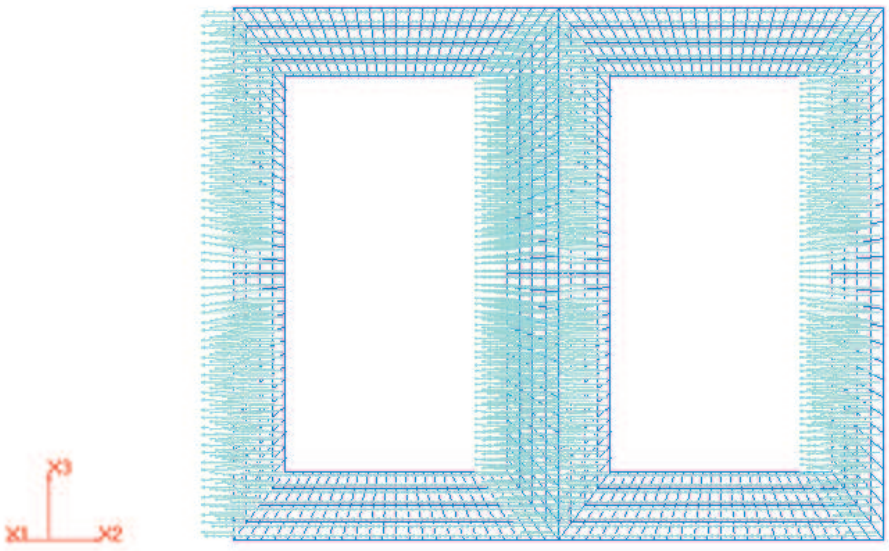

Figure 35: Example 1. Double box

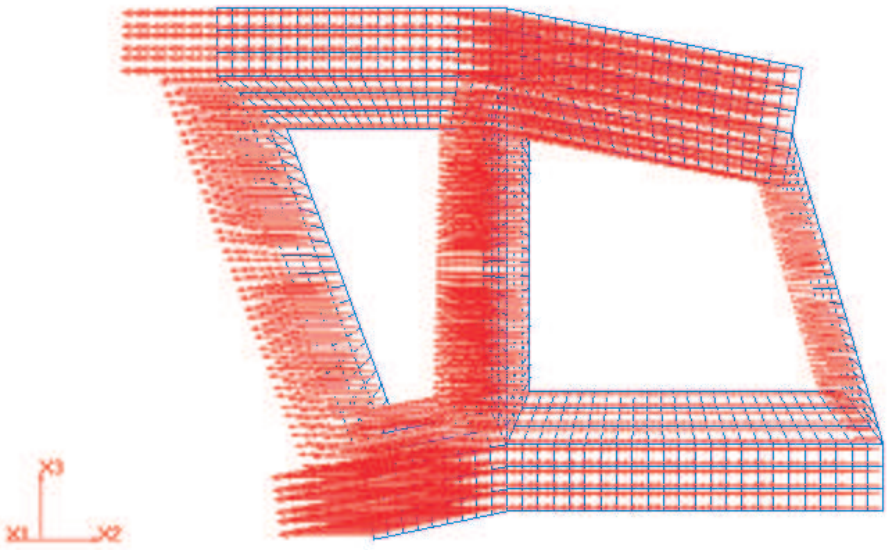

Figure 36: Example 2. Double box

3.2.6 Definition of I-sections

I-sections are parametric configurations of the shape depicted in fig. 37. They consist of an I-section, possibly reinforced by top and/or bottom flanges. The section consists of up to four zones to which independent material properties can be assigned. Note that through the use of fixed frames, the I-section can be made to look like the following shapes: H-sections.

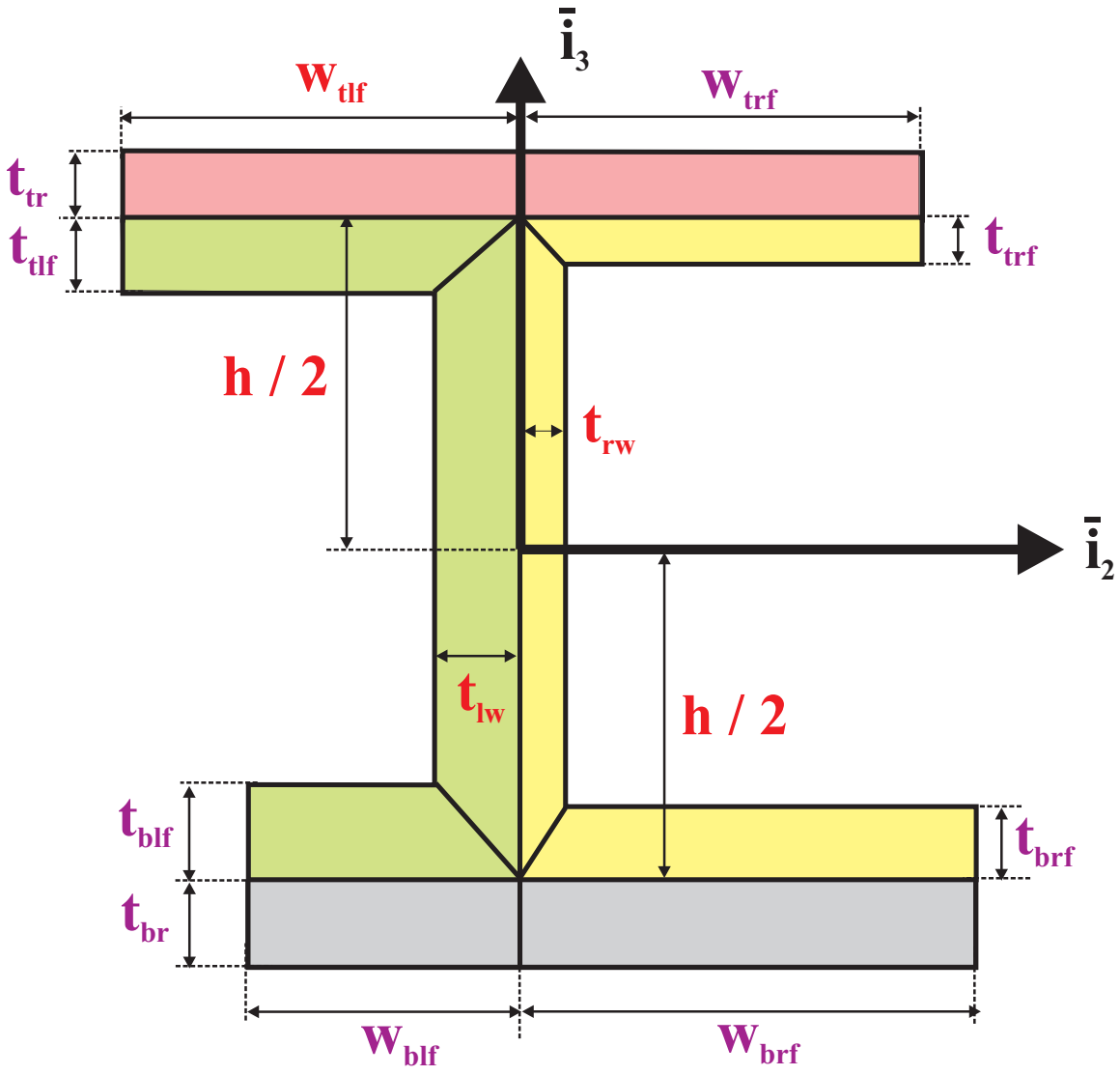

Figure 37: Configuration of the I-section

The dimensions of the I-section, shown in fig. 37, are defined by the following

parameters.

3.2.6.1 Web dimensions

1. The height, h, of the section.
2. The thickness, t_{lw}, of the left part of the web.
3. The thickness, t_{rw}, of the right part of the web.

3.2.6.2 Top left flange dimensions

1. The width, w_{tlf}, of the top left flange.
2. The thickness, t_{tlf}, of the top left flange (*default value:* $t_{\mathrm{tlf}} = t_{\mathrm{lw}}$).
3. The skew angle, α_{tlf}, of the top left flange, positive up, measured in degrees (*default value:* $\alpha_{\mathrm{tlf}} = 0$).
4. The thickness, t_{tr}, of the top reinforcement flange; this thickness applies to both left and right reinforcements that cannot exist independently of each other (*default value:* $t_{\mathrm{tr}} = 0$). This variable is also used as a flag for the presence of the top flange reinforcement: if $t_{\mathrm{tr}} > 0$, this reinforcement is present.

3.2.6.3 Top right flange dimensions

1. The width, w_{trf}, of the top right flange (*default value:* $w_{\mathrm{trf}} = w_{\mathrm{tlf}}$).
2. The thickness, t_{trf}, of the top right flange (*default value:* $t_{\mathrm{trf}} = t_{\mathrm{rw}}$).
3. The skew angle, α_{trf}, of the top right flange, positive up, measured in degrees (*default value:* $\alpha_{\mathrm{trf}} = 0$).

3.2.6.4 Bottom left flange dimensions

1. The width, w_{blf}, of the bottom left flange (*default value:* $w_{\mathrm{blf}} = w_{\mathrm{tlf}}$).
2. The thickness, t_{blf}, of the bottom left flange (*default value:* $t_{\mathrm{blf}} = t_{\mathrm{tlf}}$).

3. The skew angle, α_{blf}, of the bottom left flange, positive down, measured in degrees (*default value:* $\alpha_{\text{blf}} = 0$).

4. The thickness, t_{br}, of the bottom reinforcement flange; this thickness applied to both left and right reinforcements that cannot exist independently of each other (*default value:* $t_{\text{br}} = 0$). This variable is also used as a flag for the presence of the bottom flange reinforcement: if $t_{\text{br}} > 0$, this reinforcement is present.

3.2.6.5 Bottom right flange dimensions

1. The width, w_{brf}, of the bottom right flange (*default value:* $w_{\text{brf}} = w_{\text{trf}}$).

2. The thickness, t_{brf}, of the bottom right flange (*default value:* $t_{\text{brf}} = t_{\text{trf}}$).

3. The skew angle, α_{brf}, of the bottom right flange, positive down, measured in degrees (*default value:* $\alpha_{\text{brf}} = 0$).

As shown in fig. 38, the section is divided into four zones.

1. The top reinforcement flange consists of components labeled *TLFlgR* and *TRFlgR*

2. The left portion of the I-section itself consists of components labeled **TLFlg**, **LWeb**, and **BLFlg**.

3. The right portion of the I-section itself consists of components labeled **TRFlg**, **RWeb**, and **BRFlg**.

4. The top reinforcement flange consists of components labeled *BLFlgR* and *BRFlgR*.

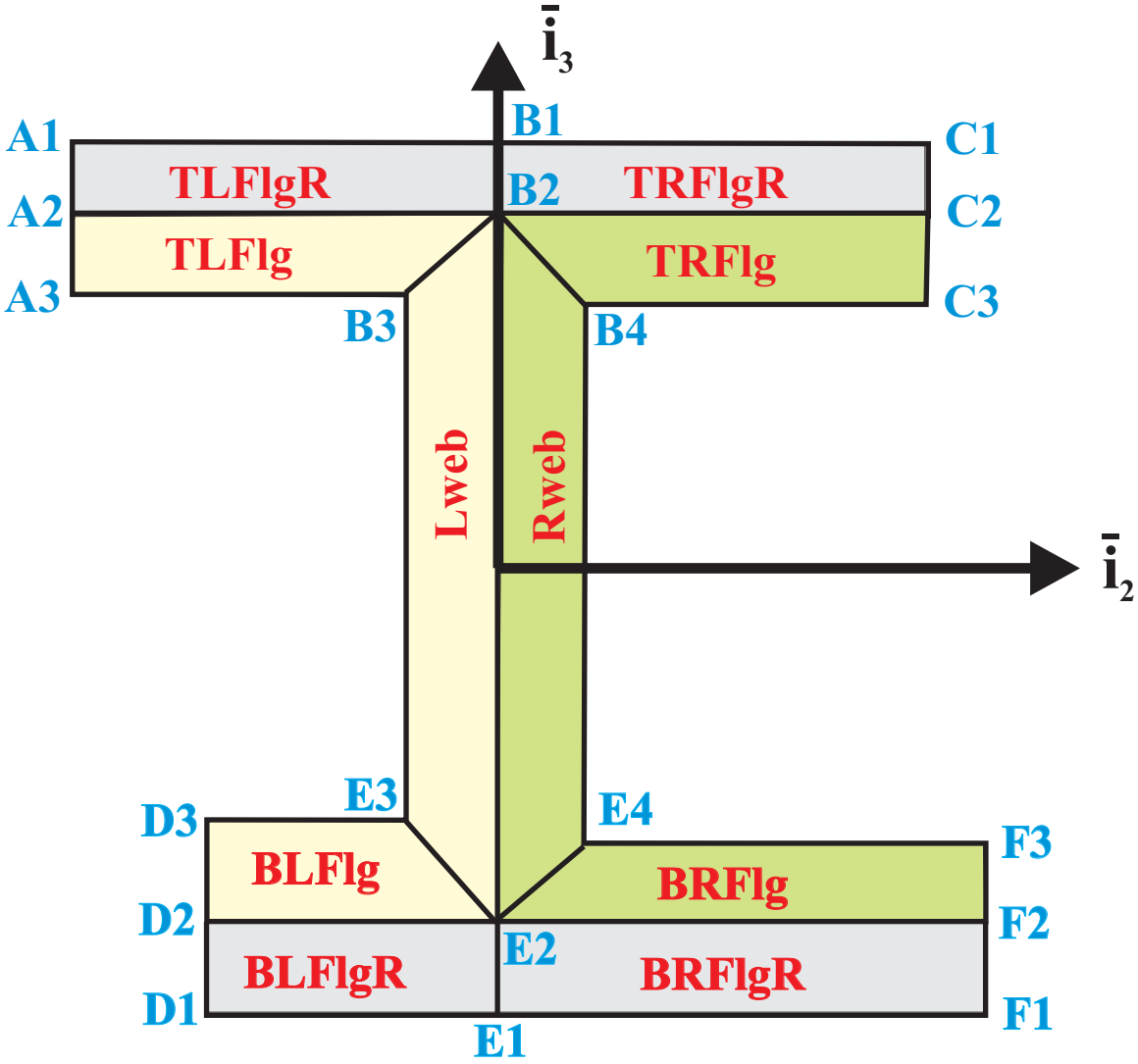

Figure 38: The four zones of the I-section

3.2.6.6 Special Cases

1. If the widths, $w_{\text{trf}} = 0$ and $w_{\text{blf}} = 0$, the section looks like Z-shape depicted in fig. 39. This Z-section does not have TRFlgR, TRFlg, BLFlgR, and BLFlg solids, shown in fig. 40. Here the coordinates of the points are also adjusted from the I-section.

2. If the widths, $w_{\text{blf}} = 0$ and $w_{\text{brf}} = 0$, the section looks like T-shape depicted in fig. 41. This T-section does not have BLFlgR, BLFlg, BRFlgR, and BRFlg

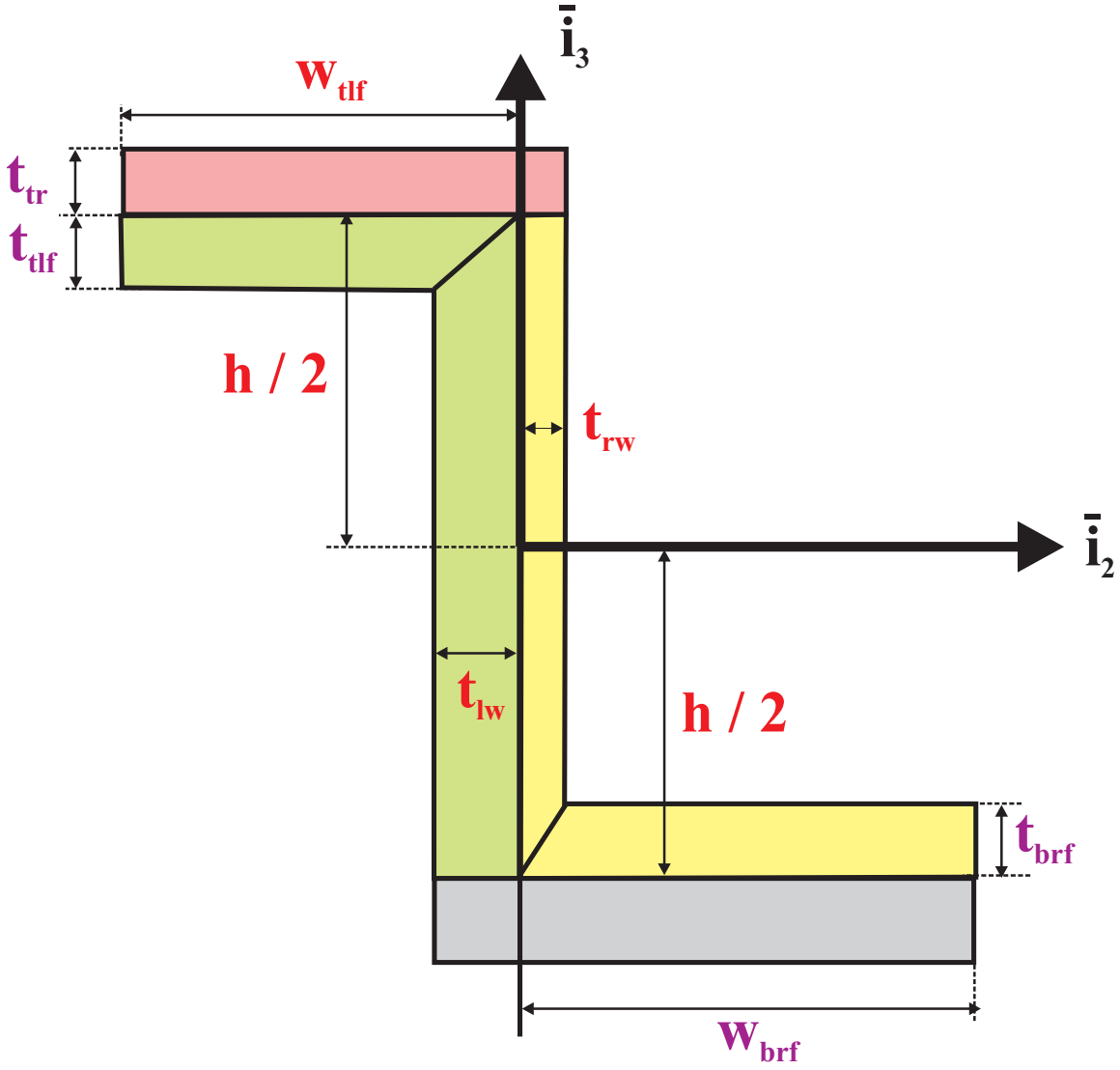

Figure 39: Configuration of the Z-section

solids, shown in fig. 42. Here the coordinates of the points are also adjusted from the I-section.

3.2.6.7 Examples

A few examples that describe the construction procedure of this type of section are shown below.

Example 1

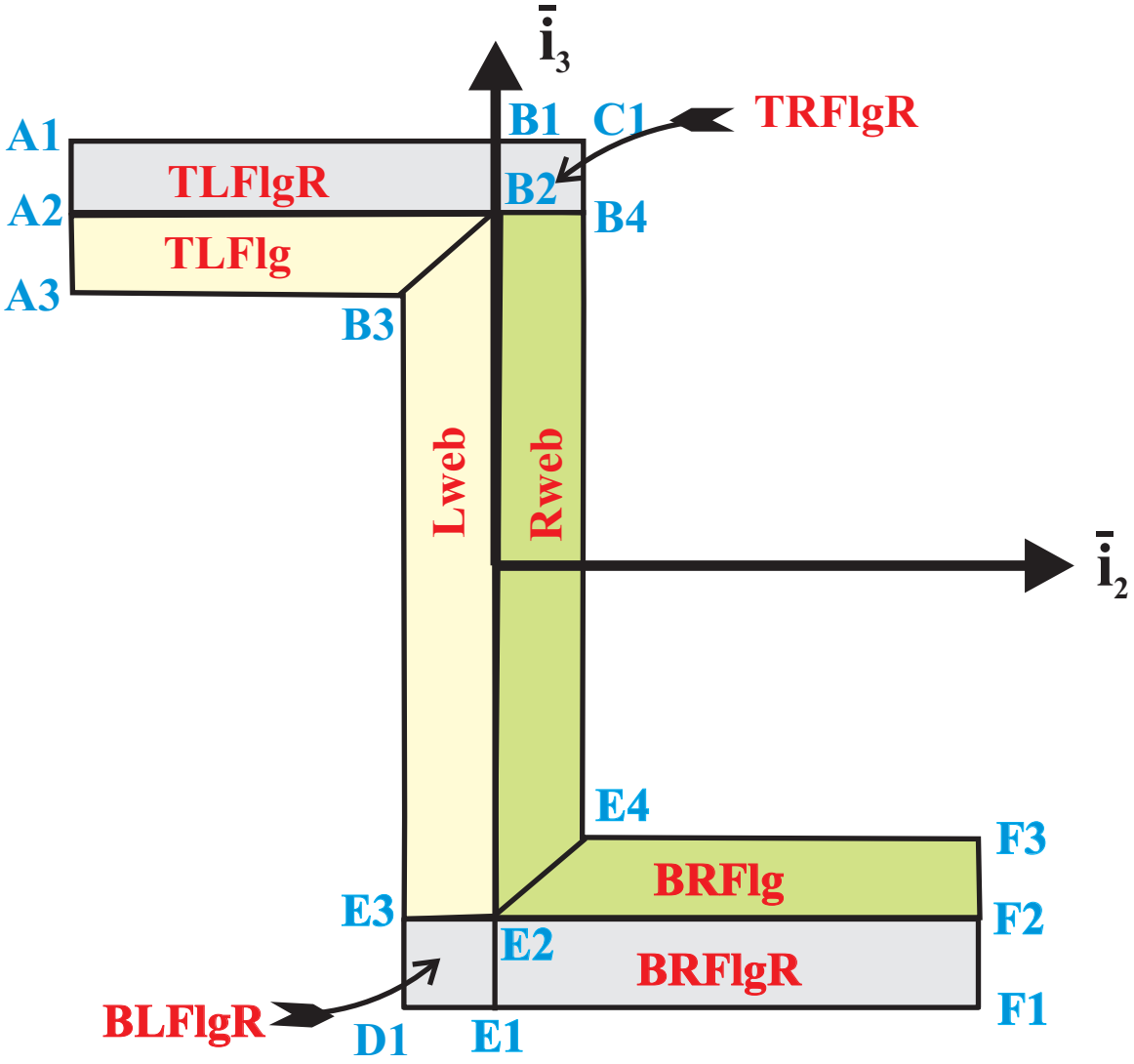

Figure 40: The zones of the Z-section

This example shows an I-section. Here web height, web thicknesses, flange widths, flange thicknesses, web materials, and mesh density are assigned for constructing this section. This example also shows the shear stress field over the cross-section under the applied sectional loads.

Example 2

This example shows an I-section with top and bottom reinforcements. Here web height, web thicknesses, flange widths, flange reinforcement thicknesses, materials, and mesh density are assigned for constructing this section. This example also shows

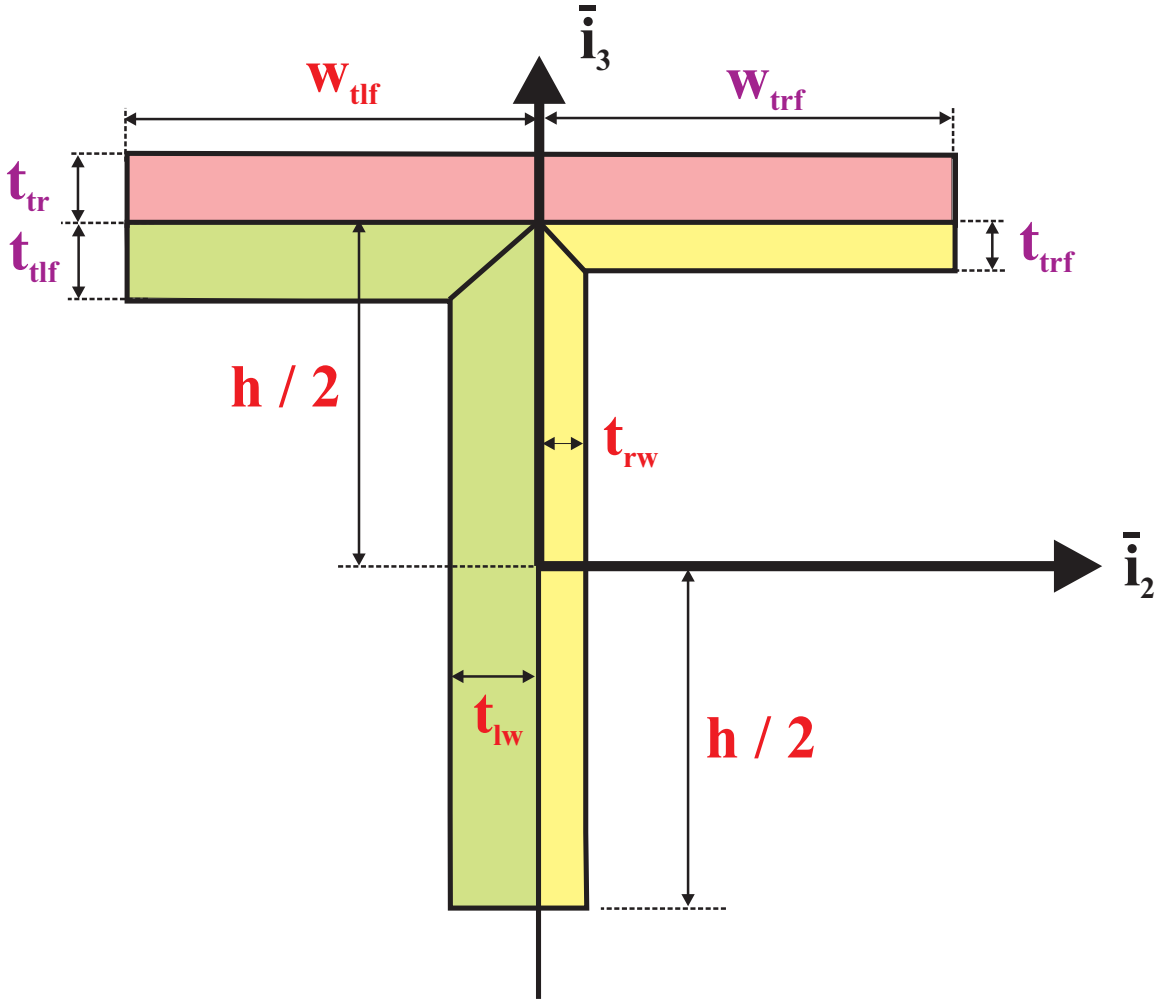

Figure 41: Configuration of the T-section

the axial strain field over the cross-section under the applied sectional loads.

Example 3

This example also shows a Z-section without any reinforcement. Here web height, web thicknesses, flange widths (here $w_{\text{trf}} = 0$ and $w_{\text{blf}} = 0$), materials and mesh density are assigned for constructing this section. This example also shows principal centroidal axes of bending.

Example 4

This example shows a Z-section with top and bottom reinforcements. Here web

height, web thicknesses, flange widths (here $w_{\mathrm{trf}} = 0$ and $w_{\mathrm{blf}} = 0$), flange reinforcement thicknesses, materials, and mesh density are assigned for constructing this section. This example also shows the axial stress field over the cross-section under the applied sectional loads.

Example 5

This example shows a T-section with top reinforcement. Here web height, web thicknesses, flange widths (here $w_{\mathrm{blf}} = 0$ and $w_{\mathrm{brf}} = 0$), flange reinforcement thicknesses, materials, and mesh density are assigned for constructing this section. This example also shows the principal axes of inertia at the mass center.

3.2.7 Definition of rectangular boxes

Rectangular boxes are parametric configurations of the shape depicted in fig. 48. They consist of a rectangular box, possibly reinforced by top and/or bottom flanges. The section consists of up to three three zones to which independent material properties can be assigned.

The dimensions of the rectangular box, as depicted in fig. 48, are defined by the following parameters.

3.2.7.1 Web dimensions

1. The height, h, of the section.
2. The thickness, t_{lw}, of the left web.
3. The thickness, t_{rw}, of the right web.

3.2.7.2 Top left flange dimensions

1. The width, w_{tlf}, of the top left flange.
2. The thickness, t_{tf}, of the top flange (*default value:* $t_{\mathrm{tf}} = t_{\mathrm{lw}}$).

3. The skew angle, α_{tlf}, of the top left flange, positive up, measured in degrees (*default value:* $\alpha_{\text{tlf}} = 0$).

4. The thickness, t_{tr}, of the top reinforcement flange; this thickness applies to both left and right reinforcements that cannot exist independently of each other (*default value:* $t_{\text{tr}} = 0$). This variable is also used as a flag for the presence of the top reinforcement flange: if $t_{\text{tr}} \neq 0$, the top reinforcement flange is present.

3.2.7.3 Top right flange dimensions

1. The width, w_{trf}, of the top right flange (*default value:* $w_{\text{trf}} = w_{\text{tlf}}$).

2. The thickness of the top right flange equals that of the top left flange.

3. The skew angle, α_{trf}, of the top right flange, positive up, measured in degrees (*default value:* $\alpha_{\text{trf}} = 0$).

3.2.7.4 Bottom left flange dimensions

1. The width, w_{blf}, of the bottom left flange (*default value:* $w_{\text{blf}} = w_{\text{tlf}}$).

2. The thickness, t_{bf}, of the bottom left flange (*default value:* $t_{\text{bf}} = t_{\text{tf}}$).

3. The skew angle, α_{blf}, of the bottom left flange, positive down, measured in degrees (*default value:* $\alpha_{\text{blf}} = 0$).

4. The thickness, t_{br}, of the bottom reinforcement flange; this thickness applied to both left and right reinforcements that cannot exist independently of each other (*default value:* $t_{\text{br}} = 0$). This variable is also used as a flag for the presence of the bottom reinforcement flange: if $t_{\text{br}} \neq 0$, the bottom reinforcement flange is present.

3.2.7.5 Bottom right flange dimensions

1. The width, w_{brf}, of the bottom right flange (*default value:* $w_{\text{brf}} = w_{\text{blf}}$).

2. The thickness of the bottom right flange equals that of the bottom left flange.

3. The skew angle, α_{brf}, of the bottom right flange, positive down, measured in degrees (*default value:* $\alpha_{\text{brf}} = 0$).

As shown in fig. 49, the section is divided into three zones.

1. The top reinforcement flange consists of the components labeled *TLFlgR* and *TRFlgR*.

2. The rectangular box consists of the components labeled **TLFlg**, **TRFlg**, **LWeb**, **RWeb**, **BLFlg**, and **BRFlg**.

3. The bottom reinforcement flange consists of the components labeled *BLFlgR* and *BRFlgR*.

3.2.7.6 Examples

A few examples that describe the construction procedure of this type of section are shown below.

Example 1

This example shows a rectangular box with skewed flanges. Here height, web thicknesses, flange widths, flange skew angles, materials, and mesh density are assigned for constructing this section.This example also shows the principal centroidal axes of bending.

Example 2

This example shows a rectangular box with top and bottom flange reinforcements. Here height, web thicknesses, flange widths, flange thickness, bottom left flange skew angle, materials, and mesh density are assigned for constructing this section. This example also shows the axial stress field over the cross-section under the applied sectional loads.

3.2.8 Definition of rectangular sections

Rectangular sections are parametric configurations of the shape depicted in fig. 52. They consist of a rectangular section, possibly reinforced by top and/or bottom flanges. The section consists of up to three three zones to which independent material properties can be assigned.

The dimensions of the rectangular section, shown in fig. 52, are defined by the following parameters.

1. The width, w, of the section.

2. The height, h, of the section.

   The thickness, t_{tr}, of the top reinforcement flange; this thickness applies to both left and right reinforcements that cannot exist independently of each other (*default value:* $t_{\mathrm{tr}} = 0$).

3. The thickness, t_{tr}, of the top reinforcement flange (*default value:* $t_{\mathrm{tr}} = 0$). This variable is also used as a flag for the presence of the top reinforcement flange: if $t_{\mathrm{tr}} \neq 0$, the top reinforcement flange is present.

4. The thickness, t_{br}, of the bottom reinforcement flange (*default value:* $t_{\mathrm{br}} = 0$). This variable is also used as a flag for the presence of the bottom reinforcement flange: if $t_{\mathrm{br}} \neq 0$, the bottom reinforcement flange is present.

As shown in fig. 53, the section is divided into three zones.

1. The top reinforcement flange consists of a single component labeled *TFlgR*.

2. The central portion of the section consists of a single component labeled **Core**.

3. The bottom reinforcement flange consists of a single component labeled *BFlgR*.

3.2.8.1 Examples

A few examples that describe the construction procedure of this type of section are shown below.

Example 1

This example shows a rectangular section. Here width, height, frame, core material, and mesh density are assigned for constructing this section. This example also shows the inverse of the reserve factor field over the cross- section under the applied sectional loads.

Example 2

This example shows also a rectangular section. Here width, height, frame, reinforcement thicknesses, composite core materials, and mesh density are assigned for constructing this section. This example also shows the shear stress field over the cross-section under the applied sectional loads.

3.2.9 Definition of circular tubes

Circular tubes are predefined sections presenting the shape, shown in fig. 56. Circular tubes consist of an area included between two circles. The section consists of a single zone to which material properties can be assigned. The circular tube is a **closed circular tube**, as shown in fig. 56. **Open circular tubes** can be defined with the help of the circular arc predefined section as described in section 3.2.2.

The dimensions of the circular tube, shown in fig. 56, are defined by two parameters.

1. The outer radius, R_O, of the circular tube.

2. The inner radius, R_I, of the circular tube.

3.2.9.1 Examples

A few examples that describe the construction procedure of this type of sections are show below.

Example 1

This example shows a circular tube section. Here inner and outer radii, frame, material, and mesh density are assigned for constructing this section. This example also shows the warping displacement of the cross-section under the applied sectional loads.

Example 2

This example shows also a circular tube section. Here inner and outer radii, frame, materials property, and mesh density are assigned for constructing this section. This example also shows the principal axes of inertia at the mass center.

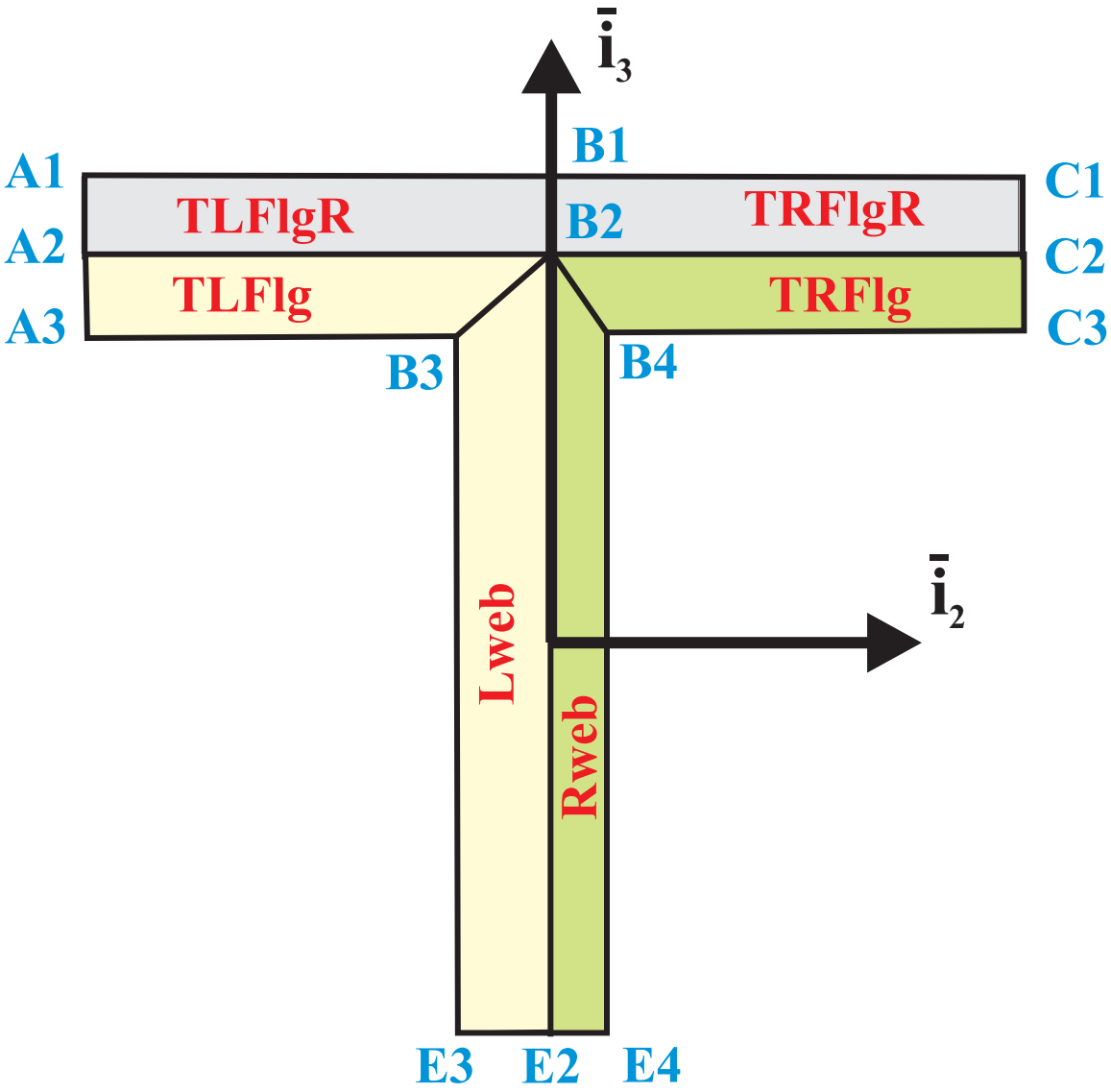

Figure 42: The zones of the T-section

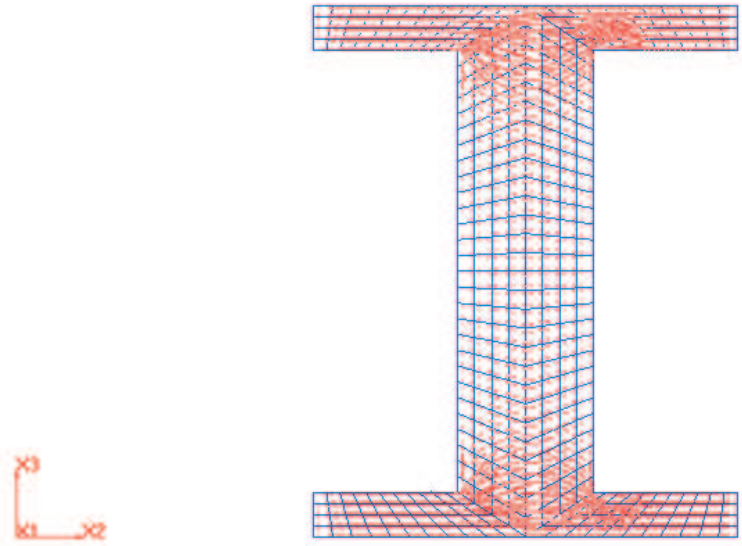

Figure 43: Example 1. I-section

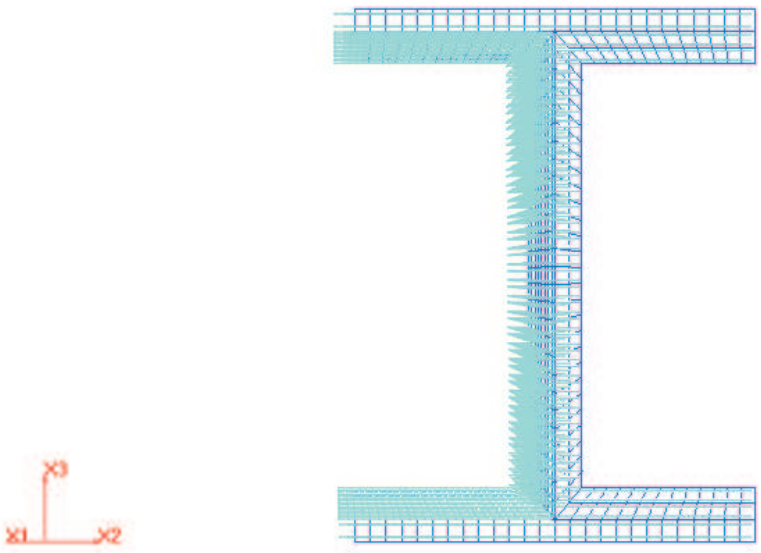

Figure 44: Example 2. I-section

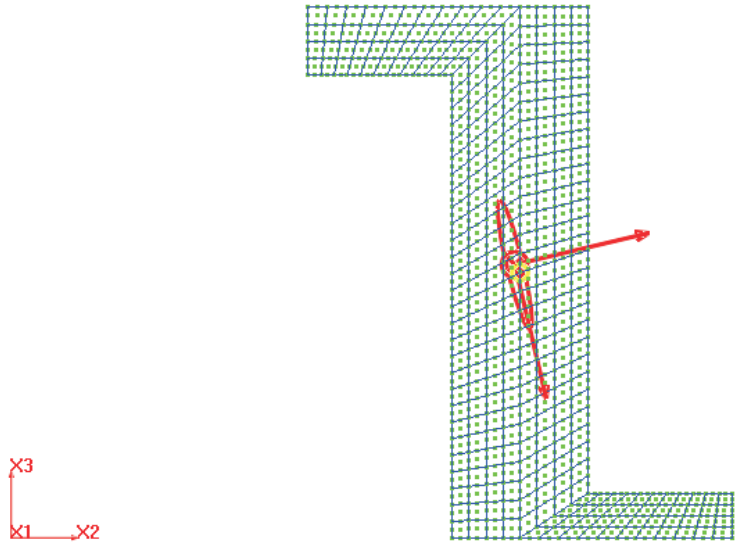

Figure 45: Example 3. Z-section

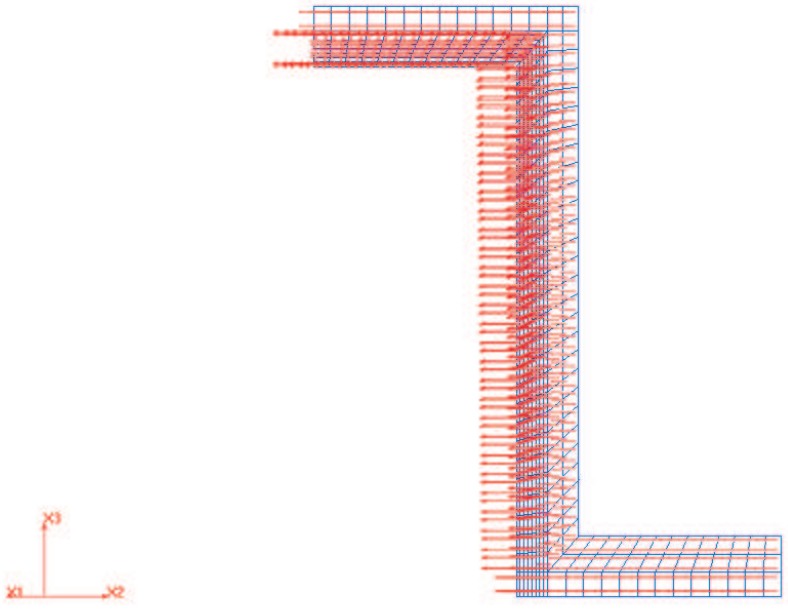

Figure 46: Example 4. Z-section

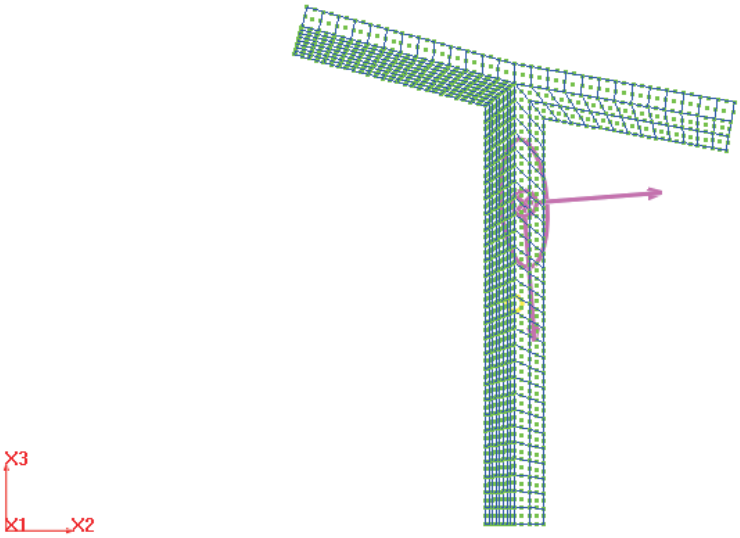

Figure 47: Example 5. T-section

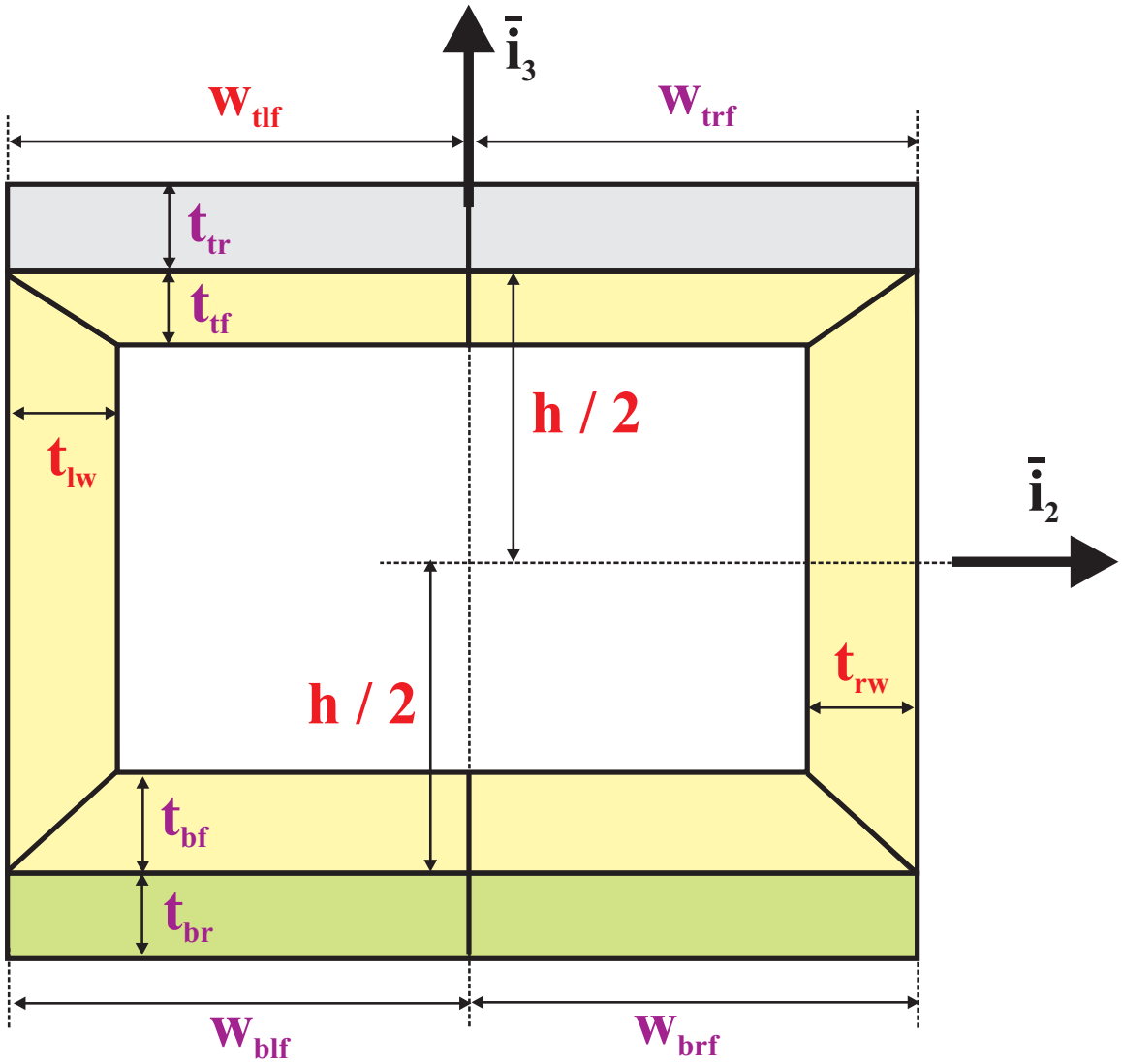

Figure 48: Configuration of the rectangular box. The dimensions of the various elements of the section are indicated on the figure. The three shaded areas correspond to the three zones of the section

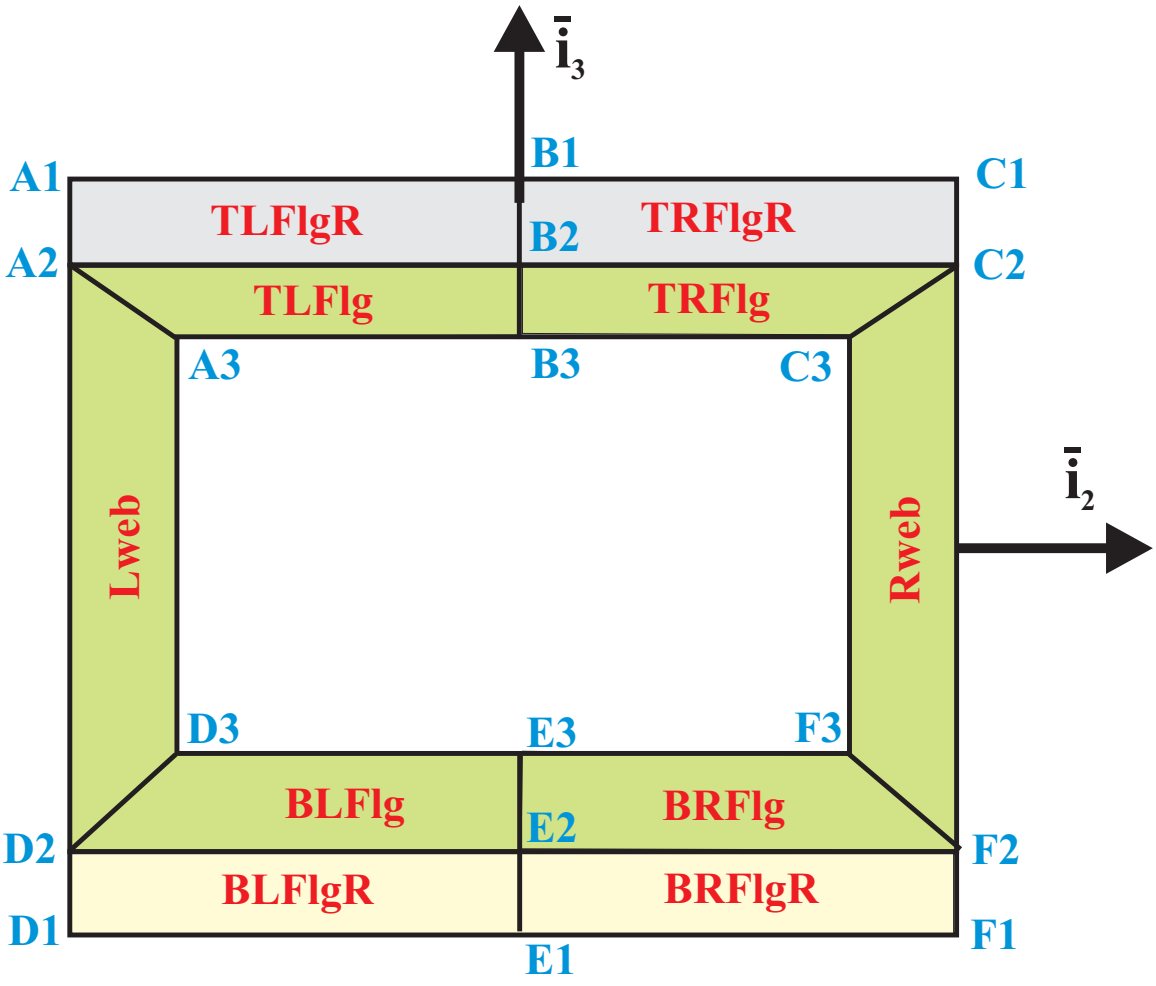

Figure 49: The three zones of the rectangular box

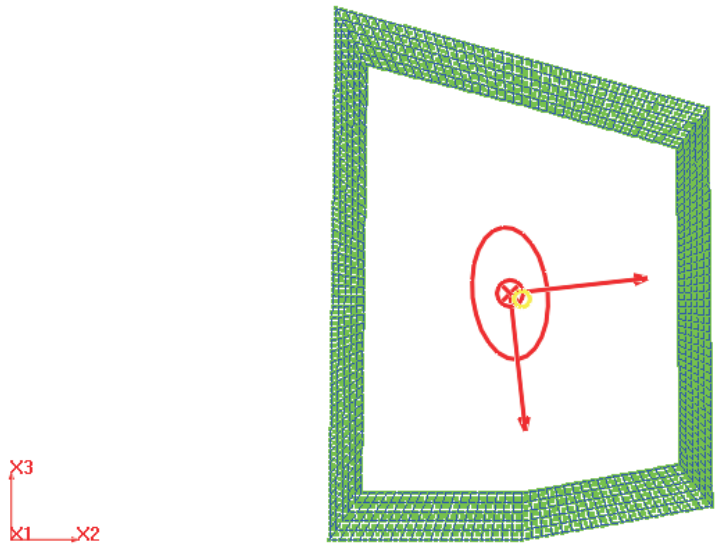

Figure 50: Example 1. Rectangular box

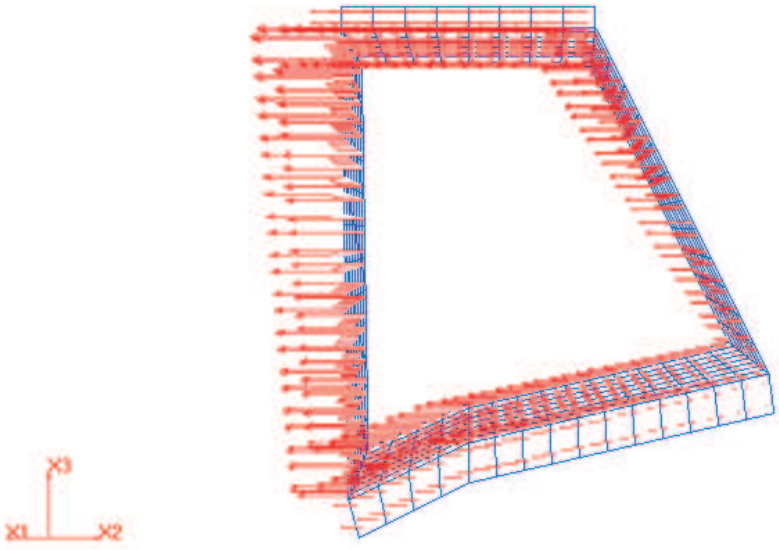

Figure 51: Example 2. Rectangular box

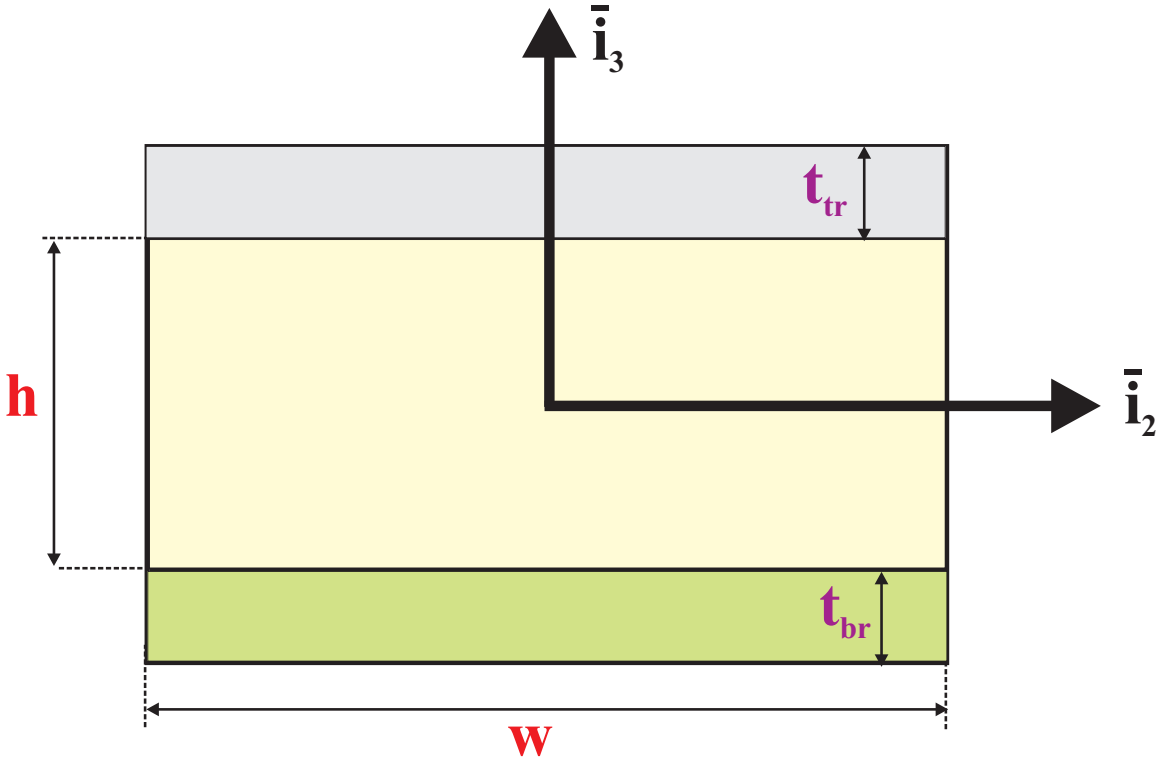

Figure 52: Configuration of the rectangular section

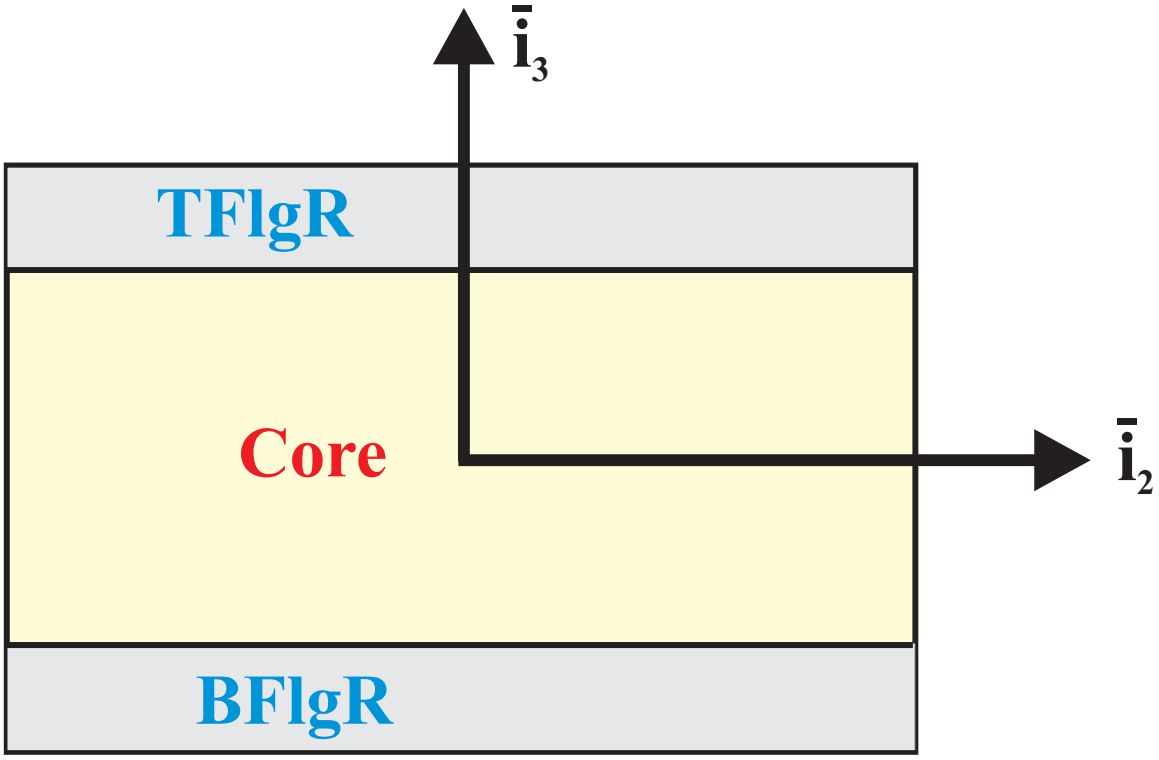

Figure 53: Solid zones of the rectangular section

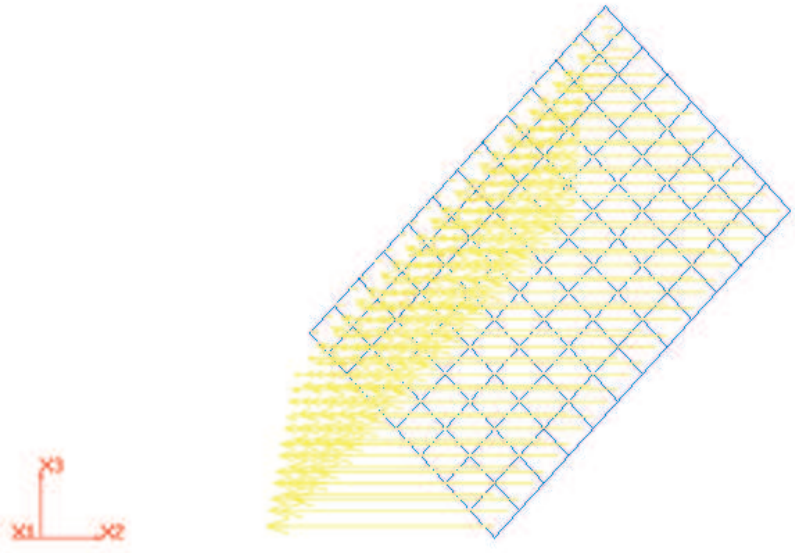

Figure 54: Example 1. Rectangular section

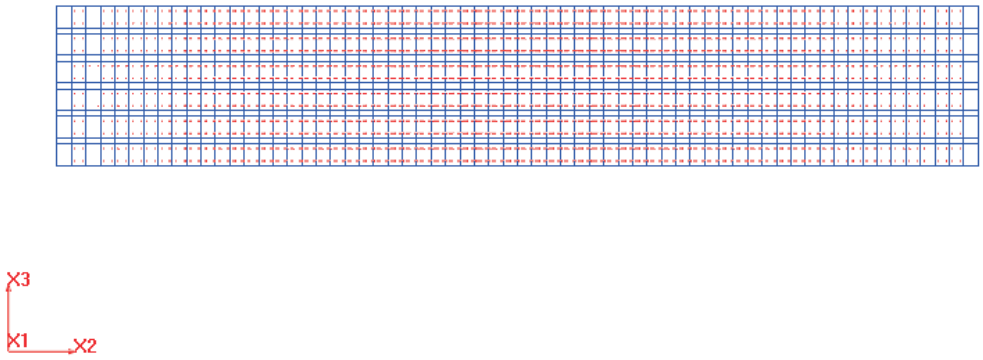

Figure 55: Example 2. Rectangular section

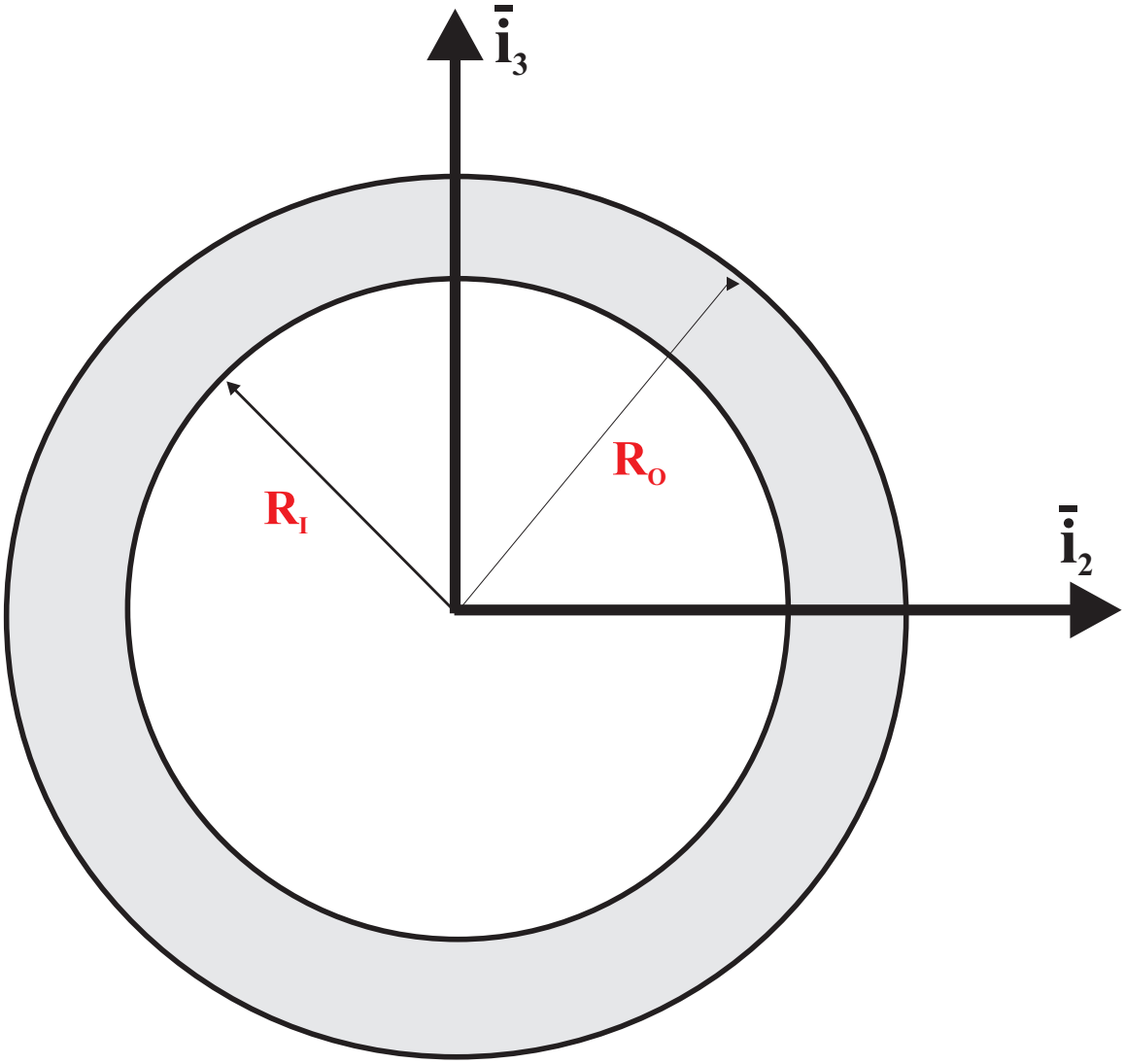

Figure 56: Configuration of the circular tube

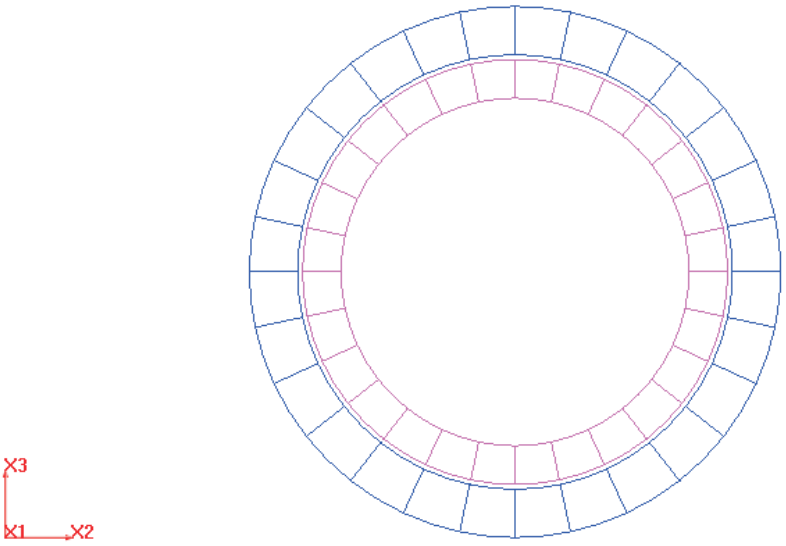

Figure 57: Example 1. Circular tube

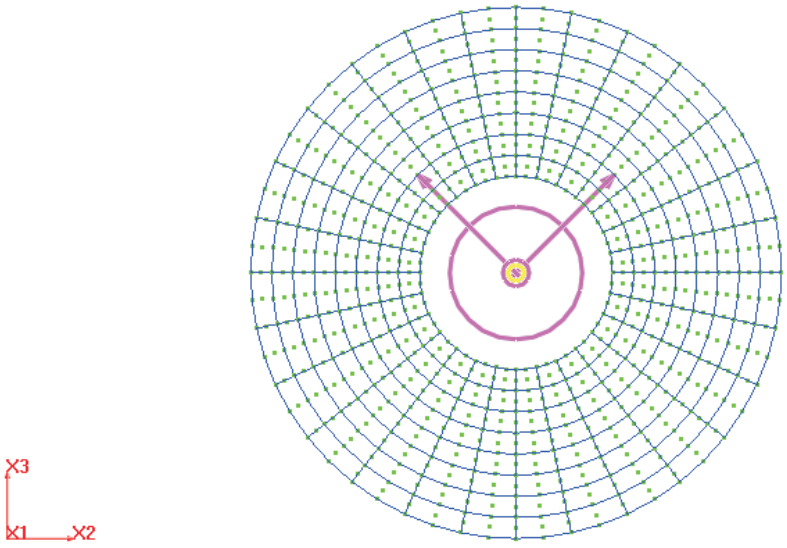

Figure 58: Example 2. Circular tube

3.2.10 Definition of triangular sections

Triangular sections are parametric configurations of the shape depicted in fig. 59. They consist of a triangular section, which can be open or closed. The section consists of a single zone which material properties can be assigned. Note that through the use of fixed frames, the triangular section can be made into the following shapes: $\triangle$, $\triangleleft$, $\triangleright$, or $\triangledown$.

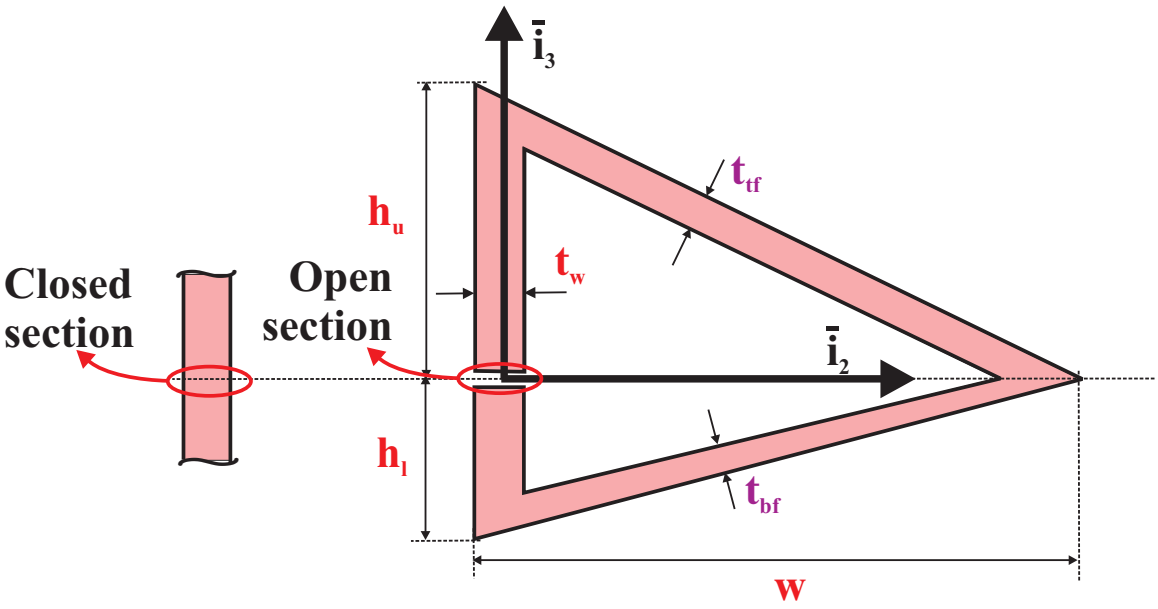

Figure 59: Configuration of the triangular section with open or closed section

The dimensions of the triangular section, shown in fig. 59, are defined by the following parameters.

3.2.10.1 Web dimensions

1. The height, h_{u}, of the top web.

2. The height, h_{b}, of the bottom web.

3. The thickness, t_{w}, of the web.

3.2.10.2 Top flange dimensions

1. The width, w, of the section.

2. The thickness, t_{tf}, of the top flange (*default value:* $t_{\mathrm{tf}} = t_{\mathrm{w}}$).

3.2.10.3 Bottom flange dimensions

1. The width, w, of the section.

2. The thickness, t_{bf}, of the bottom flange (*default value:* $t_{\mathrm{bf}} = t_{\mathrm{w}}$).

As shown in fig. 60, the section features a single zone.

1. The top reinforcement flange consists of the components labeled *TWeb*, *TFlg*, *BFlg*, and *BWeb*.

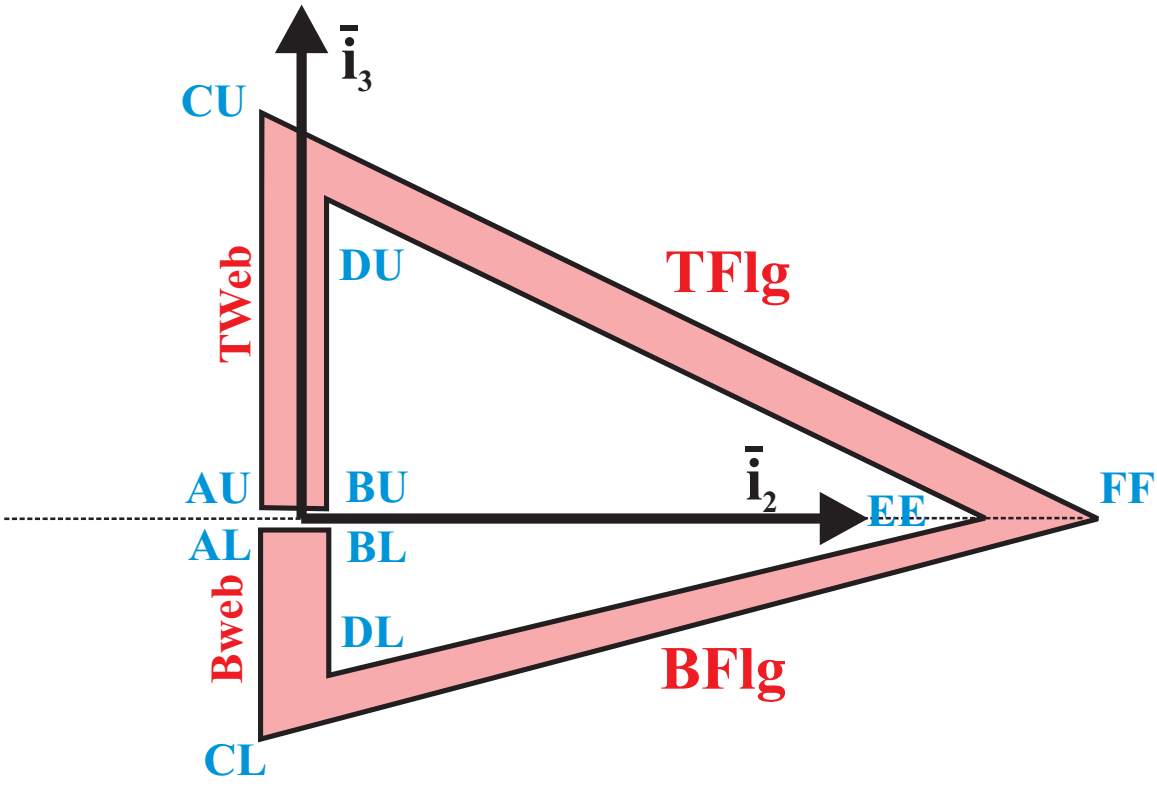

Figure 60: The three zones of the triangular section

3.2.10.4 Examples

A few examples that describe the construction procedure of this type of section are shown below.

Example 1

This example shows an open triangular section. Here top and bottom web heights, width, web thickness, material, frame, and mesh density are assigned for constructing this section. This example also shows the principal axes of shearing at the shear center.

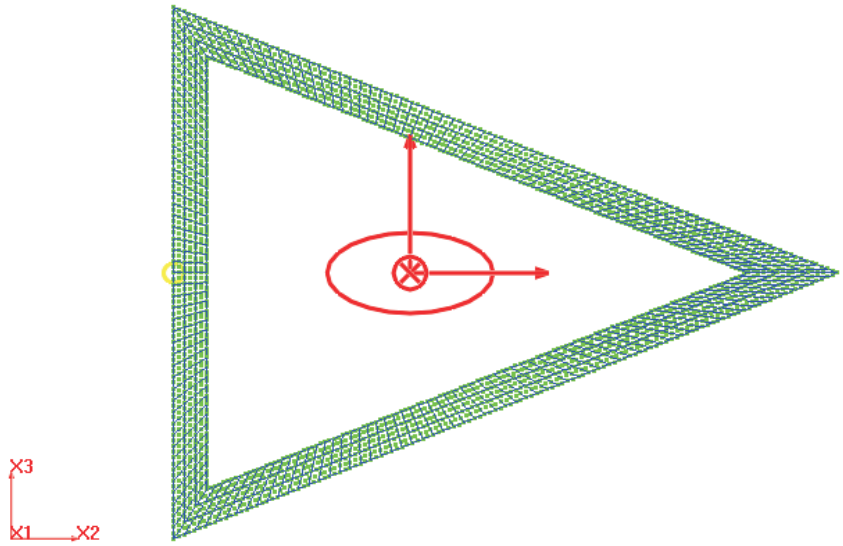

Figure 61: Example 1. Triangular section

3.2.11 Definition of T-sections

T-sections are parametric configurations of the shape depicted in fig. 62. They consist of a T-section, possibly reinforced by a top flange. The section consists of up to three zones to which independent material properties can be assigned. Note that through

the use of fixed frames, the T-section can be made into the following shapes: $\perp$, $\dashv$, $\vdash$, or $\top$.

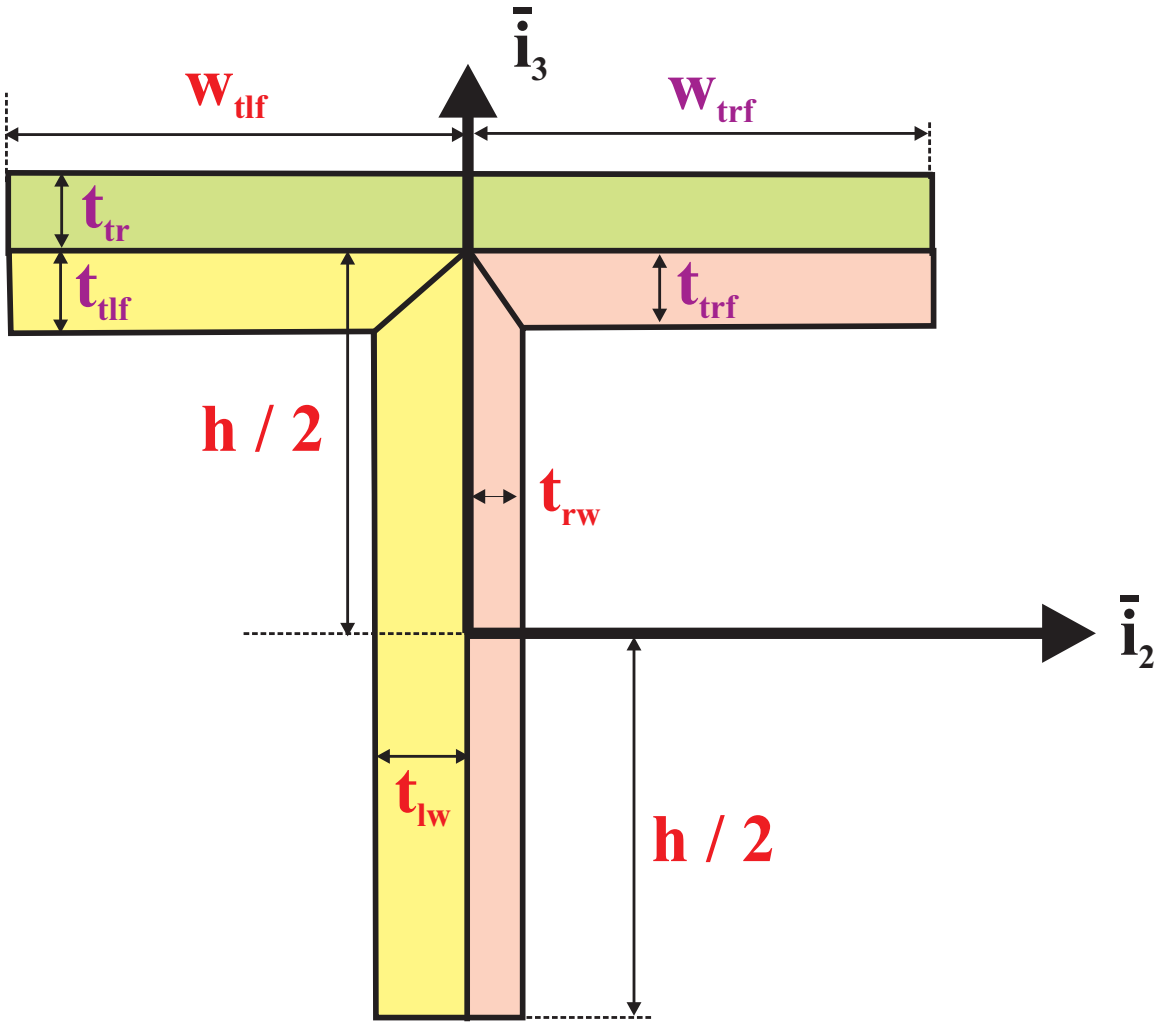

Figure 62: Configuration of the T-section

The dimensions of the T-section, shown in fig. 62, are defined by the following parameters.

3.2.11.1 Web dimensions

1. The height, h, of the section.

2. The thickness, t_{lw}, of the left part of the web.

3. The thickness, t_{rw}, of the right part of the web.

3.2.11.2 Top left flange dimensions

1. The width, w_{tlf}, of the top left flange.

2. The thickness, t_{tlf}, of the top left flange (*default value:* $t_{\mathrm{tlf}} = t_{\mathrm{lw}}$).

3. The skew angle, α_{tlf}, of the top left flange, positive up, measured in degrees (*default value:* $\alpha_{\mathrm{tlf}} = 0$).

4. The thickness, t_{tr}, of the top reinforcement flange; this thickness applied to both left and right reinforcements that cannot exist independently of each other (*default value:* $t_{\mathrm{tr}} = 0$). This variable is also used as a flag for the presence of the top flange reinforcement: if $t_{\mathrm{tr}} > 0$, this reinforcement is present.

3.2.11.3 Top right flange dimensions

1. The width, w_{trf}, of the top right flange (*default value:* $w_{\mathrm{trf}} = w_{\mathrm{tlf}}$).

2. The thickness, t_{trf}, of the top right flange (*default value:* $t_{\mathrm{trf}} = t_{\mathrm{rw}}$).

3. The skew angle, α_{trf}, of the top right flange, positive up, measured in degrees (*default value:* $\alpha_{\mathrm{trf}} = 0$).

As shown in fig. 63, the section is divided into three zones.

1. The top reinforcement flange consists of the components labeled *TLFlgR* and *TRFlgR*.

2. The left portion of the T-section consists of the components labeled **TLFlg** and **LWeb**.

3. he left portion of the T-section consists of the components labeled **TRFlg** and **RWeb**.

3.2.11.4 Examples

A few examples that describe the construction procedure of this type of section are shown below.

Example 1

This example shows a T-section with skewed flange and top reinforcement. Here web height, web thicknesses, flange widths, flange thicknesses,flange skew angles, materials, and mesh density are assigned for constructing this section. This example also shows the inverse of the reserve factor field over the cross- section under the applied sectional loads.

Example 2

This example shows a T-section with flange reinforcement. Here web height, web thicknesses, flange widths, flange thicknesses, materials, and mesh density are assigned for constructing this section. This example also shows the axial stress field over the cross-section under the applied sectional loads.

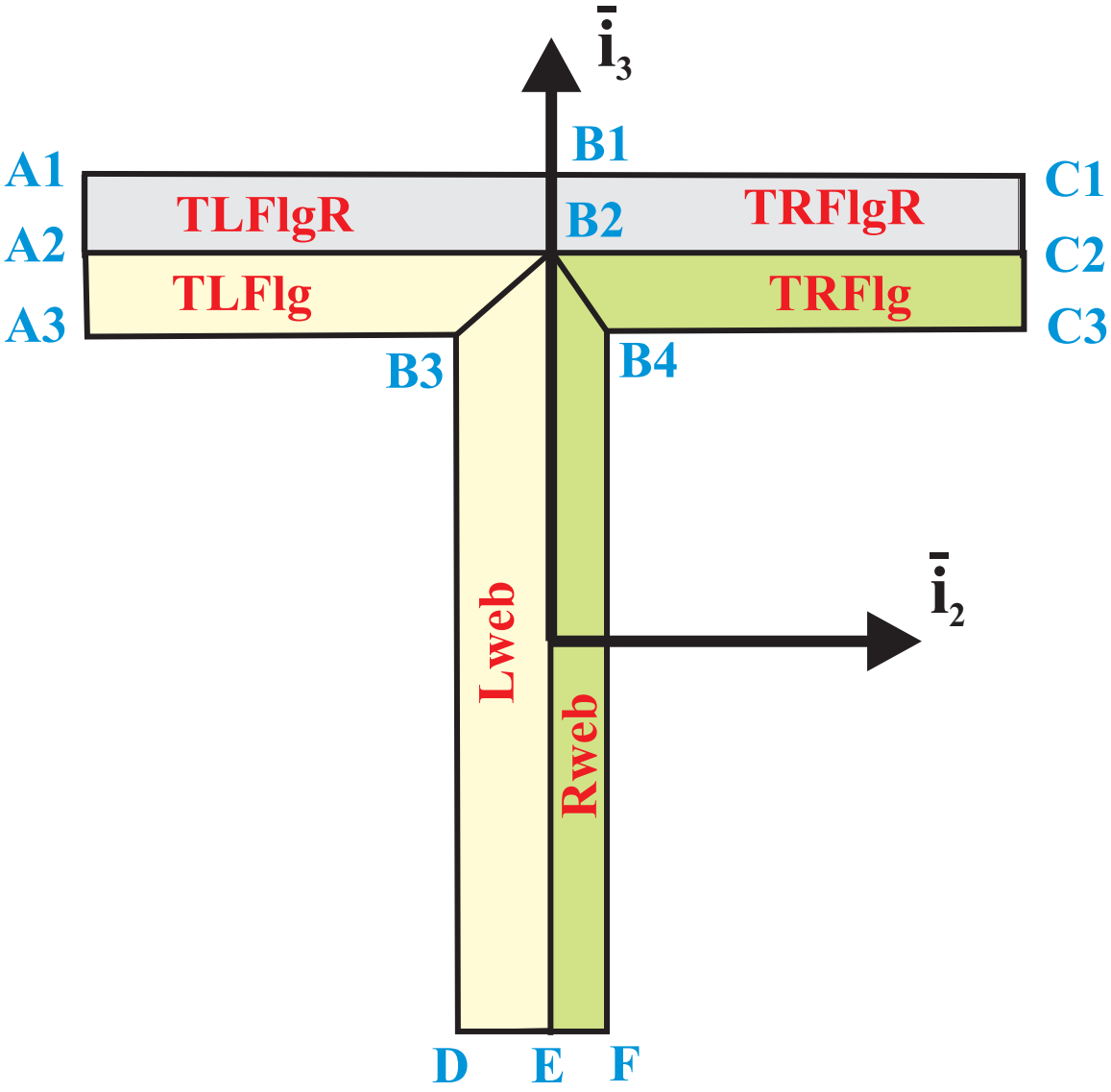

Figure 63: The three zones of the T-section

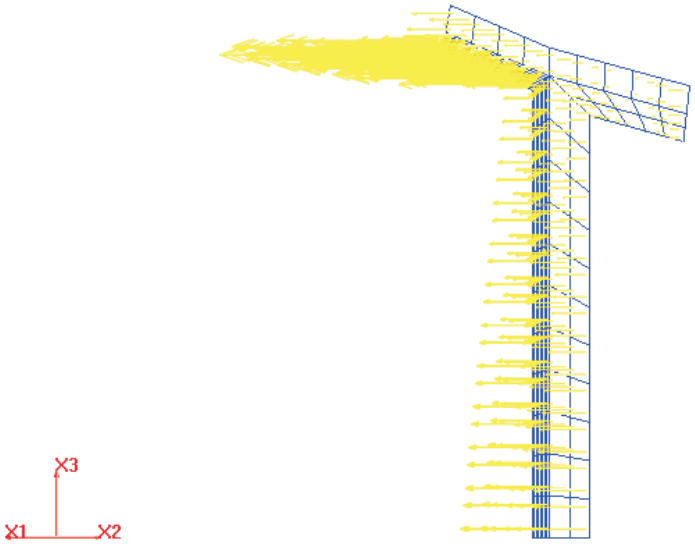

Figure 64: Example 1. T-section

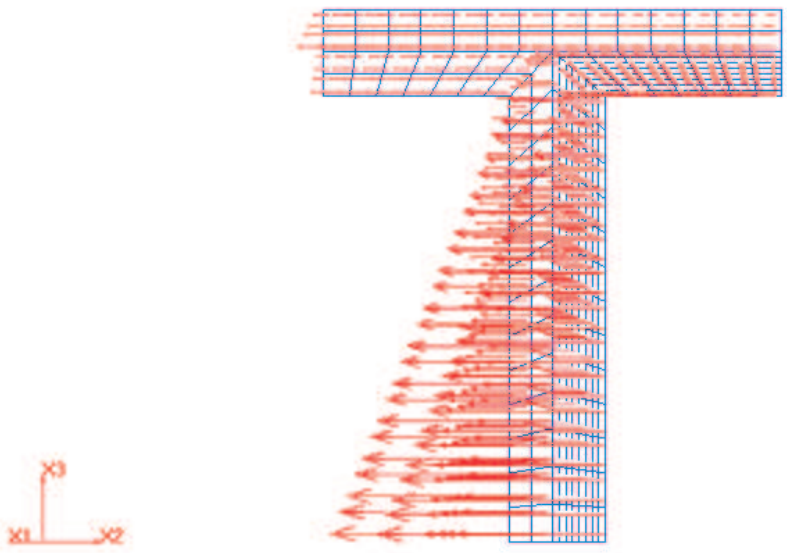

Figure 65: Example 2. T-section

3.3 Builder

A complex section is viewed as a collection of interconnected walls. Various connectors such as Split-connectors, T-connectors, and V-connectors are considered for connecting walls for creating a realistic section. The section may need to integrate core materials inside the cavities to keep the original shape during operation. The definition of walls (section 3.3.1), Split-connectors (section 3.3.2), T-connectors (section 3.3.3), V-connectors (section 3.3.4), and Core (section 3.3.5) are discussed below.

3.3.1 Definition of walls

As discussed in the introduction of chapter 3, a general beam section is defined as an assembly of interconnected walls, see fig. 6.

3.3.1.1 Wall geometry

The geometry of a wall is is defined by an oriented planar curve, as shown in fig. 66, defined in terms of its NURBS representation [42, 81]. Each point on the curve is associated with a variable η; the curve is defined between points **A**, and **B**, corresponding to $\eta = 0$, and $\eta = 1$, respectively. Along the curve, the unit tangent, and normal vectors, denoted $\bar{t}$, and $\bar{n}$, respectively, are defined such that $\bar{t}$ points in the direction of increasing values of η, and unit vectors $(\bar{t}, \bar{n})$ correspond to a planar rotation of unit vector $(\bar{\imath}_2, \bar{\imath}_3)$. It now becomes possible to define the upper, and lower portion of the wall: the upper portion of the wall is located *above the curve*, *i.e.* in the direction of $\bar{n}$, whereas the lower portion of the wall is located *below the curve*.

3.3.1.2 Wall stacking sequence

The upper, and lower walls consist of a number of layers stacked on top, and below the curve, respectively. Fig. 66 shows an upper wall consisting of three layers denoted `Layer1`, `Layer2`, and `Layer3`, whereas the lower wall consists of layers `Layer4`, `Layer5`, and `Layer6`. Each layer has a specific thickness; for instance, layers `Layer2`,

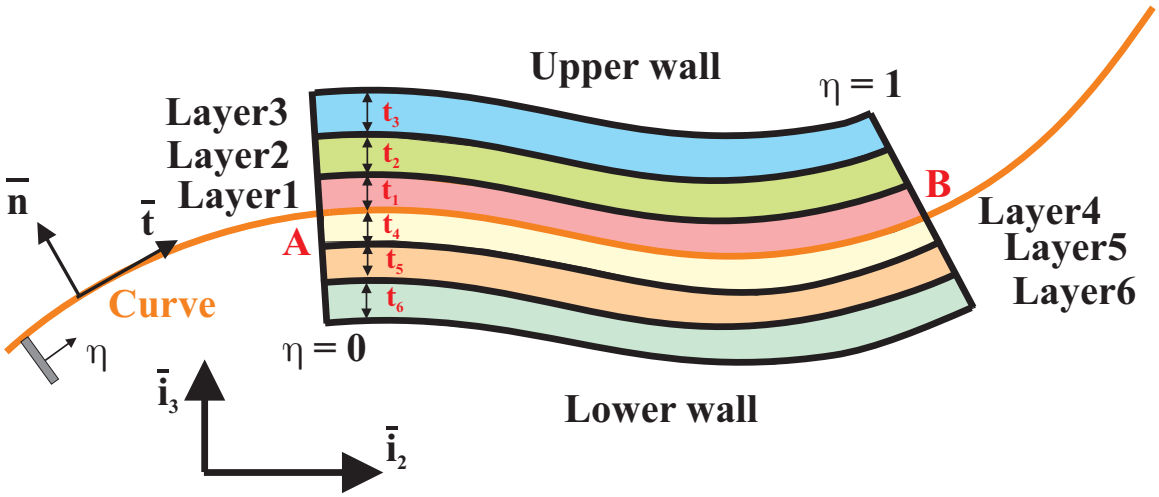

Figure 66: General configuration of a wall

and `Layer3` are of thickness t_2, and t_3, respectively.

Layers do not necessarily span the entire length of the curve defining the geometry of the wall. In general, each layer starts at a given location, η_i, along the curve, and ends at a location, η_f. The left portion of fig. 67 shows a typical configuration for a stacking sequence: layers `Layer1`, `Layer2`, and `Layer5` have the same beginning, and end coordinates, $\eta_i = 0$, and $\eta_f = 1$, respectively, whereas `Layer3` features $\eta_i = \eta_2$, and $\eta_f = \eta_3$, and `Layer4` features $\eta_i = \eta_1$, and $\eta_f = \eta_4$. Of course, when layers are dropped or added, the layers at the further distance from the curve defining the geometry of the wall drop onto the remaining layers, as illustrated on the right portion of fig. 67. An add-drop zone length defines the distance over which the layers are allowed to collapse onto a lower position.

Each layer is characterized by the following parameters *(1)* the layer name; *(2)* the layer beginning, and end coordinates, η_i, and η_f, respectively; *(3)* the layer thickness; *(4)* the material the layer is made of.

For transversely-isotropic materials, which are common for fiber reinforced composites, are easier to express materials properties as solid properties.

Walls are allowed for ply-add/drops at any position between U=0 to U=1, as

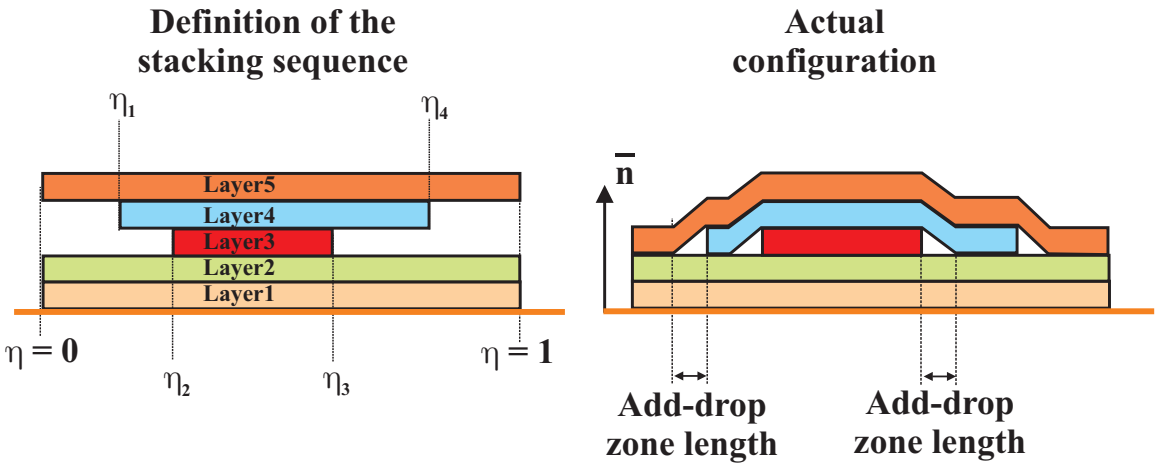

Figure 67: Definition of the stacking sequence and actual configuration of the wall

depicted in fig. 67. This ply-add/drops feature gives the freedom for designing a realistic airfoil section after connecting several walls with various connectors (i.e., T-connector, V-connector, Split-connector etc).

Two walls with arbitrary lay-ups can be connected using "@CONNECTED_AT_0" and "@CONNECTED_AT_1" commands. For connecting the initial position of a wall with the final position of another wall, "@CONNECTED_AT_0" command is used. On the other hand, "@CONNECTED_AT_1" command is considered for connecting the final position of a wall with the initial position of another wall, as depicted in fig. 68. The number of layers for walls must be equal at the connection. The layer thickness and material properties should also be compatible at the connection position of two walls.

3.3.1.3 Examples

A few examples that describe the construction procedure of this type of section are shown below.

Example 1

This example shows a wall that has five layers. Each layer may have different

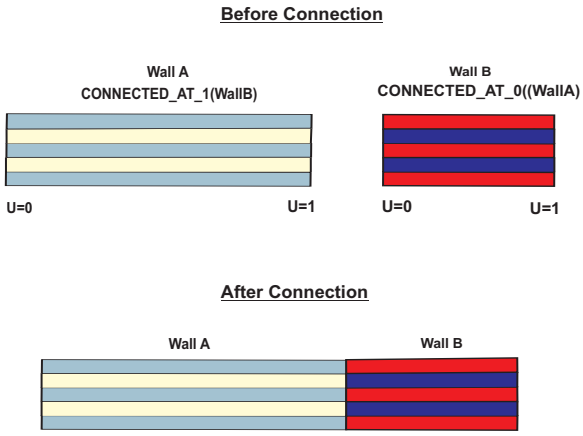

Figure 68: Connection of two walls

materials. Ply-add/drops are also shown here. The mesh density can also be adjusted base on the requirement. This example also shows the axial stress field over the cross-section under the applied sectional loads.

Example 2

This example mainly shows the connection between two walls. Both walls have equal number of layers at the connection. The material properties of the layers need to be compatible at the joining position. The tangents of the base curves of the walls should also be equal or comparable (the angle between them should be less than 10^0). Both walls may have ply-add/drops. Ply-add/drops are not allowed at the connection position. This example also shows the principal axes of shearing at the shear center.

3.3.2 Definition of Split-connector sections

Split-connector is a connector for connecting three walls. Three walls (WallA, WallB, and WallC) connected with Spilt, are depicted in fig. 71. Split-connector can be constructed at any direction. i.e., one wall can split in two walls or two walls can marge into one wall. User has to provide the WallA (connected at position A of Split-connector), WallB (connected at position B of Split-connector), and WallC (connected at position C of Split-connector) information for constructing a Split-connector.

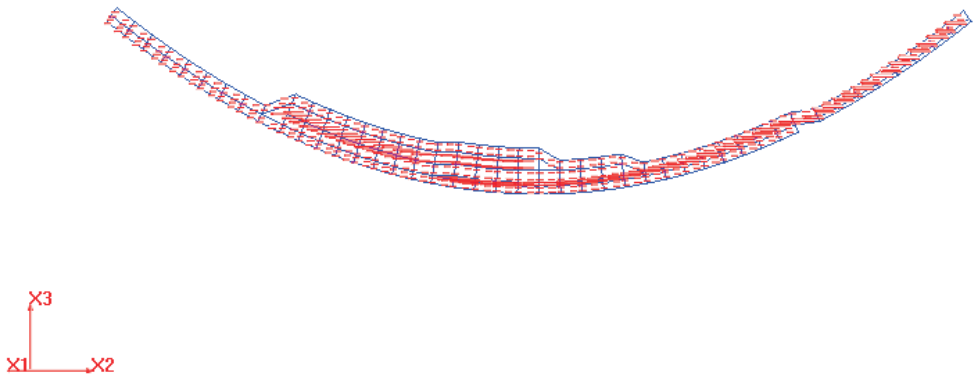

Figure 69: Example 1. Wall with arbitrary lay-ups

The detail description of Split-connector is shown in fig. 72. Basically wall information is used for Split-connector construction. Points Ki, K1i, Mi, and M1i (i= 1,2,3 ...n) are generated from WallA, WallB, and WallC. Points Ki, and Mi (or M1i) are the starting positions (at U=0) of various layers of WallA, and WallC respectively. Similarly, points K1i are the final position (at U=1) of the layers of WallB. Li are the intersection points of the tangents of the layers of WallA (at U=0) and WallC (at U=0). L1i are the intersection points of the tangents of the layers of WallB (at U=1) and WallC (at U=0). Here the sum of the layers for WallA and WallB is equal to that of WallC. Curves, and surfaces are constructed from Ki, K1i, Li, L1i, Mi, and M1i. Solids are generated using the material and mesh properties. From WallB, and lower part of WallC properties, LeftTailLo, and RightTailLo sections are generated. LeftTailUp, and RightTailUp sections are generated from WallA, and upper part of WallC properties.

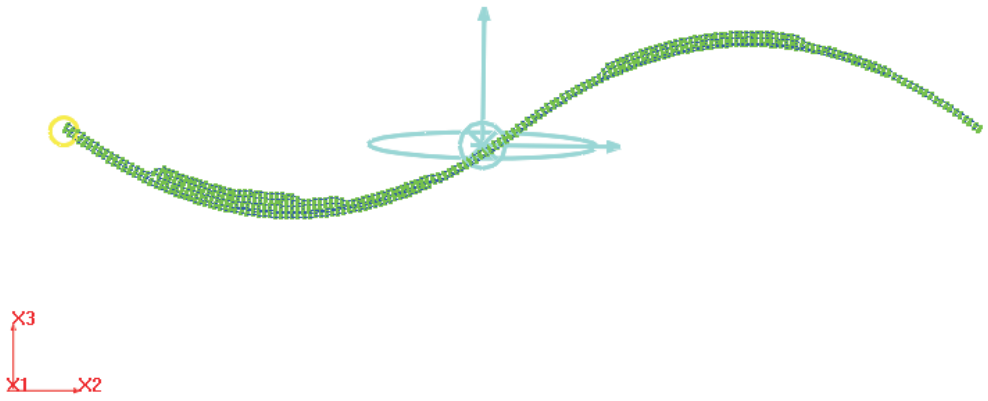

Figure 70: Example 2. Connection between two walls

3.3.2.1 Examples

An example that describes the construction procedure of this type of section is shown below.

Example 1

This example shows a Split-connector that connects three walls. WallA, WallB, and WallC have two, two, and four number of layers respectively. Here the sum of the number of layers for WallA and WallB are equal to that of WallC at the connection position. This example also shows the principal centroidal axes of bending.

3.3.3 Definition of T-connector sections

T-connector is a connector for connecting three walls like a T-shape. Three walls (WallA, WallB, and WallC) connected with a T-connector, are depicted in fig. 74, fig. 75. T-connector has three parts, and those are web, right flange, and left flange.

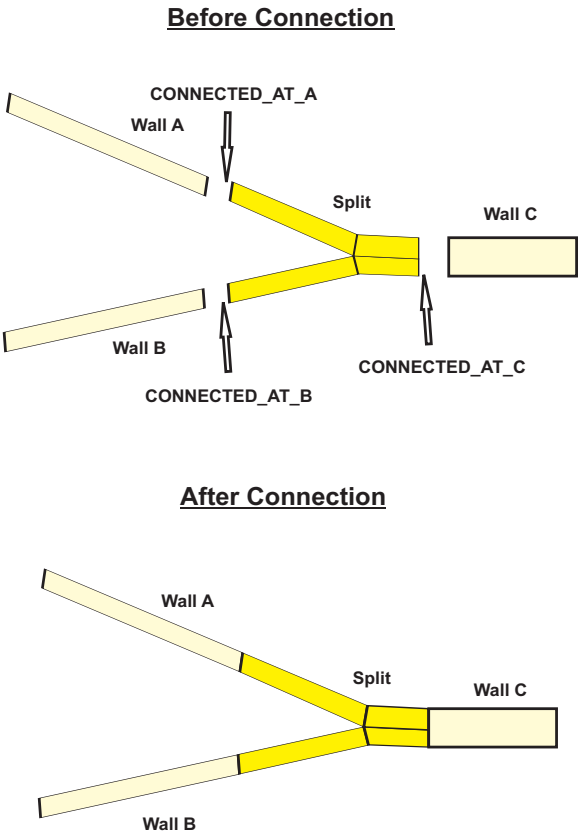

Figure 71: Three walls can be connected as above with a Split-connector

The web is constructed from the layers of the WallC. WallC has layers at upper and lower directions. Upper direction means layers are stacked at the positive normal direction of the base curve of the wall. Whereas, lower direction means the layers are stacked at the negative normal direction. Right portion of the web (RWeb) and lower part of the right flange (TRFlg) are constructed from the upper direction layers of WallC. Where as, the left part of the web (LWeb) and lower portion of the left flange (TLFlg) is constructed from the lower direction layers of the WallC. The upper portion of the left and right flanges (TLFlgR and TRFlgR) are constructed from the pass through layers. Pass through layers are the common number of layers from the WallA and WallB. User has to provide the Wall A (connected at position A of T-connector), WallB (connected at position B of T-connector), WallC (connected at position C of T-connector), and number of pass through layers information for

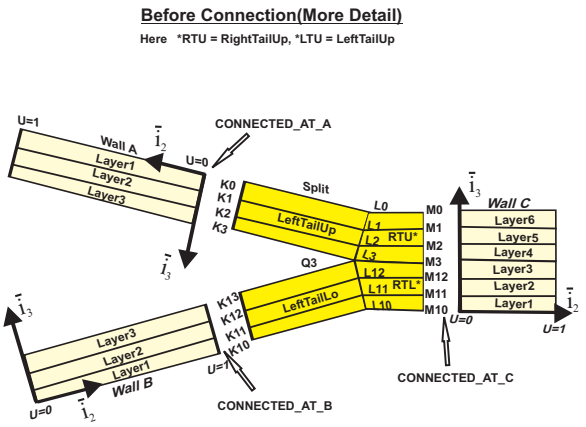

Figure 72: Three walls and a Split-connector (in detail)

constructing a T-connector.

The detail description of T-connector is shown in fig. 76. Wall information is used for T-connector construction. For a T-connector (shown in fig. 76), points Ai, and Bi (i= 1,2,3....n) are generated from the pass through layers information of WallA, (at U=0) and WallB (at U=1). Di are the middle points of Ai and Bi. Aai, and Bbi (i= 1,2,3....n) are generated from the rest of the layers information of WallA (at U=0), and WallB (at U=1). Ci, and Cci are constructed from the upper, and lower parts of WallC (at U=0) respectively. Ei are the intersection points of the tangents of the layers of WallA (at U=0) and upper part of WallC (at U=0). Fi are the intersection points of the tangents of the layers of WallB (at U=1) and lower part of WallC (at U=0). Curves and surfaces are constructed using these points. Finally solid is defined using the material and mesh properties. TRFlgR, and TLFlgR are constructed form the pass through layers information of WallA, and WallB respectively. TRFlg, and TLFlg are constructed form the other layers information of WallA, and WallB. Whereas, RWeb, and LWeb are constructed form the upper, and lower parts of WallC information respectively.

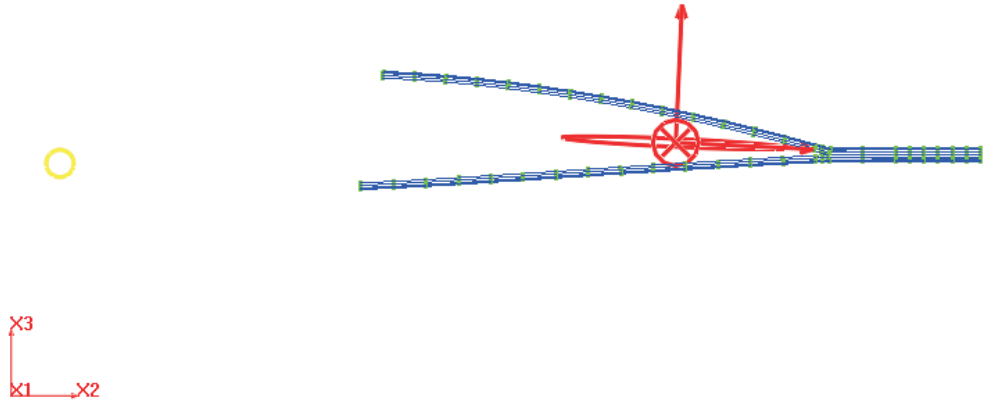

Figure 73: Example 1. Split-connector with three walls

3.3.3.1 Examples

A few examples that describe the construction procedure of this type of section are shown below.

Example 1

This example shows a simple T-connector that connects three walls. All walls have two layers. This example also shows the axial strain field over the cross-section under the applied sectional loads.

Example 2

This example shows the connection among five walls using two T-connectors. This example also shows the inverse of the reserve factor over the cross- section under the applied sectional loads.

Example 3

This example shows the connection among eight walls using six T-connectors.

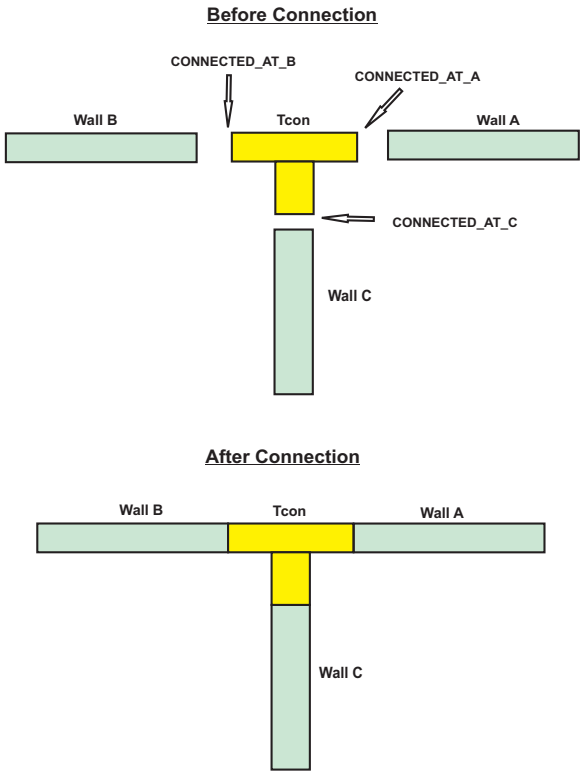

Figure 74: Three walls can be connected as above with a T-connector

All walls have more than two layers and ply-add/drops are also shown here. This example also shows the shear strain field over the cross-section under the applied sectional loads.

3.3.4 Definition of V-connector sections

V-connector is a connector for connecting two walls like a V-shape. Two walls (WallA and WallB) connected with a V-connector, are depicted in fig. 80. V-connector has the same number of layers of walls at the junction. It is very useful for the trailing-edge construction of an airfoil section. User needs to provide the WallA (connected at position A of V-connector) and WallB (connected at position B of V-connector) information for constructing a V-connector.

The detail description of V-connector is shown in fig. 81. Basically wall information is used for V-connector construction. Points Pi, and Ri (i= 1,2,3.....n) are

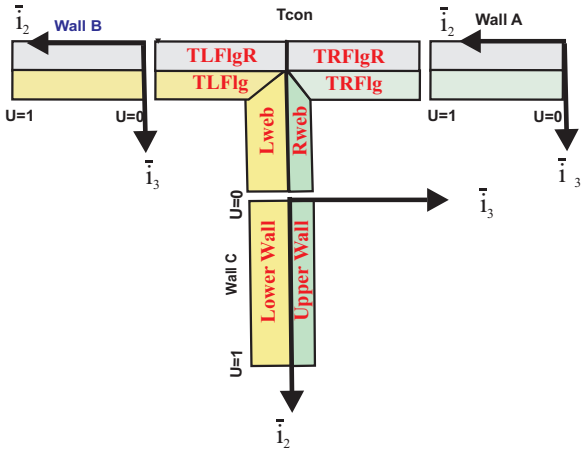

Figure 75: Three walls can be connected as above with a T-connector

generated from WallA, and WallB. Points Pi are the starting positions (U=0) of various layers of WallA. Similarly, points Ri are the final positions (at U=1) of the layers of WallB. Qi are the intersection points of the tangents of the layers of WallA (at U=0) and WallB (at U=1). Curves, and surfaces are constructed from Pi, Qi, and Ri. Solids are generated using the material and mesh properties. From WallA, and WallB properties VconUp, and VconLo sections are constructed.

3.3.4.1 Examples

An example that describes the construction procedure of this type of section is shown below.

Example 1

This example shows a V-connector that connects two walls. These walls have two layers. This example also shows the principal axes of inertia at the mass center.

3.3.5 Definition of core sections

SectionBuilder can integrate core materials inside the cavities of the cross-sections. After integrating the core materials with the cross-sections, meshes are created for

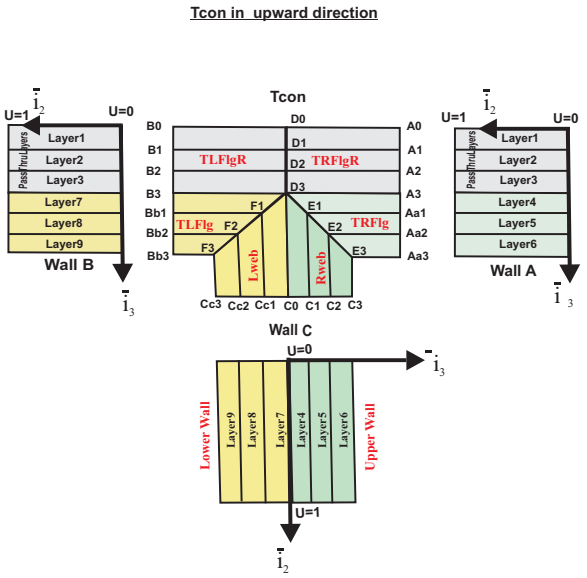

Figure 76: Three walls and T-connector in upward direction (in detail)

finite element analysis, and computing the sectional properties. For example, the cross-sections that are shown in fig. 7 need to integrate core material inside the desired cavity. At this point, closed Boundary curves, and corresponding points from the walls are only available as input information shown in fig. 7. Free mesh is considered for generating meshes inside the arbitrary closed boundary curve. The Delaunay triangulation [43, 76], is the most popular, and efficient technique for free mesh generation for this kind of situation. This technique ensures the minimum angle of the triangles is equal or greater than that generated by any other techniques and produces the best possible meshes. As a result, the Delaunay triangulation technique is considered here for creating the free meshes of the core material. The Delaunay triangulation technique is discussed in appendix B. But this technique can not serve this purpose properly due to the presence of non-convex hull (explained in appendix A), few scattered points presence from the boundary curve, three points presence in the same straight line, and four points presence in the circumference of the same circle. As a result, a new algorithm based on the Delaunay refinement algorithm is proposed here. This algorithm can produce fine mesh for core material of hollow

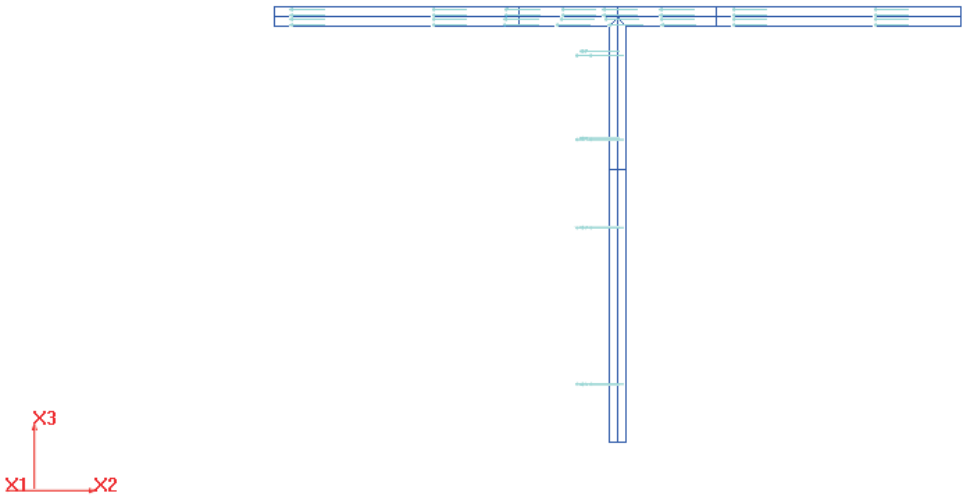

Figure 77: Example 1. T-connector with three walls

cross-section. A few examples of cross-sections with core materials are shown in the section 4. The proposed algorithm is explained below.

3.3.5.1 The proposed algorithm

The Delaunay triangulation technique does not create free meshes properly inside non-convex hull. A new algorithm based on the Delaunay refinement algorithm is considered for creating free meshes inside any arbitrary closed boundary curve (with convex or non-convex hull). This algorithm has five steps, shown in fig. 83, and fig. 84. The steps are:

(1) Create the initial (coarse) triangles using the input data (points from the boundary curves) considering the Delaunay triangulation technique that is explained in the appendix B. Delete the triangles that stay outside the boundary curve (Optional at this stage).

(2) Insert new point at the circumcenter of the triangles, which area, and aspect ratio (AR) are higher than the preassigned $Area_{max}$, and AR_{max}. The Inserted

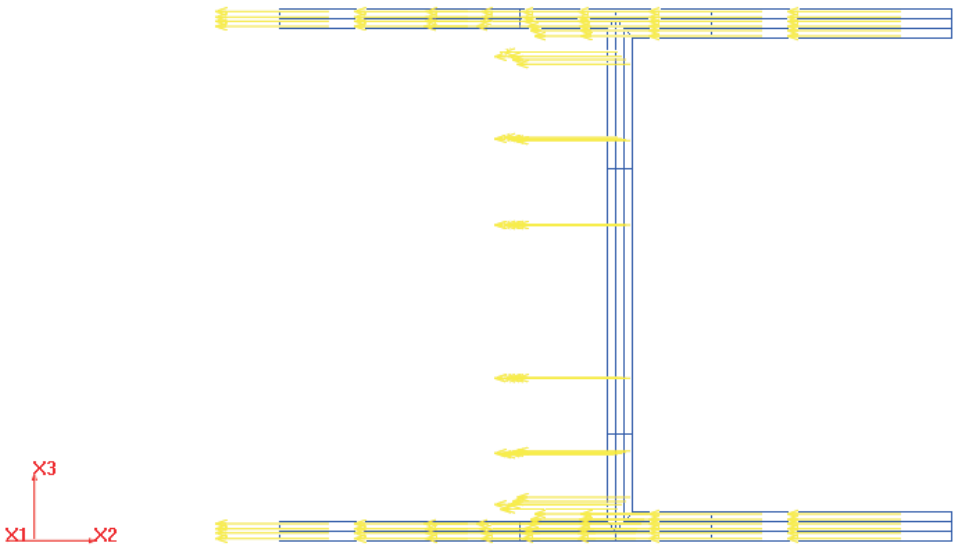

Figure 78: Example 2. Two T-connectors with five walls

point must remain inside the boundary. This way the big and sliver triangles can be removed.

(3) Create again the Delaunay triangles using all data points (including inserted points).

(4) Delete the triangles that stay outside the boundary curve.

(5) Repeat the process until all the big, and sliver triangles are removed, and get a fine mesh.

The proposed algorithm for free mesh generation for arbitrary sections is used for constructing the free meshes inside two arbitrary closed boundaries are also shown in fig. 85 and fig. 86.

Few triangles look very small because minimum value of area of triangle is not set for these examples. The higher aspect ratio triangles are considered for further refinement although the triangles are small. The proposed algorithm is used to integrate core materials for analyzing the realistic rotor blade cross-sections. The quality of free

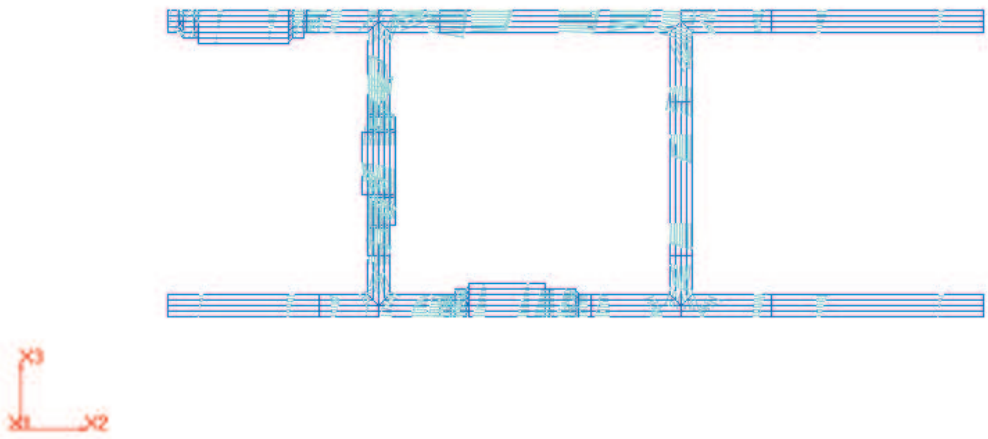

Figure 79: Example 3. Four T-connectors with eight walls

mesh depends on the points selected from the boundary curves for initial Delaunay triangulation. The quality of free mesh becomes nice if the total number of boundary points are high and uniformly spaced. But poor mesh can be generated if only a few number of points with non-uniformly spaced is considered for initial Delaunay triangulation. The sectional properties, computed by SectionBuilder, are validated, and given in detail in section 4.

This algorithm is considered for creating triangular free mesh to integrate core materials inside the closed boundaries, generated by walls. The detail procedure for creating triangular free mesh to integrate core material inside the boundary developed by two walls is given below:

(1) For this particular example, shown in fig. 87: both the walls have three layers, ply add/drops, and five zones. From the topmost curves of the zones, the initial, and final station points are picked up (two walls have 12 points). These points are considered for initial Delaunay triangulation. The triangles that contain all three

vertices from wallA or wallB (i.e., triangles lie outside the boundary curves) are deleted from the available Delaunay triangles. The remaining triangles are drawn by joining vertices with straight line(s) except the curves available from walls. For SectionBuilder, these triangles are known as GSols, and shown in fig.1 of fig. 87.

(2) The connection among walls and triangular GSols is resolved by setting proper triangular GSol at the top of the proper quadrilateral GSol from walls.

(3) Every triangular GSol is considered for creating fine triangular mesh. The outmost boundary curve for each zone are divided by the number of elements. The number of element of each zone can be calculated from the walls, zones, and mesh curves information. The characteristic length of an element is calculated by dividing the total length of two walls with the total mesh density of two walls. The length of every straight line curve for GSol is divided by this characteristic length for finding out the total number of points on the straight line curves. This way, the points on the GSol boundary curves are found out based on mesh density information of walls. These points are considered for the Delaunay triangulation and course mesh can be generated. This course mesh generation of a triangular GSol is shown in fig.2 of fig. 87.

(4) Big and high aspect ratio triangles are considered for further refinement by inserting points at the middle of the longest edge of the triangles, as shown in fig.3 of fig. 87. (The points can also be inserted at the circumcenter or centroid of the triangles. But points insertion at the middle of the longest edge is considered here and fine quality mesh can be generated.) But the points can not be inserted on or outside the boundary curves of the walls. At the time of inserting points, it is always necessary to make sure that the inserted points are not too close to the other points and always maintain a minimum distance between each pair of points. After inserting points, the Delaunay triangulation is carried out again. Points insertion and the Delaunay triangulation are continued until desired quality mesh is achieved.

Finally the triangles are deleted those lie outside the boundary curves of the triangular GSol. The triangles from the refined mesh are known as Sol for SectionBuilder, as shown in fig.4 of fig. 87.

(5) The position of vertices are known for all available Sols (shown as big points in fig.4 of fig. 87). The edges are created by joining vertices with straight line unless available from curves of the walls. These three vertices are considered as three corner nodes and other three nodes are inserted at the middle of the edges. Finally the Sol is considered as six noded triangular element for finite element analysis.

The same technique can be applied for creating triangular free mesh to integrate core material among more than two walls. The mesh generation to integrate core material among three or four walls (airfoil, rotor blade section) are given as examples in the section 4.

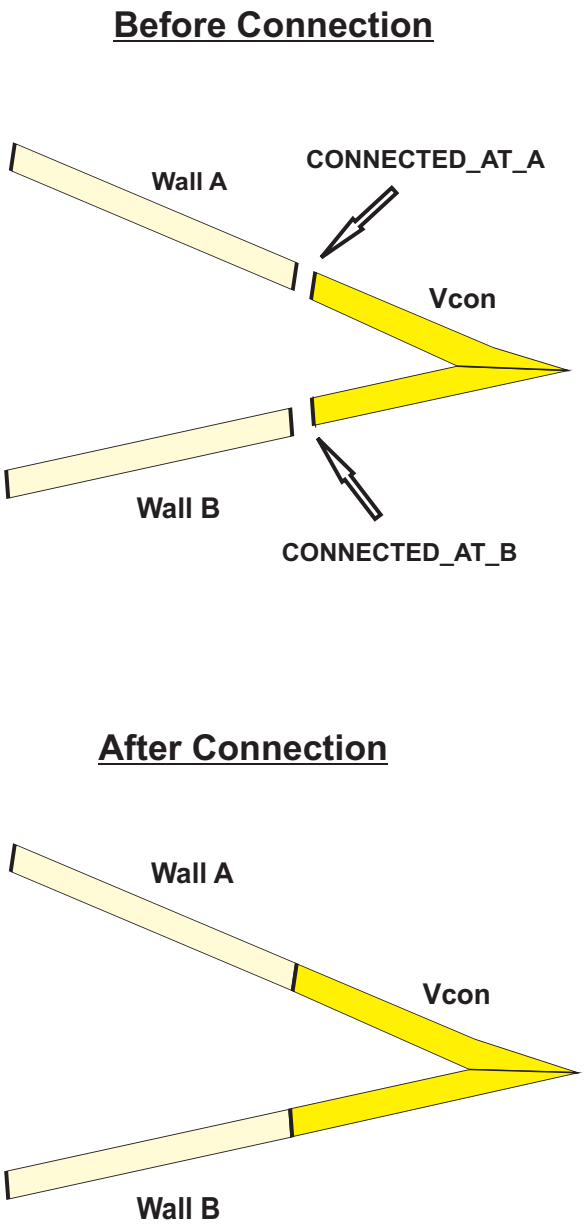

Figure 80: Two walls can be connected as above with a V-connector

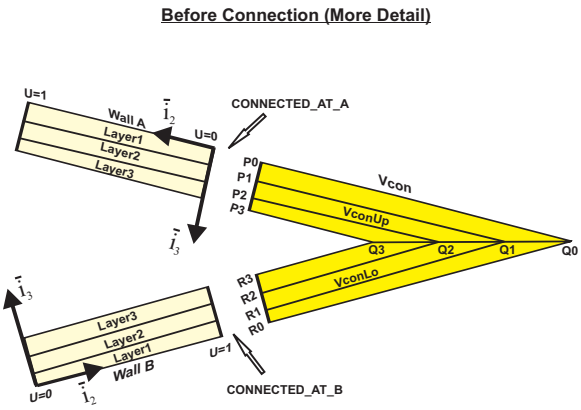

Figure 81: Two walls and a V-connector (in detail)

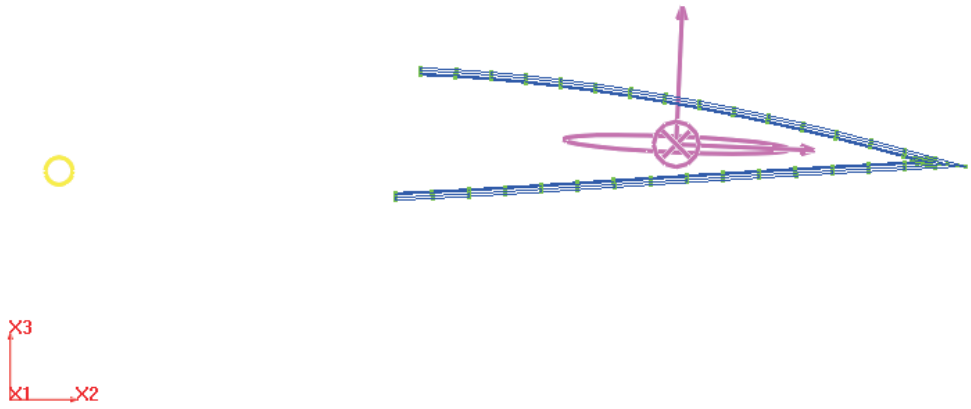

Figure 82: Example 1. V-connector with two walls

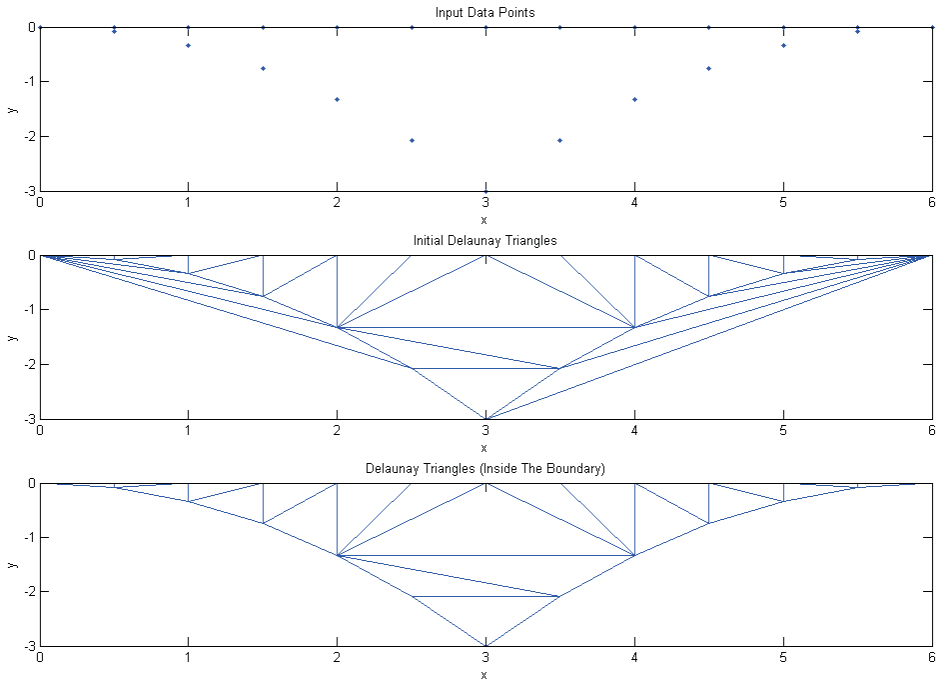

Figure 83: Free mesh generation steps

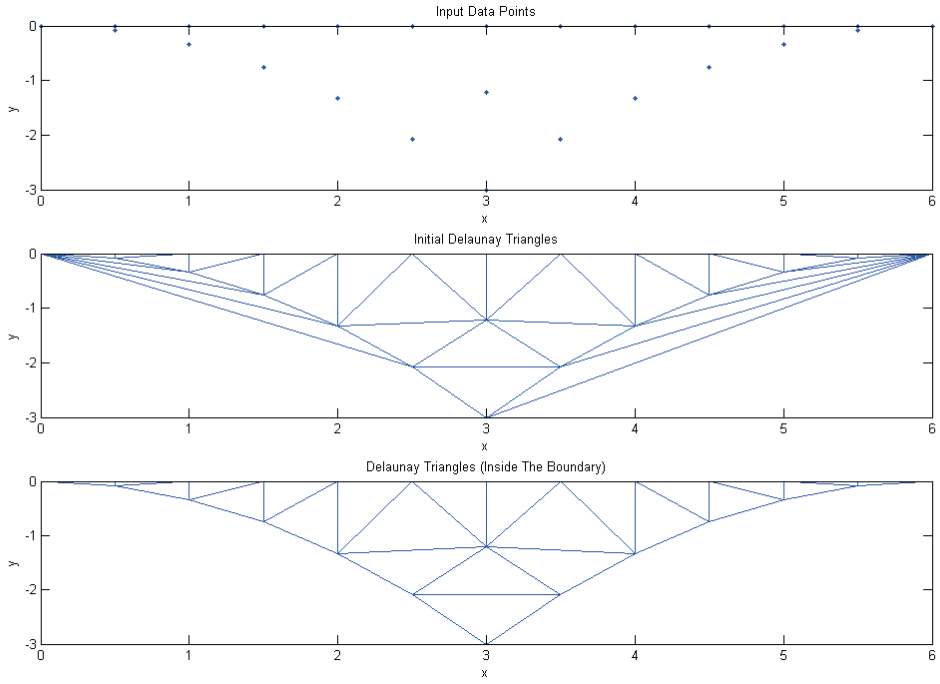

Figure 84: Free mesh generation steps (continued)

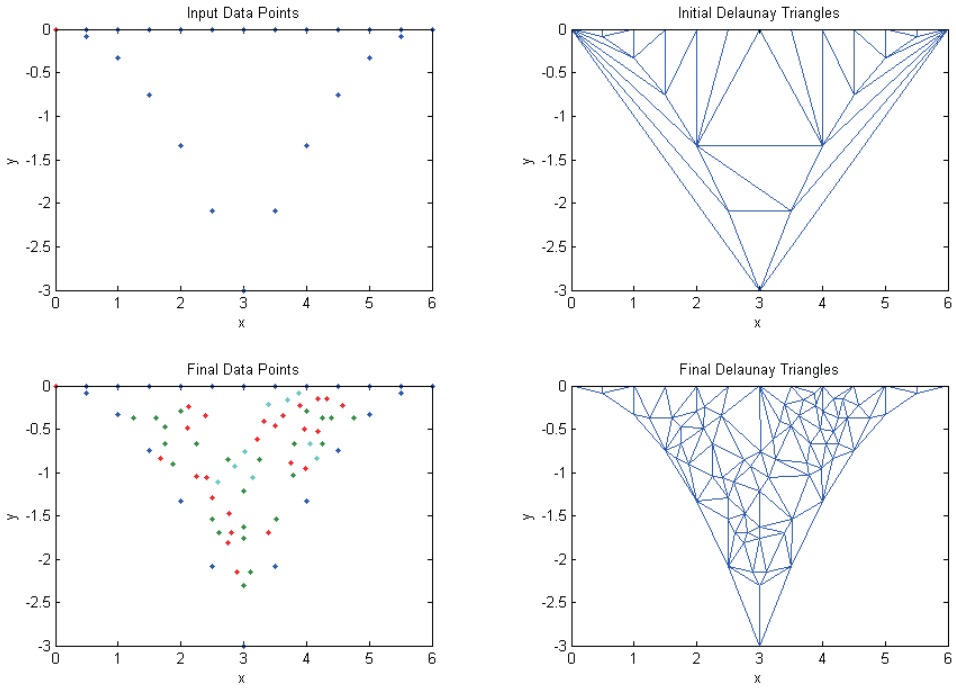

Figure 85: Example 1. Free mesh generation

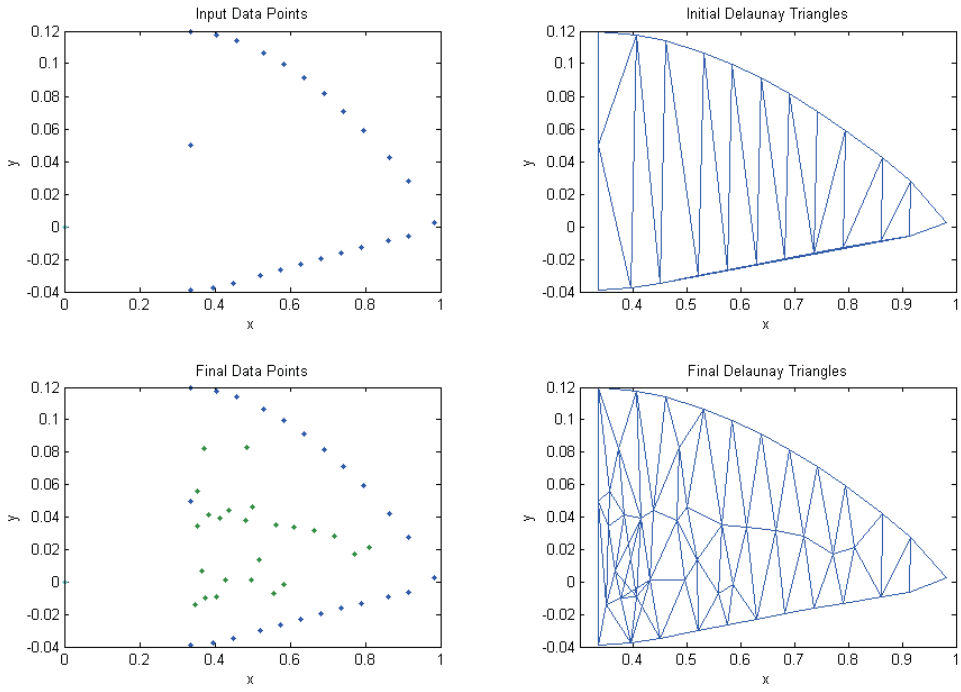

Figure 86: Example 2. Free mesh generation

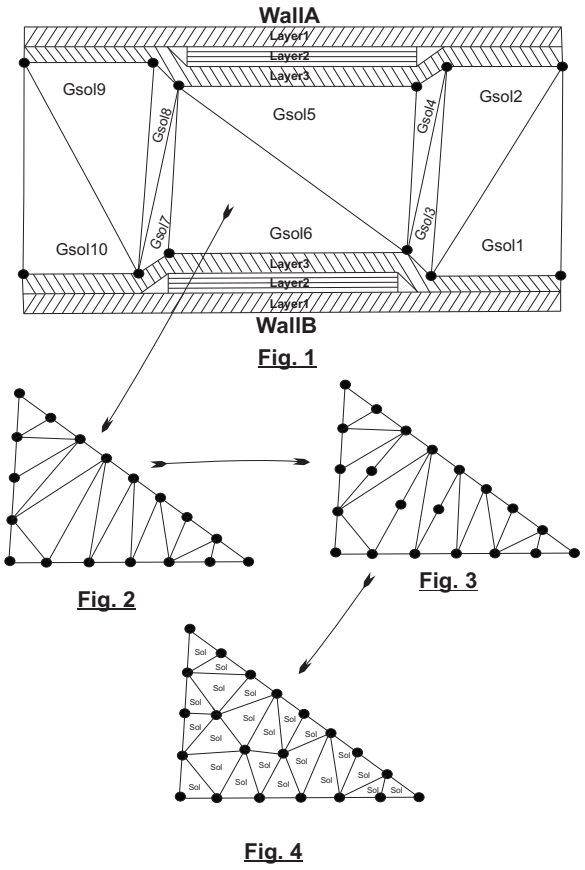

Figure 87: Free mesh generation technique to integrate core material between two walls

CHAPTER IV

RESULTS AND DISCUSSION

A simple NACA four digit series (0012) airfoil cross-section shown in fig. 88 is considered as a first example. This cross-section has a chord length 1.0 m and thickness 0.005 m. Steel is considered as the material. The cross-sectional properties are computed and stiffnesses at 382 elements (6,876 DOF) are shown in fig. 90. The variation of axial stiffness with the number of elements is also plotted and the difference is negligible for higher number of elements, as shown in fig. 89. The results are also compared with those computed by the VABS-ANSYS Toolset. Cross-sectional area differs by 2.5% and almost all stiffnesses differ by less than 2.0% at higher number of elements for the two methods of computation.

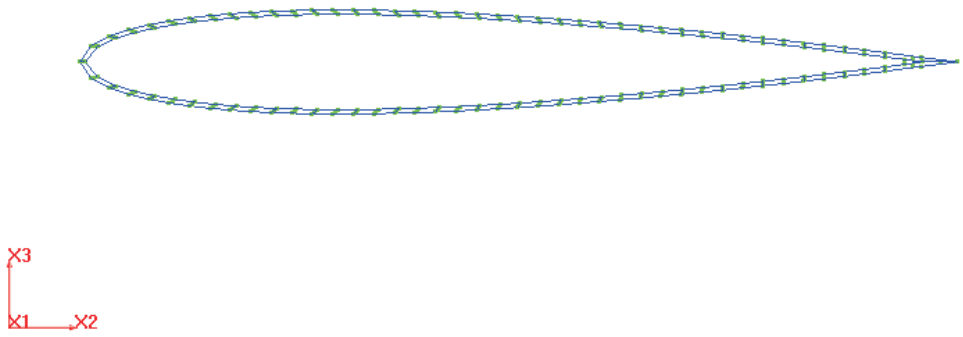

Figure 88: Simple airfoil cross-section with mesh generation

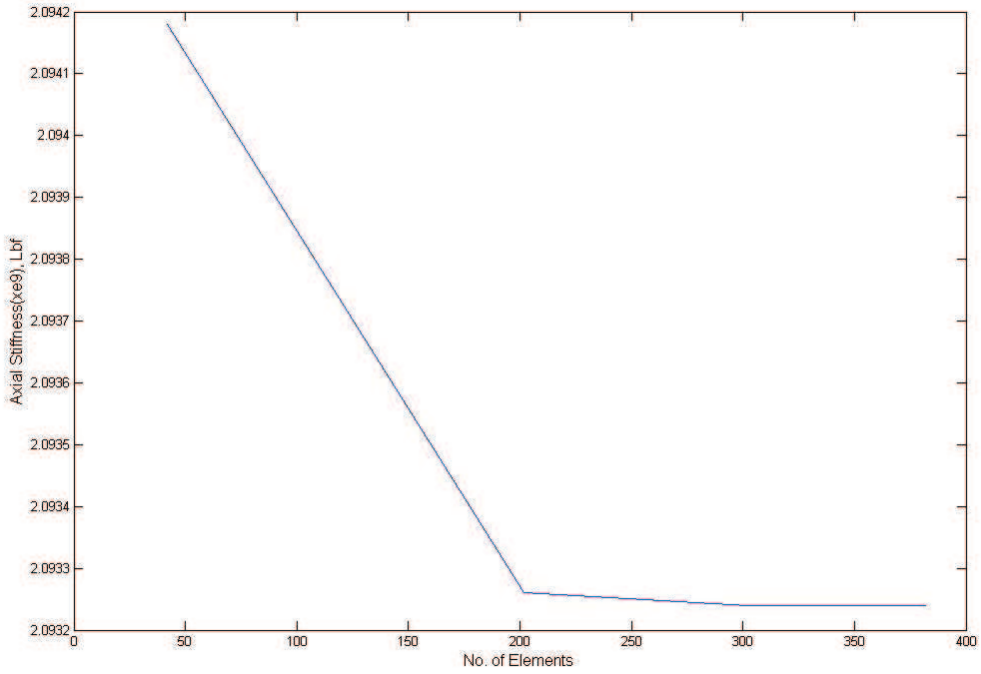

Figure 89: Variation of axial stiffness with number of elements plot

--- Sectional stiffness matrix (4x4) ---

S T R A I N	*<---*	*C U R V A T U R E S*	*--->*
Axial S1	*Twist K1*	*Bending K2*	*Bending K3*
2.09324e+009	*0.00000e+000*	*1.35141e-001*	*-1.02359e+009*
0.00000e+000	*4.83821e+006*	*0.00000e+000*	*0.00000e+000*
1.35140e-001	*0.00000e+000*	*3.71649e+006*	*2.75871e-004*
-1.02359e+009	*0.00000e+000*	*2.75930e-004*	*6.76887e+008*

Figure 90: Stiffnesses for simple airfoil section

An airfoil cross-section of NACA four digit series (4416) with one web and chord length 1.0 m as shown in fig. 91 is constructed next. This cross-section is made of five walls with arbitrary lay-ups and ply add/drops. These walls are connected with various connectors (two T-connectors and one V-connector). Two adjacent walls at the tip are connected between themselves. Steel, and aluminum are used as materials for the various layers of the airfoil cross-section. The cross-sectional properties are computed at 3,162 DOF and stiffness and compliance matrices are shown in fig. 92. Sectional mass matrix of the cross-section is depicted in fig. 93. The axial stress distribution with principal axes of bending due to axial loading is also shown in fig. 91.

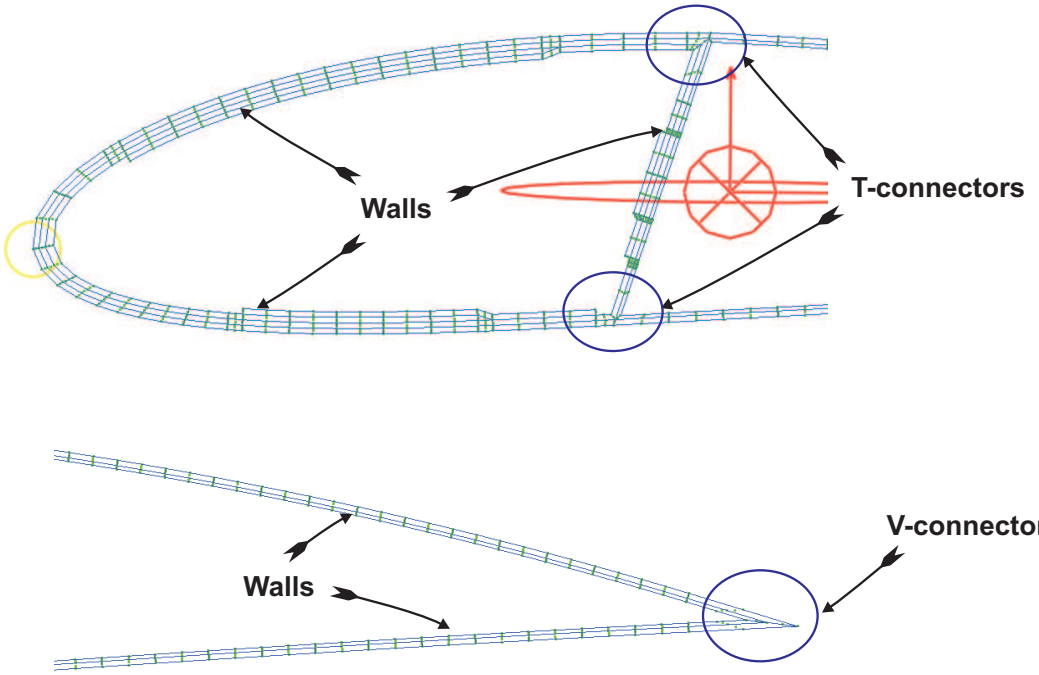

(a) Geometric details

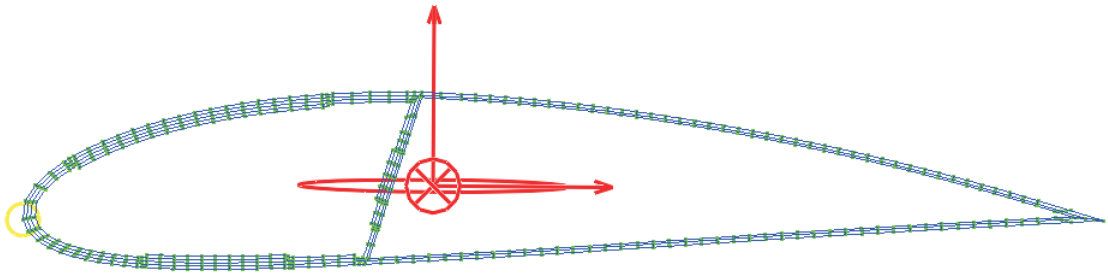

(b) Principal axes of bending

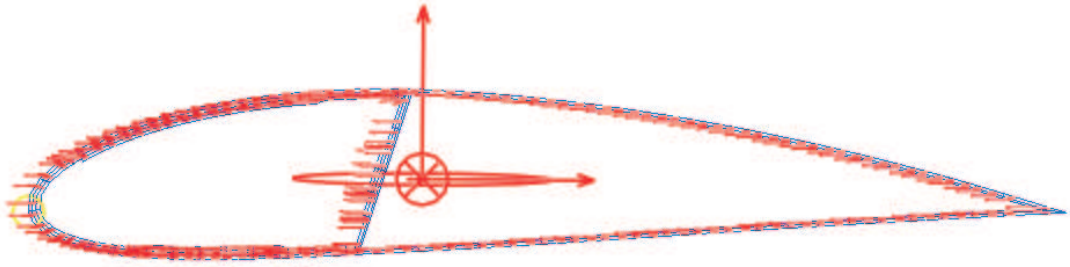

(c) Axial stress distribution for axial loading

Figure 91: Geometry and analysis results for airfoil cross-section with one web

--- Sectional stiffness matrix (4x4) ---

S T R A I N <---		C U R V A T U R E S --->	
Axial S1	Twist K1	Bending K2	Bending K3
2.13603e+009	0.00000e+000	6.71088e+007	-8.19370e+008
0.00000e+000	7.63282e+006	0.00000e+000	0.00000e+000
6.71088e+007	0.00000e+000	9.16746e+006	-2.46366e+007
-8.19370e+008	0.00000e+000	-2.46366e+007	4.70972e+008

--- Sectional stiffness matrix (6x6) ---

<--- S T R A I N S --->			<--- C U R V A T U R E S --->		
Axial S1	Shear S2	Shear S3	Twist K1	Bending K2	Bending K3
2.13603e+009	0.00000e+000	0.00000e+000	0.00000e+000	6.71088e+007	-8.19370e+008
0.00000e+000	4.85892e+008	3.39475e+007	-1.39633e+007	0.00000e+000	0.00000e+000
0.00000e+000	3.39475e+007	7.60613e+007	1.95605e+007	0.00000e+000	0.00000e+000
0.00000e+000	-1.39633e+007	1.95605e+007	1.37572e+007	0.00000e+000	0.00000e+000
6.71088e+007	0.00000e+000	0.00000e+000	0.00000e+000	9.16746e+006	-2.46366e+007
-8.19370e+008	0.00000e+000	0.00000e+000	0.00000e+000	-2.46366e+007	4.70972e+008

--- Sectional compliance matrix ---

<--- F O R C E S --->			<--- M O M E N T S --->		
Axial F1	Shear F2	Shear F3	Torque M1	Bending M2	Bending M3
1.57255e-009	0.00000e+000	0.00000e+000	0.00000e+000	-4.83964e-009	2.48266e-009
0.00000e+000	2.42879e-009	-2.70826e-009	6.31590e-009	0.00000e+000	0.00000e+000
0.00000e+000	-2.70826e-009	2.37456e-008	-3.65113e-008	0.00000e+000	0.00000e+000
0.00000e+000	6.31590e-009	-3.65113e-008	1.31013e-007	0.00000e+000	0.00000e+000
-4.83964e-009	0.00000e+000	0.00000e+000	0.00000e+000	1.41819e-007	-1.00116e-009
2.48266e-009	0.00000e+000	0.00000e+000	0.00000e+000	-1.00116e-009	6.39009e-009

Figure 92: Stiffnesses and compliance matrices for airfoil section with one web

--- Sectional mass matrix ---

<--- V E L O C I T I E S --->			<--- A N G U L A R V E L O C I T I E S --->		
V1	V2	V3	OMEGA1	OMEGA2	OMEGA3
7.99021e+001	0.00000e+000	0.00000e+000	0.00000e+000	2.51199e+000	-3.06359e+001
0.00000e+000	7.99021e+001	0.00000e+000	-2.51199e+000	0.00000e+000	0.00000e+000
0.00000e+000	0.00000e+000	7.99021e+001	3.06359e+001	0.00000e+000	0.00000e+000
0.00000e+000	-2.51199e+000	3.06359e+001	1.79398e+001	0.00000e+000	0.00000e+000
2.51199e+000	0.00000e+000	0.00000e+000	0.00000e+000	3.42993e-001	-9.21685e-001
-3.06359e+001	0.00000e+000	0.00000e+000	0.00000e+000	-9.21685e-001	1.75968e+001

Figure 93: Sectional mass matrix for airfoil section with one web

A complex rotor blade cross-section of NACA four digit series (0012) airfoil with four webs and chord length 2.24 m as shown in fig. 94 is next constructed. This cross-section is made of 14 walls with arbitrary lay-ups and ply add/drops. Each wall has at least 24 layers of composite materials. These walls are connected with various connectors (eight T-connectors and one V-connector). Two adjacent walls at the tip are connected between themselves. CYTEC5250-4-IM7/6K (Carbon/5250-4) with various orientation angles (-45^0 to $+45^0$) is selected as material for the airfoil cross-section. The cross-sectional properties are computed at 33,540 DOF and few of them are shown in fig. 95. The axial stress distribution due to axial loading is also shown in fig. 94.

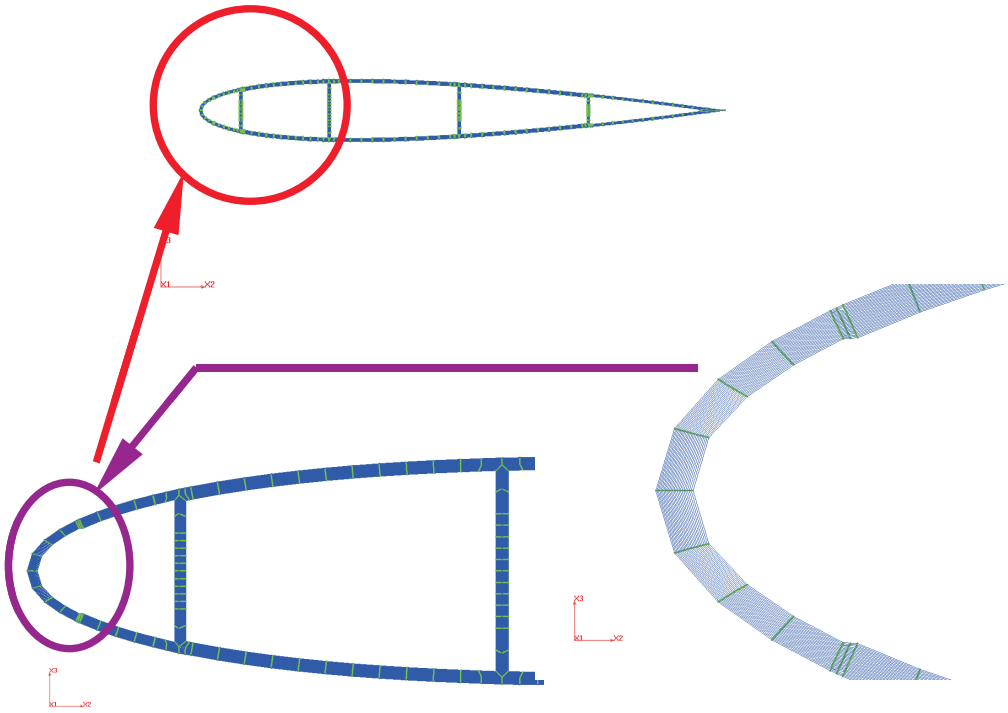

(a) Geometric details

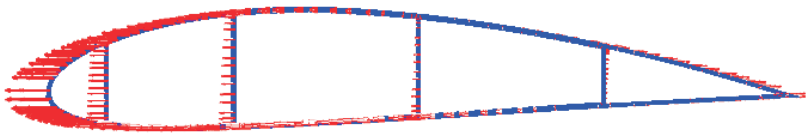

(b) Axial stress distribution due to axial loading

Figure 94: Geometry and analysis results for complex rotor blade cross-section

--- Sectional stiffness matrix ---

<--- STRAINS --->			<--- CURVATURES --->		
Axial S1	Shear S2	Shear S3	Twist K1	Bending K2	Bending K3
1.45287e+008	3.73475e+004	-3.47244e+004	7.40790e+003	1.39609e+003	-1.51446e+008
3.73475e+004	3.24297e+007	-2.47513e+006	-1.96810e+006	-8.02481e+003	-7.63949e+003
-3.47244e+004	-2.47513e+006	2.04730e+006	1.62911e+006	6.02005e+002	9.68373e+003
7.40790e+003	-1.96810e+006	1.62911e+006	2.74531e+006	6.54648e+002	1.55576e+004
1.39609e+003	-8.02481e+003	6.02005e+002	6.54648e+002	1.23635e+006	-2.06475e+003
-1.51446e+008	-7.63949e+003	9.68373e+003	1.55576e+004	-2.06475e+003	2.14196e+008

--- Sectional compliance matrix ---

<--- FORCES --->			<--- MOMENTS --->		
Axial F1	Shear F2	Shear F3	Torque M1	Bending M2	Bending M3
2.61735e-008	1.59904e-012	9.41785e-010	-7.33223e-010	1.29031e-012	1.85058e-008
1.59904e-012	3.39705e-008	4.10967e-008	-3.43094e-011	2.00500e-010	4.88637e-013
9.41785e-010	4.10967e-008	9.75203e-007	-5.49246e-007	8.27710e-011	6.63154e-010
-7.33223e-010	-3.43094e-011	-5.49246e-007	6.90170e-007	-9.83084e-011	-5.43721e-010
1.29031e-012	2.00500e-010	8.27710e-011	-9.83084e-011	8.08835e-007	8.71966e-012
1.85058e-008	4.88637e-013	6.63154e-010	-5.43721e-010	8.71966e-012	1.77531e-008

--- Sectional area ---

Omega = (8.87641e-002) [ft^2]

Figure 95: Sectional properties of complex rotor blade section

SectionBuilder can integrate core materials inside the cavities of the cross-section. A simple rectangular cross-section of thickness 0.5 m with two walls of dimension: 1.0 m width and 0.006 m thickness, forming the upper and lower surfaces and with a core between them is considered at first. The core material is integrated between these two walls and is shown in fig. 96. Mapped meshes are employed for the two walls, and free meshes are used for the core material.

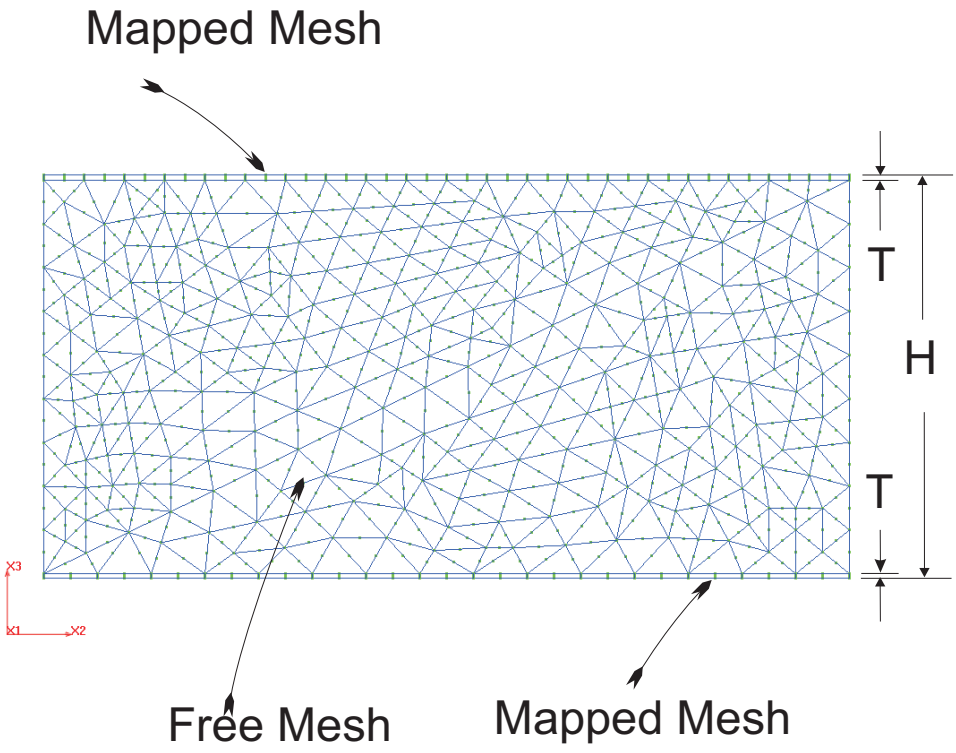

Figure 96: Mesh generation of rectangular cross-section with two walls and core material

The sectional properties are computed and the axial stiffness variation with the thickness of the walls expressed as the ratio of wall thickness to rectangular cross-section thickness is shown in fig. 97. The variation of stiffness is minimal and converged for all ratios. Steel is considered for both walls and core material of the cross-section (E=207 GPa, ν=0.3, and isotropic elasticity.)

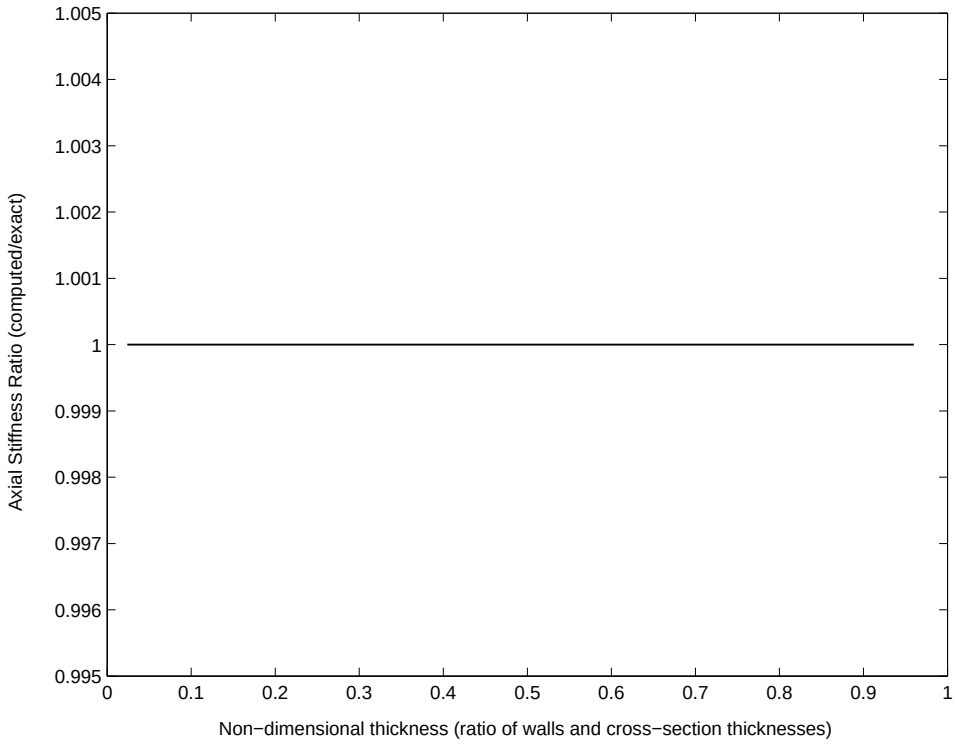

Figure 97: Variation of axial stiffness with the thickness of walls for the rectangular cross-section

The sectional properties of this cross-section with 2T/H=2.4% are computed at 4,200 DOF and few of them are shown in fig. 98. It is clear from fig. 97 that at this mesh size both mapped and free meshes yield the same axial stiffness.

```
   --- Sectional stiffness matrix (4x4) ---

  S T R A I N   <---        C U R V A T U R E S        --->
     Axial S1      Twist   K1      Bending K2      Bending K3
 1.03500e+011    0.00000e+000    2.58750e+010   -5.17500e+010
 0.00000e+000    2.27585e+009    0.00000e+000    0.00000e+000
 2.58750e+010    0.00000e+000    8.62500e+009   -1.29375e+010
-5.17500e+010    0.00000e+000   -1.29375e+010    3.45000e+010


   --- Sectional stiffness matrix ---

<---           S T R A I N S           --->   <---        C U R V A T U R E S        --->
     Axial S1        Shear S2        Shear S3      Twist   K1      Bending K2      Bending K3
 1.03500e+011    0.00000e+000    0.00000e+000    0.00000e+000    2.58750e+010   -5.17500e+010
 0.00000e+000    3.25625e+010   -1.66162e+009   -8.97144e+009    0.00000e+000    0.00000e+000
 0.00000e+000   -1.66162e+009    2.65869e+010    1.37089e+010    0.00000e+000    0.00000e+000
 0.00000e+000   -8.97144e+009    1.37089e+010    1.13731e+010    0.00000e+000    0.00000e+000
 2.58750e+010    0.00000e+000    0.00000e+000    0.00000e+000    8.62500e+009   -1.29375e+010
-5.17500e+010    0.00000e+000    0.00000e+000    0.00000e+000   -1.29375e+010    3.45000e+010


   --- Sectional compliance matrix ---

<---            F O R C E S            --->   <---           M O M E N T S           --->
     Axial F1        Shear F2        Shear F3      Torque  M1      Bending M2      Bending M3
 6.76329e-011    0.00000e+000    0.00000e+000    0.00000e+000   -1.15942e-010    5.79710e-011
 0.00000e+000    5.82707e-011   -5.29991e-011    1.09849e-010    0.00000e+000    0.00000e+000
 0.00000e+000   -5.29991e-011    1.47582e-010   -2.19698e-010    0.00000e+000    0.00000e+000
 0.00000e+000    1.09849e-010   -2.19698e-010    4.39396e-010    0.00000e+000    0.00000e+000
-1.15942e-010    0.00000e+000    0.00000e+000    0.00000e+000    4.63768e-010   -2.97420e-024
 5.79710e-011    0.00000e+000    0.00000e+000    0.00000e+000   -3.29527e-024    1.15942e-010


   --- Sectional mass matrix ---

<---        V E L O C I T I E S        --->   <--- A N G U L A R   V E L O C I T I E S --->
          V1              V2              V3          OMEGA1          OMEGA2          OMEGA3
 3.90000e+003    0.00000e+000    0.00000e+000    0.00000e+000    9.75000e+002   -1.95000e+003
 0.00000e+000    3.90000e+003    0.00000e+000   -9.75000e+002    0.00000e+000    0.00000e+000
 0.00000e+000    0.00000e+000    3.90000e+003    1.95000e+003    0.00000e+000    0.00000e+000
 0.00000e+000   -9.75000e+002    1.95000e+003    1.62500e+003    0.00000e+000    0.00000e+000
 9.75000e+002    0.00000e+000    0.00000e+000    0.00000e+000    3.25000e+002   -4.87500e+002
-1.95000e+003    0.00000e+000    0.00000e+000    0.00000e+000   -4.87500e+002    1.30000e+003


* Sectional area
   Omega = ( 5.00000e-001) [m^2].
```

Figure 98: Sectional properties of the rectangular cross-section with two walls and core material

The variation of axial stiffness with number of degrees of freedom (DOF) is observed to be less than that of torsional stiffness. So the torsional stiffness variation with number of degrees of freedom (DOF) is shown in fig. 99. The stiffnesses of these two cross-sections are almost identical and the variation is only 0.0057% at higher number of DOF. The stiffness is also compared with the St. Venant solution and the variation is 0.17%.

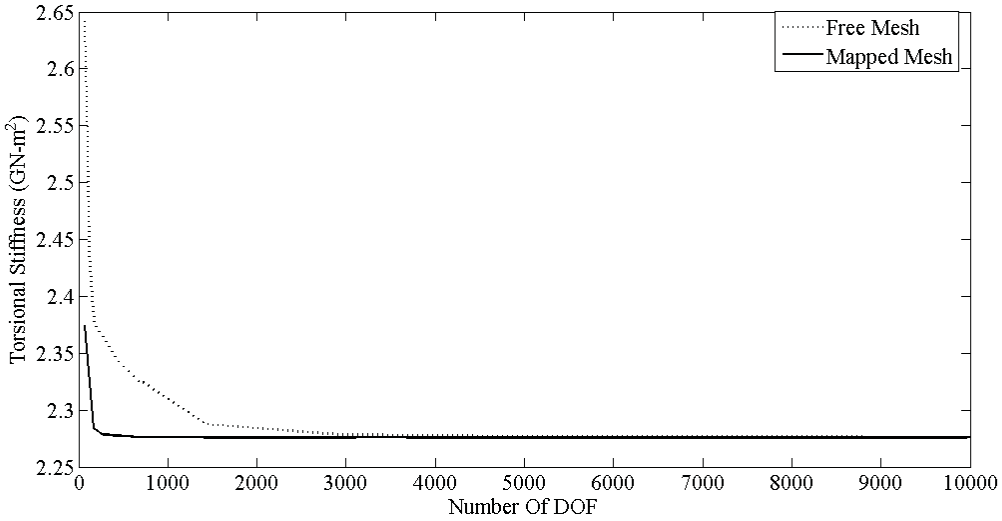

Figure 99: Variation of torsional stiffness with DOF for mapped and free meshes

The mapped mesh produces nine noded quadrilateral elements with 27 DOF, and the free mesh generates six noded triangular elements with 18 DOF. The number of DOF for quadrilateral elements is higher than that for triangular elements. As a result, the cross-sectional properties (fig. 99) and stresses (fig. 101 and fig. 102) for the rectangular cross-section with mapped meshes converge more rapidly than those for rectangular cross-section with free meshes due to higher number of DOF for quadrilateral elements than that for triangular elements.

In order to investigate the effect of mesh shape on stresses, a torsional loading is applied and the shear stress is computed at selected locations. Torsional loading is considered because it was found to produce the greatest variation from nominal values. The shear stresses and torsional stiffness are computed for a torque of 100 N.m at the centroid of the rectangular cross-section shown in fig. 96 with different meshed areas.

The maximum shear stress which occurs at the location, x2=0.5 m and x3=0.0 or 0.5 m (midpoint of the long sides) varies with the relative areas of mapped and free mesh (defined by ratio of walls thickness to section thickness defined in fig. 96) is shown in fig. 100. In this figure the ratio of the computed to exact shear stress (St. Venant solution) is plotted. The variation is minimal and the shear stress is converged.

These results show that the use of mapped or free mesh of comparable size has essentially no effect on computed stiffness or stress. To study the effect of mesh size or number of DOF, the same rectangular steel cross-section is analyzed using different mesh sizes.

The shear stress, τ_{12}, as a function of the number of DOF is shown in fig. 101 at the location, x2=0.5 m and x3=0.3 m (where bottom left corner is assigned as origin in fig. 96.) The shear stress is almost identical to the exact (St. Venant) solution even at lower number of DOF. The effect of free mesh on shear stress is also small as

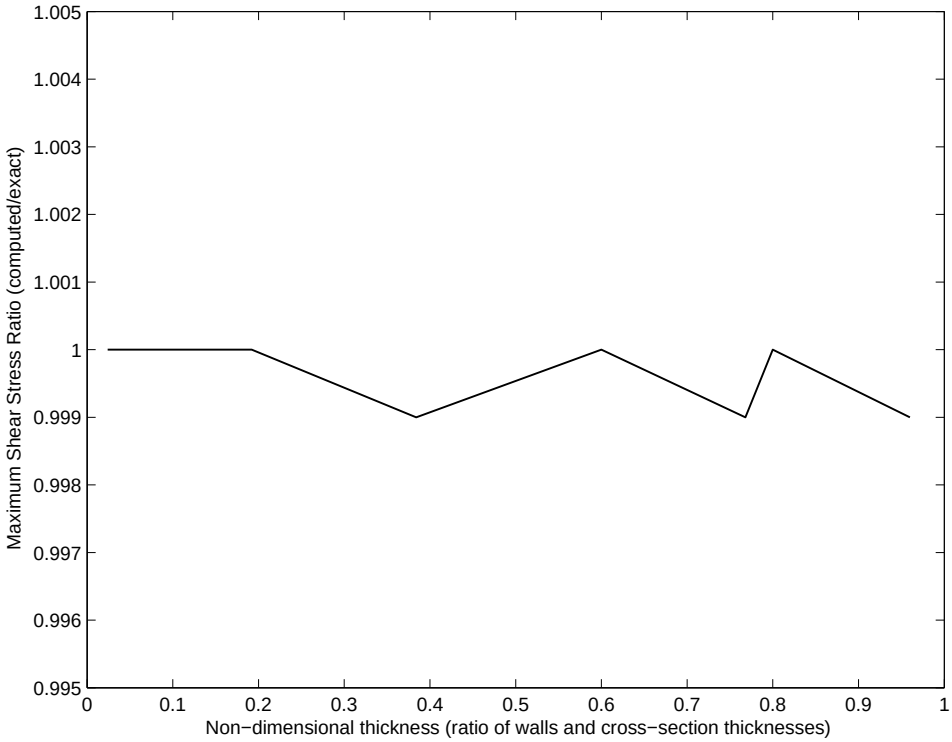

Figure 100: Variation of maximum shear stress with the thickness of walls for the rectangular cross-section

compared to the exact (St. Venant) solution and the difference is 0.405% at higher numbers of DOF.

The shear stress, τ_{12}, as a function of the number of degrees of freedom (DOF) is also shown in fig. 102 at another selected location, x2=0.6 m and x3=0.4 m (where bottom left corner is assigned as origin in fig. 96.) The shear stress for the rectangular cross-section with mapped mesh is almost identical to the exact (St. Venant) solution even at lower number of DOF. The effect of free mesh on shear stress for the rectangular cross-section is also minimal as compared to the exact (St. Venant) solution and the variation is 0.913% at higher number of DOF.

The shear stresses distribution along two different paths on the cross-section is shown in fig. 103. Shear stress, τ_{12} is shown along path A (x2=0.5m) while τ_{13} is shown along path B (x3=0.25m). The shear stresses for the rectangular cross-section with

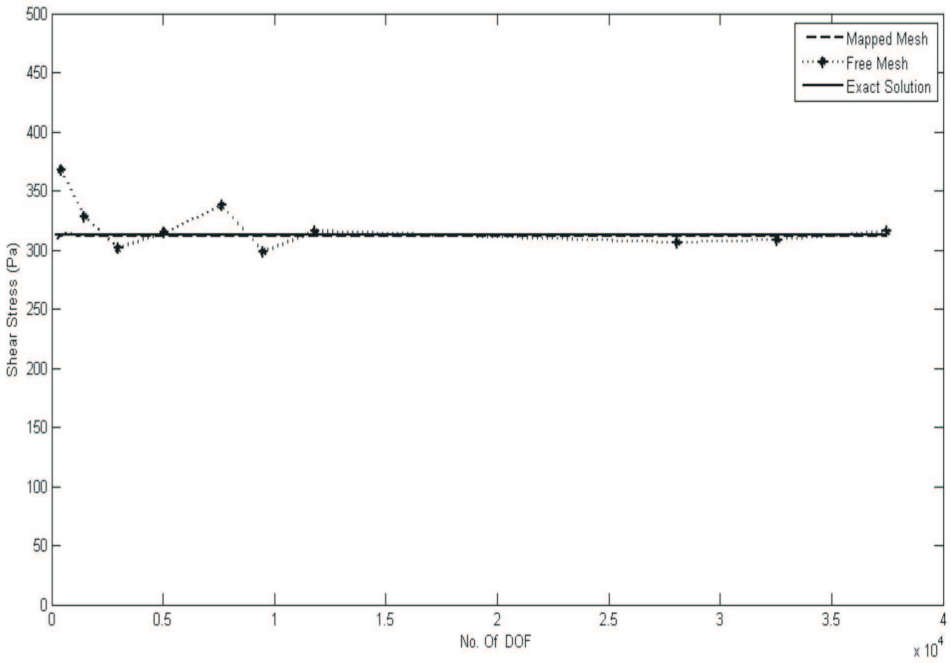

Figure 101: Variation of shear stress with number of DOF at the location, x2=0.5 m and x3=0.3 m

mapped meshes (at 15,453 DOF) are identical to the exact (St. Venant) solution. On the other hand, the shear stresses for the rectangular cross-section with free meshes (at 15,321 DOF) are also quite as compared to the exact (St. Venant) solution and the variation is up to 2.8%. Shear stresses for the rectangular cross-section with free meshes converge more slowly to the exact (St. Venant) solution due to the courser and more irregular free meshes over the cross-section for comparable DOF. In all cases the convergence of the stresses is expedited by considering finer and more uniform free meshes that can be attained by selecting a higher number of elements (i.e., higher number of DOF) for the cross-section. So, the error in the stresses for the cross-section with free meshes can be reduced by computing them at higher numbers of DOF to ensure convergence, as shown in fig. 101 and fig. 102.

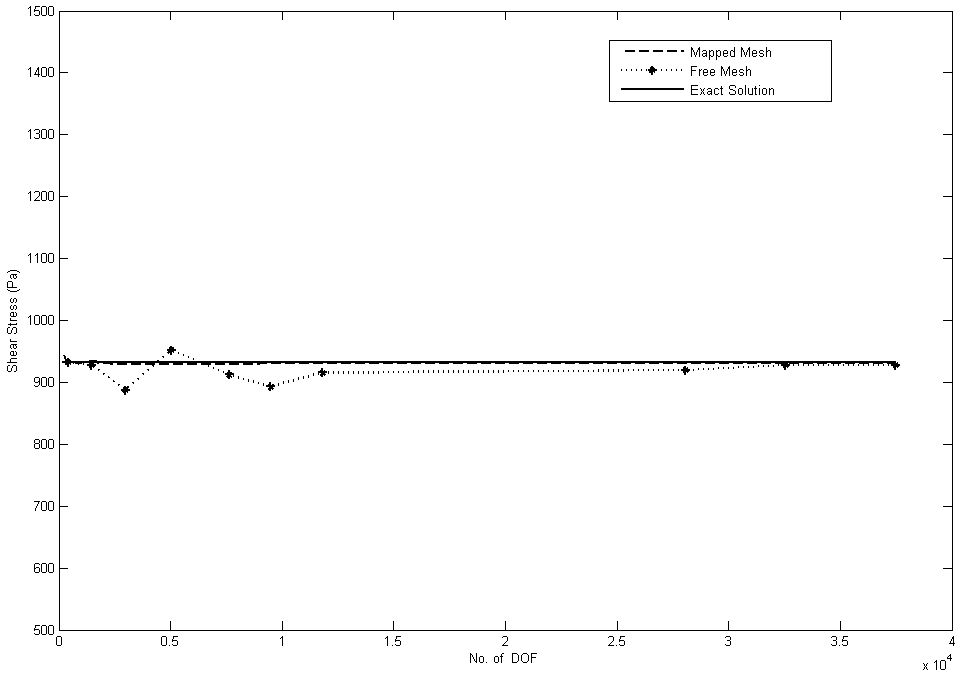

Figure 102: Variation of shear stress with number of DOF at the location, x2=0.6 m and x3=0.4 m

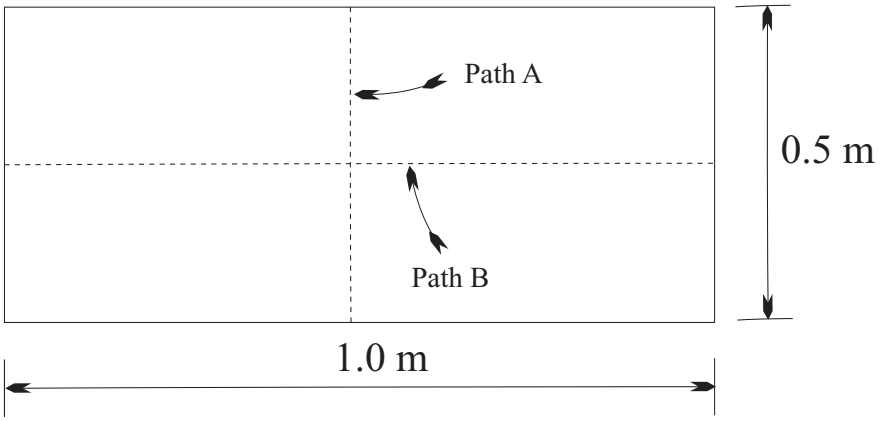

(a) Paths A and B on cross-section

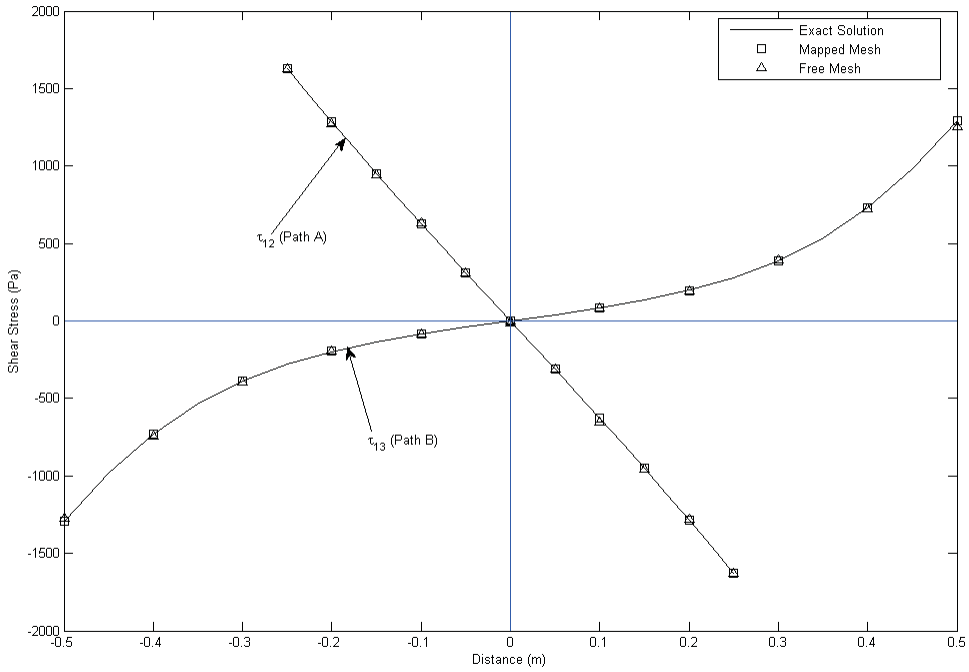

(b) Shear stress along path (measured from centroid)

Figure 103: Variation of shear stresses, (τ_{12} and τ_{13}) across cross-section along paths A and B

An airfoil cross-section of NACA four digit series (4416) with one web, chord length 1.0 m, and core material inside the aft cavity is constructed, as shown in fig. 104. This cross-section is made of five walls with arbitrary lay-ups and ply add/drops. These walls are connected with various connectors (two T-connectors and one V-connector). Two adjacent walls at the trailing edge are connected together. Free meshes are generated inside the aft cavity of the airfoil cross-section to model a core material. The inside boundary node points of the three walls are used for free mesh generation in the core material. Steel and aluminum are used as materials for various layers of the airfoil cross-section. HexWebACG Honeycomb is used as the core material. The cross-sectional properties are computed at 3,174 DOF and few of them are shown in fig. 105. The axial stress distribution is also shown in fig. 104.

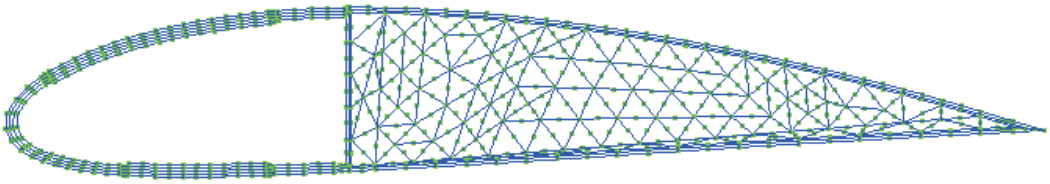

(a) Geometry

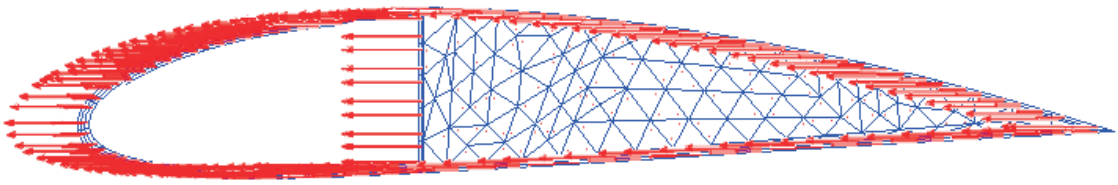

(b) Axial stress distribution for axial loading

Figure 104: Airfoil cross-section with core material

The axial stiffness variation with the numbers of DOF for the airfoil cross-section with core material is shown in fig. 106. 813 DOF can be reached as minimum for this cross-section when mesh density equal to one is considered for all five walls. The

--- Sectional stiffness matrix ---

<--- S T R A I N S --->			<--- C U R V A T U R E S --->		
Axial S1	Shear S2	Shear S3	Twist K1	Bending K2	Bending K3
2.09942e+009	0.00000e+000	0.00000e+000	0.00000e+000	6.24054e+007	-8.17877e+008
0.00000e+000	5.02396e+008	1.24213e+007	-1.99880e+007	0.00000e+000	0.00000e+000
0.00000e+000	1.24213e+007	1.03856e+008	3.19680e+007	0.00000e+000	0.00000e+000
0.00000e+000	-1.99880e+007	3.19680e+007	1.90382e+007	0.00000e+000	0.00000e+000
6.24054e+007	0.00000e+000	0.00000e+000	0.00000e+000	8.73661e+006	-2.32042e+007
-8.17877e+008	0.00000e+000	0.00000e+000	0.00000e+000	-2.32042e+007	4.78813e+008

--- Sectional compliance matrix ---

<--- F O R C E S --->			<--- M O M E N T S --->		
Axial F1	Shear F2	Shear F3	Torque M1	Bending M2	Bending M3
1.57662e-009	0.00000e+000	0.00000e+000	0.00000e+000	-4.71604e-009	2.46454e-009
0.00000e+000	2.27651e-009	-2.08629e-009	5.89326e-009	0.00000e+000	0.00000e+000
0.00000e+000	-2.08629e-009	2.18415e-008	-3.88654e-008	0.00000e+000	0.00000e+000
0.00000e+000	5.89326e-009	-3.88654e-008	1.23974e-007	0.00000e+000	0.00000e+000
-4.71604e-009	0.00000e+000	0.00000e+000	0.00000e+000	1.45477e-007	-1.00553e-009
2.46454e-009	0.00000e+000	0.00000e+000	0.00000e+000	-1.00553e-009	6.24953e-009

--- Sectional mass matrix ---

<--- V E L O C I T I E S --->			<--- A N G U L A R V E L O C I T I E S --->		
V1	V2	V3	OMEGA1	OMEGA2	OMEGA3
8.07563e+001	0.00000e+000	0.00000e+000	0.00000e+000	2.41223e+000	-3.18483e+001
0.00000e+000	8.07563e+001	0.00000e+000	-2.41223e+000	0.00000e+000	0.00000e+000
0.00000e+000	0.00000e+000	8.07563e+001	3.18483e+001	0.00000e+000	0.00000e+000
0.00000e+000	-2.41223e+000	3.18483e+001	1.89979e+001	0.00000e+000	0.00000e+000
2.41223e+000	0.00000e+000	0.00000e+000	0.00000e+000	3.32068e-001	-9.09228e-001

* Sectional area
  Omega = (7.24427e-002) [m^2].

Figure 105: Sectional properties of airfoil cross-section with core material

axial stiffness variation is minimal and converges quickly.

The shear stress for a torque of 100 N.m at the centroid is computed at the top of the upper skin and half chord location. The variation of stress with the numbers of DOF for the cross-section is shown in fig. 107. The shear stress variation is minimal and also converges quickly.

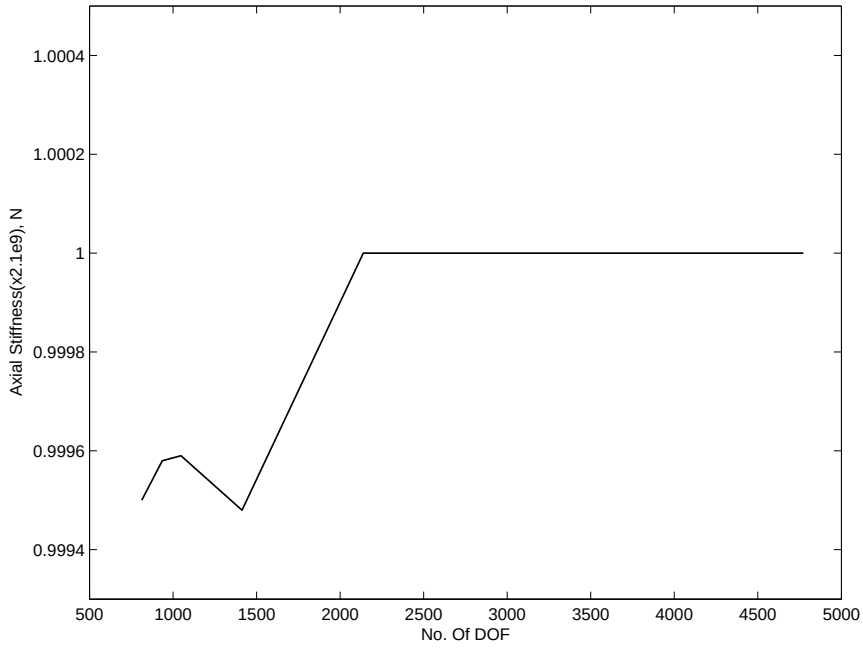

Figure 106: Variation of axial stiffness with DOF for the airfoil cross-section with core material

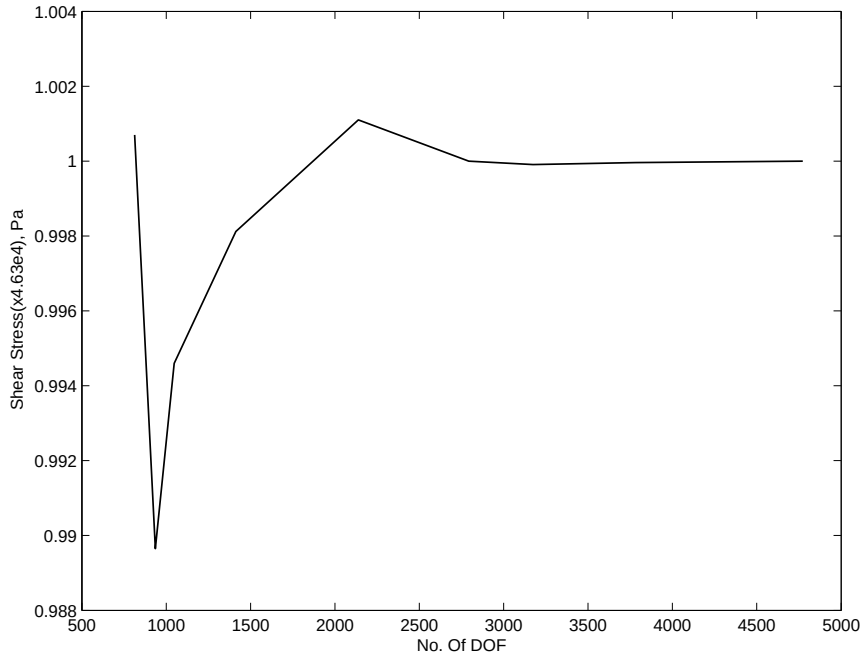

Figure 107: Variation of shear stress with DOF for the airfoil cross-section with core material at the top of the upper skin and half chord location

The previously considered complex rotor blade cross-section of NACA four digit series (0012) airfoil with four webs and chord length 2.24 m as shown in fig. 94, integrated with core materials inside various cavities is constructed and shown in fig. 108. This cross-section is made of 14 walls with arbitrary lay-ups and ply add/drops. Walls have between 24 to 36 layers of composite materials. These walls are connected with various connectors (eight T-connectors and one V-connector). Two adjacent walls at the tip are connected between themselves. Free meshes are generated for integrating core materials inside the front, middle, and aft cavities of the airfoil cross-section. The boundary points from the inside curves of the three (for front and aft cavities) or four (for middle cavity) walls are considered for free mesh generation of core materials. CYTEC5250-4-IM7/6K (Carbon/5250-4) with various orientation angles (-45^0 to $+45^0$) is considered as material for airfoil cross-section. HexWebACG Honeycomb is used as core material. The cross-sectional properties are computed and few of them at 34,275 DOF are shown in fig. 109. The axial stress distribution is also shown in fig. 108.

The axial stiffness variation with the numbers of DOF for the airfoil cross-section with core material is shown in fig. 110. The variation of the stiffness with DOF over a range of 2:1 is almost negligible and varies by no more than 0.02%.

The shear stress for a torque of 100 N.m at the centroid is computed at the top of the upper skin and near quarter chord location (at x2= 0.588 m.) The variation of stress with the numbers of DOF for this cross-section is shown in fig. 111. The shear stress variation is very small.

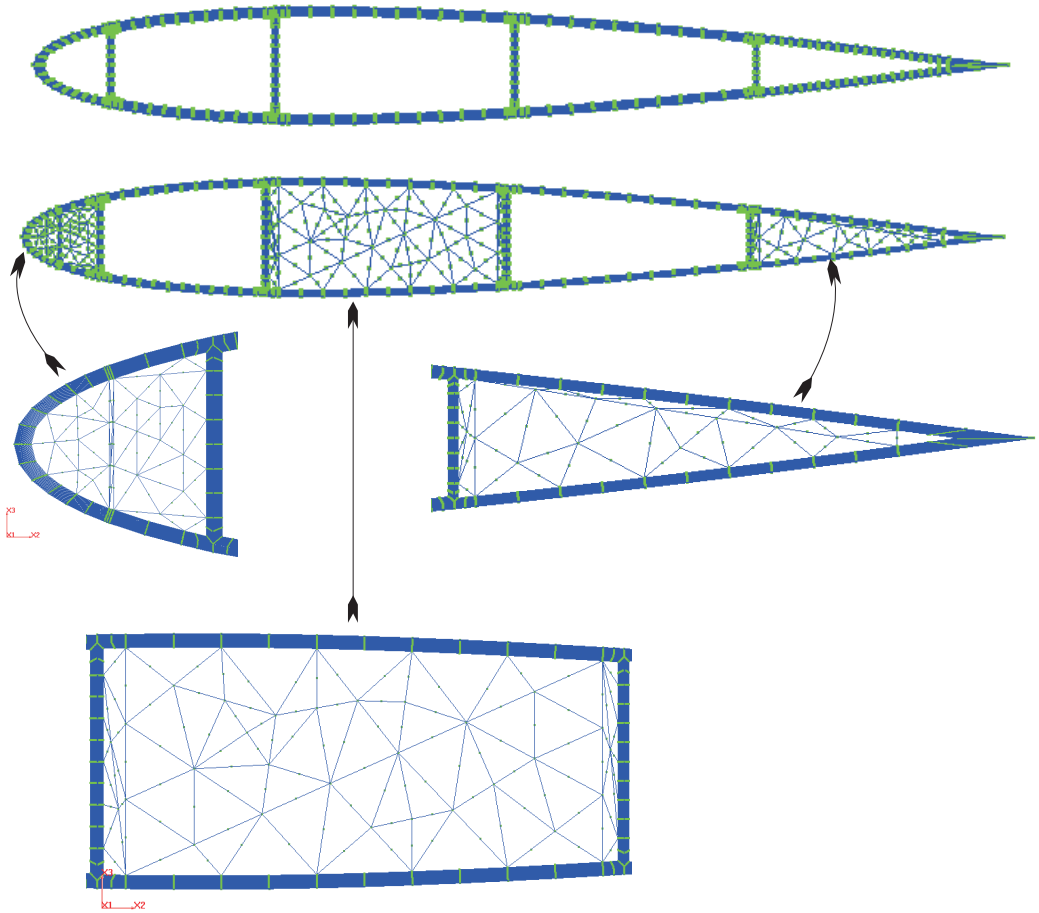

(a) Geometry and meshes

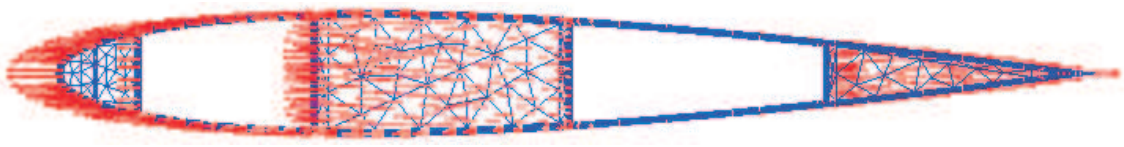

(b) Axial stress distribution due to axial loading

Figure 108: Complex rotor blade cross-section with core material

```
   --- Sectional stiffness matrix (4x4) ---

  S T R A I N   <---        C U R V A T U R E S        --->
     Axial S1      Twist   K1      Bending K2      Bending K3
 7.62607e+008    3.31956e+004   -6.98185e+002   -7.82854e+008
 3.31956e+004    4.03103e+006    1.96767e+001   -6.62972e+003
-6.98185e+002    1.96767e+001    3.27717e+006    2.78525e+001
-7.82854e+008   -6.62972e+003    2.78525e+001    9.63171e+008


   --- Sectional stiffness matrix ---

<---           S T R A I N S           --->   <---        C U R V A T U R E S        --->
     Axial S1        Shear S2        Shear S3      Twist   K1      Bending K2      Bending K3
 7.62607e+008    4.50294e+003   -9.55226e+003    2.50984e+004   -6.98249e+002   -7.82854e+008
 4.50294e+003    2.59487e+007   -1.27910e+007   -1.08428e+007   -2.93602e+002   -1.39772e+003
-9.55226e+003   -1.27910e+007    2.78643e+007    2.36199e+007    1.82306e+002    2.52998e+003
 2.50984e+004   -1.08428e+007    2.36199e+007    2.40530e+007    1.74214e+002   -4.48512e+003
-6.98249e+002   -2.93602e+002    1.82306e+002    1.74214e+002    3.27717e+006    2.78715e+001
-7.82854e+008   -1.39772e+003    2.52998e+003   -4.48512e+003    2.78715e+001    9.63171e+008


   --- Sectional compliance matrix ---

<---            F O R C E S            --->   <---           M O M E N T S           --->
     Axial F1        Shear F2        Shear F3      Torque  M1      Bending M2      Bending M3
 7.91684e-009    2.88747e-014    4.84365e-011   -5.46123e-011    1.63229e-012    6.43471e-009
 2.88747e-014    4.98081e-008    2.28629e-008    1.62149e-012    3.19040e-012    3.57016e-014
 4.84365e-011    2.28629e-008    2.24638e-007   -2.10287e-007    7.40713e-013    3.78325e-011
-5.46123e-011    1.62149e-012   -2.10287e-007    2.48076e-007   -1.50077e-012   -4.26807e-011


   --- Sectional mass matrix ---

<---        V E L O C I T I E S        --->   <--- A N G U L A R   V E L O C I T I E S --->
          V1              V2              V3          OMEGA1          OMEGA2          OMEGA3
 2.61658e+000    0.00000e+000    0.00000e+000    0.00000e+000   -1.91448e-006   -2.60250e+000
 0.00000e+000    2.61658e+000    0.00000e+000    1.91448e-006    0.00000e+000    0.00000e+000
 0.00000e+000    0.00000e+000    2.61658e+000    2.60250e+000    0.00000e+000    0.00000e+000
 0.00000e+000    1.91448e-006    2.60250e+000    3.17178e+000    0.00000e+000    0.00000e+000


* Sectional area
   Omega = ( 2.35156e-001) [ft^2].
```

Figure 109: Sectional properties of complex rotor blade cross-section with core material

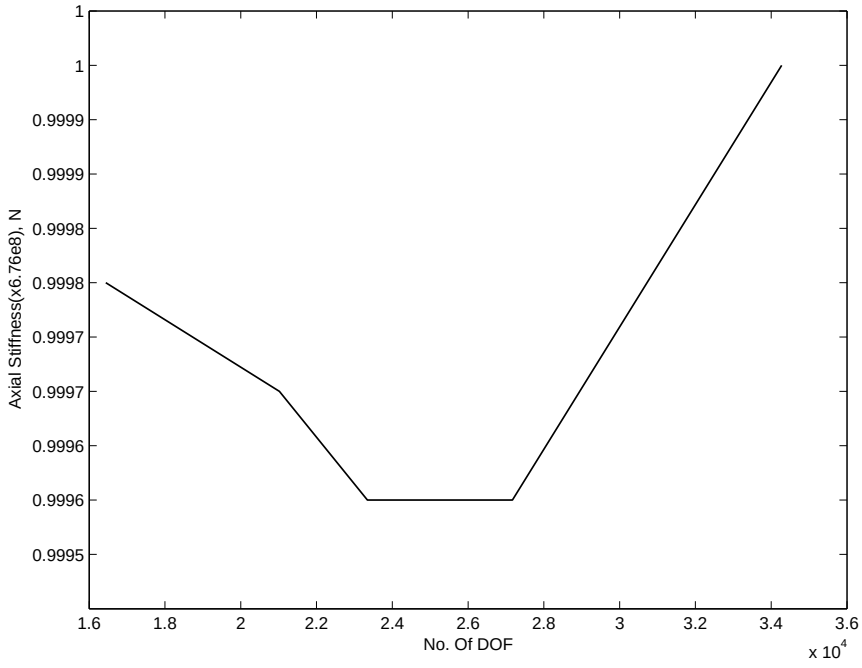

Figure 110: Variation of axial stiffness with DOF for complex rotor blade cross-section with core material

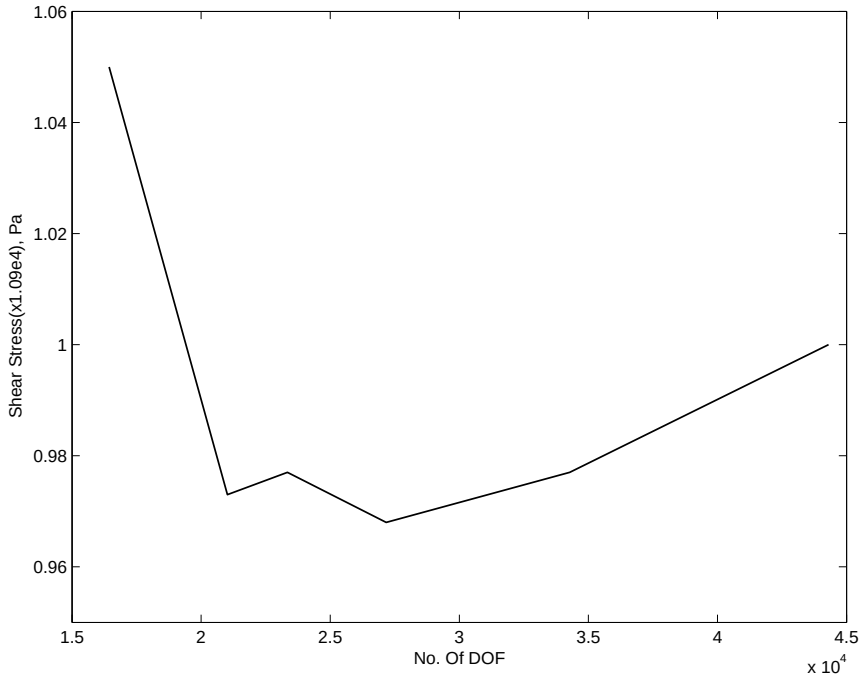

Figure 111: Variation of shear stress with DOF for complex rotor blade cross-section with core material at the top of the upper skin and near quarter chord location

CHAPTER V

CONCLUSIONS

SectionBuilder is a new and versatile tool, developed based on finite element analysis for generating meshes and rapidly computing the sectional properties of composite beam cross-sections. It also speeds up the analysis process. It has the ability to create multi-cell and multiply connected walls, and airfoil sections. This tool can handle the complex lay-up sequences and arbitrary material properties for each layer of the cross-section. It has also the ability to handle the variation of thickness of skin and D-spars of airfoil cross-sections that can be found in rotor blades. It integrates core materials into the cross-sections for modeling realistic rotor blade cross-sections. A visualization environment is integrated with the tool for visualizing the stress and strain distributions over the cross-sections. Post-processing and visualization of stress and strain fields are also complete for this tool.

CHAPTER VI

RECOMMENDATIONS FOR FUTURE WORK

The SectionBuilder code can be enhanced to improve the capabilities of modeling and analysis of beam sections in more realistic sense. SectionBuilder could be modified to accept parametric inputs in terms of the design variables of the optimization process. Optimization tools could be used to drive the design process. A hierarchical approach could be used to break the overall design and optimization processes into manageable problems. So the technical objectives would be:

(1) Incorporate the capabilities for optimization and sensitivity studies into SectionBuilder.

(2) Incorporate a suite of sectional optimization tools in SectionBuilder for composite rotor blade design.

(3) Develop procedures for coupled global (rotor/aircraft) and local (blade cross-section) design optimization.

(4) Develop procedures for handling more flexible geometric layout of beam cross-sections.

APPENDIX A

CONVEX HULL

The convex hull of a planar set is the minimum area convex polygon containing the planar set. For two-dimensional case:

Formally: It is the smallest convex set containing the points.

Informally: It is a rubber band wrapped around the outside points.

For a point (x, y) to be a vertex (i.e on the convex hull) the interior/reflex angle (RA) formed by joining (x, y) to its immediate neighboring vertices must be less than 180^0 (π). An upper hull is the part of the convex hull, which is visible from the above. Lower hull is the remaining part of the convex hull. The convex and non-convex hulls are shown in fig. 112 (where 3D defines three-dimensional.) For three-dimensional case, this hull looks like gift wrapping.

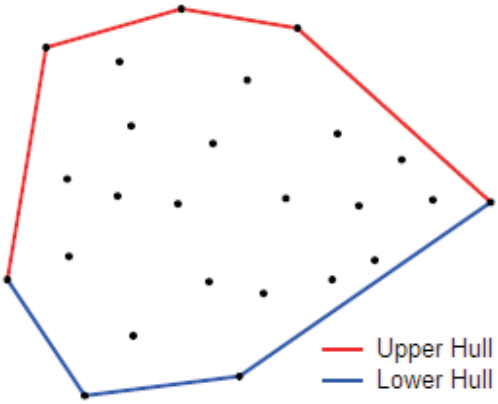

Convex hull

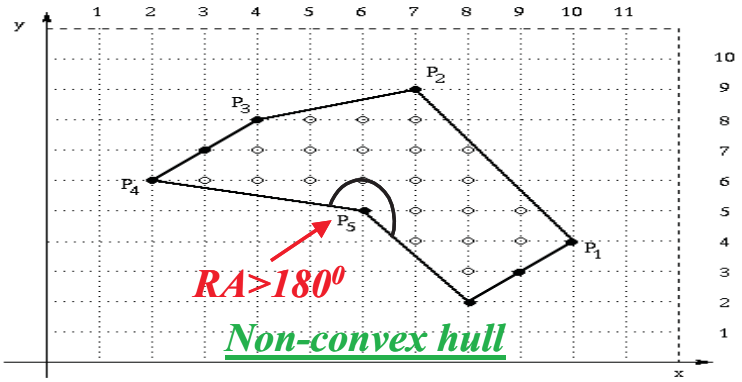

Non-convex hull

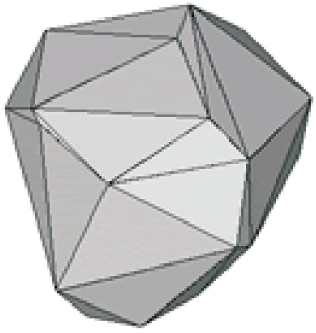

Convex hull (3D)

Figure 112: Convex and non-convex hulls

APPENDIX B

DELAUNAY TRIANGULATION

In general, the Delaunay triangulation is the most efficient technique to construct triangles among scattered points in a plane. Every point is connected by lines to its closest neighbors, in such a way that all lines are edges of triangles, and do not intersect each other. Triangles can not overlap and finally, the surface is totally covered with one fine layer of different triangular tiles.

The Russian mathematician Boris Nikolaevich Delaunay (1890-1980) invented this triangulation technique in 1934 and from then it is known as Delaunay triangulation. It has various applications in science and computer graphics. It is frequently used in the graphic representation of geometrically irregularly distributed data, such as weather maps or altitude maps. Its three-dimensional variant is very important in creating virtual worlds for video games and animated movies among many other things.

In computational geometry and mathematics, the Delaunay triangulation for a set Np of points in a particular plane is the triangulation Dt(Np) in such a way that there is no point of Np inside the circumcircle of any triangle in Dt(Np). Delaunay triangulations maximize the minimum angle of all the angles of the triangles in the triangulation process; they have a tendency to avoid sliver triangles.

For n-dimensional case and for a set Np of points in the Euclidean space, a Delaunay triangulation is a triangulation Dt(Np) in such a way that no point in Np is inside the circum-hypersphere of any simplex in Dt(Np).

It is well known that there is a unique Delaunay triangulation for a set Np, if Np is a set of points in general position; i.e., no (n + 1) points are on the same hyperplane

and no (n + 2) points are on the same hypersphere, for n-dimensional case. For two dimensional case, this triangulation can be found if no three points are on the same line and no four are on the same circle. The proof of this fact is outlined in the following paragraph.

The riddle of finding the Delaunay triangulation of a set of points in n-dimensional Euclidean space can be converted to the puzzle of finding the convex hull of a set of points in (n + 1)-dimensional space, by assigning each point Np an extra coordinate equal to $|Np|^2$, considering the bottom view of the convex hull, and tracing back to n-dimensional space by omitting the last coordinate. As the convex hull is unique, so is the triangulation, assuming all facets of the convex hull are simplices. A facet not being a simplex implies that (n + 2) of the original points lay on the same d-hypersphere and the points are not in general position.

It is easily viewed that for the set of three points on the same line there is no triangulation and so Delaunay triangulation is not possible. For the case of 4 points on the same circle, the vertices of a rectangle, the Delaunay triangulation is not unique. In this situation two possible triangulations that split the quadrangle into two triangles fulfilling the Delaunay triangulation rules.

Generalizations are possible to metrics other than Euclidean. However in these cases a Delaunay triangulation is not guaranteed to exist or be unique.

B.1 Properties

Let n be the number of points and d the number of dimensions.

(1)The union of all simplices in the triangulation is the convex hull of the points.

(2) The Delaunay triangulation contains at most $O(d^{n/2})$ simplices.

(3) In the plane ($d = 2$), if there are b vertices on the convex hull, then any triangulation of the points has at most $(2n - 2 - b)$ triangles, plus one exterior face.

(4) The Delaunay triangulation maximizes the minimum angle. Compared to any

other triangulation of the points, the smallest angle in the Delaunay triangulation is at least as large as the smallest angle in any other triangulation. The converse is not true: the Delaunay triangulation does not necessarily minimize the maximum angle.

B.2 Algorithm

From the above description, the Delaunay triangulation technique seems to be easy, but in fact it is quite complicated. There are many algorithms as described in the literature review section, although the field is the subject of ongoing research, available for Delaunay triangulation construction. The Delaunay triangulation technique, discovered by Edelsbrunner and Seidel (1986), is easy to implement, and efficient for triangulation among scattered points in a two-dimensional plane. This technique is considered for the Delaunay triangulation in this thesis.

In 1986, Edelsbrunner and Seidel [76] discovered a connection between Delaunay triangulation and convex hulls in one and higher dimensional Euclidean space. This insight was based on earlier work of Brown (1979) [76], who was the first to establish a connection to convex hulls. The Delaunay triangulation of a set of n-dimensional points is the projection of the convex hull of (n+1)-dimensional points in n-dimensional space. For example, the Delaunay triangulation of a set of two-dimensional points with coordinates (x,y) is just the projection of the convex hull of three-dimensional points with coordinates $(x, y, x^2 + y^2)$ in two-dimensional plane. This triangles are the projection of three-dimensional convex hull in the $xy - plane$ (viewed from $z \rightarrow -\infty$) and shown in fig. 113.

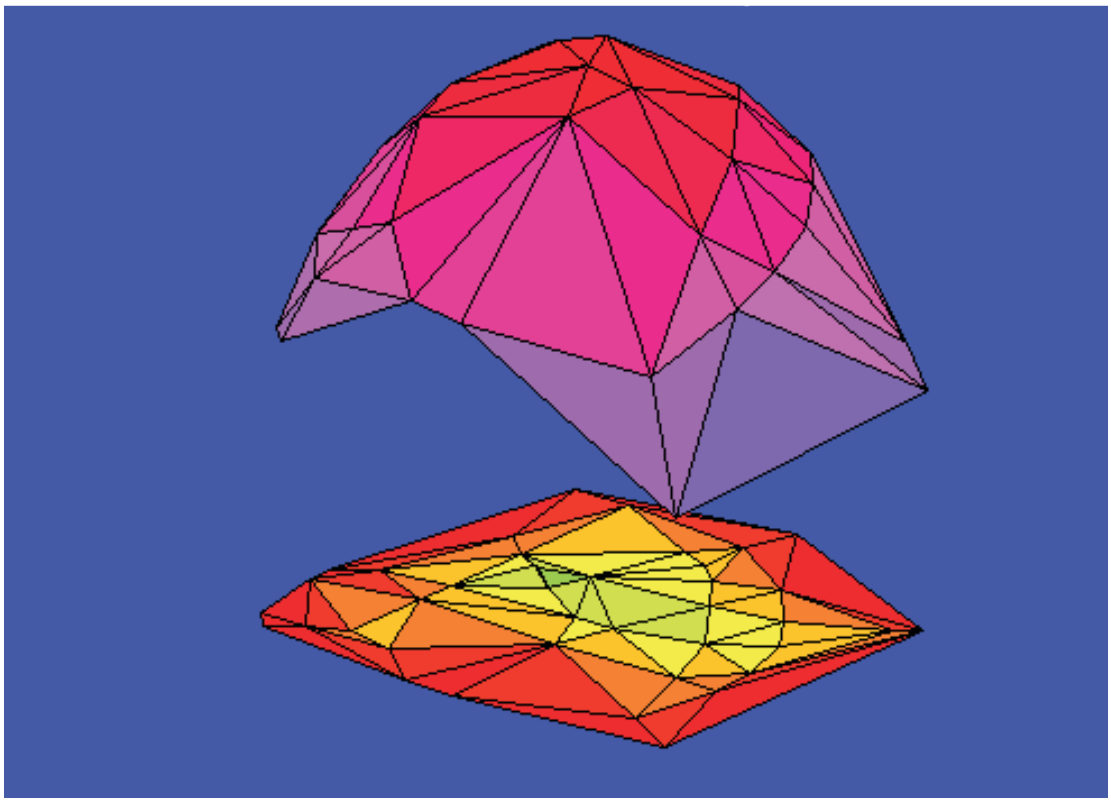

Figure 113: Delaunay triangles: the projection of three-dimensional convex hull in two-dimensional plane

REFERENCES

[1] Amenta, N., Bern, M., and Kamvysselis, M., "A new Voronoi-based surface reconstruction algorithm," in *Proceedings SIGGRAPH '98*, pp. 415–421, 1998.

[2] Amenta, N., Choi, S., and Kolluri, R., "The power crust, unions of balls, and the medial axis transform," vol. 19, pp. 127–153, 2001.

[3] Barber, C. B., *Computational Geometry with Imprecise Data and Arithmetic*. Princeton, New Jersey: PhD thesis, 1993.

[4] Bathe, K. J., *Finite Element Procedures*. Englewood Cliffs, New Jersey: Prentice Hall, Inc., 1996.

[5] Bauchau, O. A., "Computational Schemes for Flexible, Nonlinear Multi-Body Systems," *Multibody System Dynamics*, vol. 2, no. 2, pp. 169–225, 1998.

[6] Bauchau, O. A., *DYMORE User's Manual*. Georgia Institute of Technology, Atlanta, Georgia, 2007.

[7] Bauchau, O. A. and Hong, C. H., "Finite Element Approach to Rotor Blade Modeling," *Journal of the American Helicopter Society*, vol. 32, no. 1, pp. 60–67, 1987.

[8] Bauchau, O. A. and Hong, C. H., "Large Displacement Analysis of Naturally Curved and Twisted Composite Beams," *AIAA Journal*, vol. 11, no. 25, pp. 1469–1475, 1987.

[9] Bauchau, O. A. and Hong, C. H., "Nonlinear Composite Beam Theory," *Journal of Applied Mechanics*, vol. 55, pp. 156–163, 1988.

[10] Bauchau, O. A. and Hong, C. H., "Nonlinear Response and Stability Analysis of Beams Using Finite Elements in Time," *AIAA Journal*, vol. 26, no. 9, pp. 1135–1142, 1988.

[11] Bauchau, O. A. and Kang, N. K., "A multi-body Formulation for Helicopter Structural Dynamic Analysis," *Journal of the American Helicopter Society*, vol. 38, pp. 3–14, 1993.

[12] Berdichevsky, V. L., "On a Variational Principle," *Dokl. Akad. Nauk SSSR*, vol. 215, no. 6, 1974.

[13] Berdichevsky, V. L., "Variational-Asymptotic Method of Constructing a Theory of Shells," *PMM*, vol. 43, no. 4, pp. 711–736, 1979.

[14] Berdichevsky, V. L., Armanios, E. A., and Badir, A. M., "Theory of anisotropic thin-walled closed-section beams," *Composites Engineering*, vol. 2, no. 5-7, pp. 411–432, 1992.

[15] Berdichevsky, V. L. and Misiura, V. A., "On a Dual Variational Principle in Geometrically Nonlinear Elasticity Theory," *PMM*, vol. 43, no. 2, pp. 343–352, 1979.

[16] Bern, M. W. and Eppstein, D., "Mesh generation and optimal triangulation," in *D. Du and F. K. Hwang, editors, computing in Euclidean Geometry, world Scientific*, pp. 23–90, 1992.

[17] Bhaskar, K. and Varadan, T. K., "Benchmark elasticity solution for locally loaded laminated orthotopic cylindrical shells," *AIAA Journal*, vol. 32, no. 3, pp. 627–632, 1994.

[18] Boissonat, J. D. and Cazals, F., "Smooth surface reconstruction via natural neighbor interpolation of distance functions," in *Symposium on Computational Geometry*, pp. 223–232, 2000.

[19] Boissonat, J. D. and Yvinec, M., *Algorithmic Geometry*. Cambridge University Press, 1998.

[20] Borri, M., Ghiringhelli, G. L., and Merlini, T., "Linear analysis of naturally curved and twisted anisotropic beams," *Composites Engineering*, vol. 2, no. 5-7, pp. 433–456, 1992.

[21] Bowyer, A., "Computing Dirichlet tessellations," *The Computer Journal*, vol. 24, no. 2, pp. 162–166, 1981.

[22] Brown, K., "Voronoi diagrams from convex hulls," *IPL*, pp. 223–228, 1979.

[23] Buannic, N. and Cartraud, P., "Higher-order asymptotic model for a heterogeneous beam, including corrections due to end effects," in *Proceedings of the 4lst Structures, Structural Dynamics and Materials Conference*, no. 2000-1495, (AIAA, Atlanta, Georgia), Apr. 2000.

[24] Cesnik, C. E. S., *Cross-Sectional Analysis of Initially Twisted and Curved Composite Beams*. PhD thesis, Aerospace Engineering, Georgia Institute of Technology, May 1994.

[25] Cesnik, C. E. S. and Hodges, D. H., "Stiffness constants for initially twisted and curved composite beams," *Applied Mechanics Reviews*, vol. 46, no. 11, Part 2, pp. S211–S220, 1993.

[26] Cesnik, C. E. S. and Hodges, D. H., "Variational-asymptotical analysis of initially twisted and curved composite beams," *International Journal for Engineering Analysis and Design*, vol. 1, pp. 177–187, Apr. 1994.

[27] Cesnik, C. E. S. and Hodges, D. H., "Stiffness constants for composite beams including large initial twist and curvature effects," *Applied Mechanics Reviews*, vol. 48, no. 11, Part 2, pp. S61–S67, 1995.

[28] Cesnik, C. E. S. and Hodges, D. H., "VABS: a new concept for composite rotor blade cross-sectional modeling," *Journal of the American Helicopter Society*, vol. 42, pp. 27–38, Jan. 1997.

[29] Cheng, S., "On the sizes of Delaunay meshes," *Computational Geometry*, vol. 33, pp. 130–138, 2006.

[30] Chew, L. P., "Constrained Delaunay Triangulations," *Algorithmica*, vol. 4, no. 1, pp. 97–108, 1989.

[31] Chew, L. P., "Guaranteed-Quality Triangular Meshes," Tech. Rep. TR-89-983, Department of Computer Science, Cornell University, 1989.

[32] Chew, L. P., "Guaranteed-Quality Mesh Generation for Curved Surfaces," in *Proceedings of the Ninth Annual Symposium on Computational Geometry*, (Association for Computing Machinery, San Diego, California), pp. 274–280, May 1993.

[33] Clarkson, K. L. and Shor, P. W., "Applications of random sampling in computational geometry," *Discrete and Computational Geometry*, vol. 4, pp. 387–421, 1989.

[34] Cook, R. D., Malkus, D. S., and Plesha, M. E., *Concepts And Applications Of finite element analysis*. New York: John Wiley and Sons, 2000.

[35] Curless, B. and Levoy, M., "A volumetric method for building complex models from range images," in *Proceedings SIGGRAPH '96*, pp. 303–312, 1996.

[36] Danielson, D. A. and Hodges, D. H., "Nonlinear beam kinematics by decomposition of the rotation tensor," *Journal of Applied Mechanics*, vol. 54, no. 2, pp. 258–262, 1987.

[37] Dwyer, R. A., "Higher dimensional Voronoi diagrams in linear expected time," *Discrete and Computational Geometry*, vol. 6, pp. 343–367, 1991.

[38] Dwyer, R. A., "A Faster Divide-and-Conquer Algorithm for Constructing Delaunay Triangulations," *Algorithmica*, vol. 2, no. 2, pp. 137–151, 1987.

[39] Edelsbrunner, H., Kirkpatrick, D. G., and Seidel, R., "On the shape of a set of points in the plane," *IEEE Transactions on Information Theory*, vol. 29, pp. 551–559, 1983.

[40] Edelsbrunner, H. and Mucke, E. P., "Three-dimensional alpha shapes," *ACM Transactions on Graphics*, vol. 13, pp. 43–72, 1994.

[41] Fang, T. P. and Piegl, L. A., "Delaunay triangulation using a uniform grid," *IEEE Computer Graphics and Applications*, vol. 13, no. 3, pp. 36–47, 1993.

[42] Farin, G. E., *Curves and Surfaces for Computer Aided Geometric Design*. Boston, Massachusetts: Academic Press, Inc., third ed., 1992.

[43] Farrashkhalvat, M. and Miles, J. P., *Basic Structured Grid Generation with an introduction to unstructured grid generation*. Massachusetts: Butterworth-Heinemann, 2003.

[44] Fortune, S., "A sweepline algorithm for Voronoi diagrams," *Algorithmica*, vol. 2, pp. 153–174, 1987.

[45] Fortune, S., "Voronoi diagrams and Delaunay triangulations," in *D. Du and F. K. Hwang, editors, computing in Euclidean Geometry*, vol. world Scientific, pp. 193–233, 1992.

[46] Giavotto, V., Borri, M., Mantegazza, P., Ghiringhelli, G., Carmaschi, V., Maffioli, G. C., and Mussi, F., "Anisotropic beam theory and applications," *Computers and Structures*, vol. 16, no. 1-4, pp. 403–413, 1983.

[47] Green, P. J. and Sibson, R. R., "Computing Dirichlet tessellations in the plane," *The Computer Journal*, pp. 168–123, 1978.

[48] Guibas, L. J., Knuth, D. E., and Sharir, M., "Randomized incremental construction of Delaunay and Voronoi diagrams," *Algorithmica*, vol. 2, pp. 381–413, 1992.

[49] Guibas, L. J. and Stolfi, J., "Primitives for the Manipulation of General Subdivisions and the Computation of Voronoi Diagrams," *ACM Transactions on Graphics*, vol. 4, pp. 74–123, Apr. 1985.

[50] Hodges, D. H., "A review of composite rotor blade modeling," *AIAA Journal*, vol. 28, no. 3, pp. 561–565, 1990.

[51] Hodges, D. H., "Non-linear in-plane deformation and buckling of rings and high arches," *International Journal of Non-Linear Mechanics*, vol. 34, no. 4, pp. 723–737, 1999.

[52] Hodges, D. H., Atilgan, A. R., Cesnik, C. E. S., and Fulton, M. V., "On a simplified strain energy function for geometrically nonlinear behaviour of anisotropic beams," *Composites Engineering*, vol. 2, no. 5-7, pp. 513–526, 1992.

[53] Hodges, D. H., Harursampath, D., Volovoi, V. V., and Cesnik, C. E. S., "Non-classical effects in non-linear analysis of anisotropic strips," *International Journal of Non-Linear Mechanics*, vol. 34, pp. 259–277, Mar. 1999.

[54] Hodges, D. H., *Nonlinear Composite Beam Theory*. Virginia: American Institute of Aeronautics and Astronautics, Inc., 2006.

[55] Hoppe, H., DeRose, T., Duchamp, T., McDonald, J., and Stuetzle, W., "Surface reconstruction from unorganized points," in *Proceedings SIGGRAPH '92*, pp. 71–78, 1992.

[56] Ie, C. A. and Kosmatka, J. B., "On the Static Behavior of Shear-Deformable Prismatic Beams Including In-Plane Cross-Section Deformations," in *Proceedings of the 32nd Structures, Structural Dynamics, and Materials Conference*, (Baltimore, Maryland), pp. 1453–1461, Apr. 1991.

[57] Ie, C. A. and Kosmatka, J. B., "A Nonlinear Theory for Spinning Anisotropie Beams Using Restrained Warping Functions," in *Proceedings of the 34th Structures, Structural Dynamics, and Materials Conference*, vol. AIAA, (La Jolla, California), 1993.

[58] Jing, H. S. and Tzeng, K. G., "Elasticity solution for laminated anisotropic cylindrical panels in cylindrical bending," *Composite Structures*, vol. 30, pp. 307–317, 1995.

[59] Jones, R. M., *Mechanics of Composite Materials*. Philadelphia, Pensylvania: Taylor Francis, second ed., 1999.

[60] Jung, S. N., Nagaraj, V. T., and Chopra, I., "Assessment of composite rotor blade modeling techniques," *Journal of the American Helicopter Society*, vol. 44, pp. 188–205, July 1999.

[61] Kim, C. and White, S. R., "Thick-walled composite beam theory including 3-d elastic effects and torsional warping," *International Journal of Solids and Structures*, vol. 34, no. 31-32, pp. 4237–4259, 1997.

[62] Kosmatka, J. B., "Extension, Bending, and Torsion of Anisotropie Beams with Initial Twist," in *Proceedings of the 3Oth Structures, Structural Dynamics, and Materials Conference*, no. 89-1364, pp. 1799–1806, Apr. 1989.

[63] Kosmatka, J. B., "On the Behavior of Pretwisted Beams with Irregulr Cross Sections Having Applications to Rotor Blades," in *Proceedings of the 31st Structures, Structural Dynamics, and Materials Conference*, no. 90-0963, pp. 783–793, Apr. 1990.

[64] Kosmatka, J. B., "Extension-Bend-Twist Coupling Behavior of Thin-Walled Advanced Composite Beams with Initial Twist," (Baltimore, Maryland), pp. 1037–1049, Apr. 1991.

[65] Kosmatka, J. B., "Flexure-Torsion Behavior of Shear-Deformable Beams with Applications to Aircraft Wing Sections," in *Proceedings of the 33rd Structures, Structural Dynamics, and Materials Conference*, (Dallas, Texas), pp. 763–773, Apr. 1992.

[66] Kosmatka, J. B., "On the Behavior of Pretwisted Beams with Irregulr Cross Sections," *ASME Journal of Applied Mechanics*, vol. 59, no. 1, pp. 146–152, 1992.

[67] Kruithof, N. G. H. and Vegter, G., "Meshing skin surfaces with certified topology," *Computational Geometry*, vol. 36, pp. 166–182, 2007.

[68] Lawson, C. L., "Thansforming triangulation," *Discrete Math*, vol. 3, pp. 365–372, 1972.

[69] Lawson, C. L., "Software for surface interpolation," *Mathematical Software III*, pp. 161–194, 1977.

[70] Lee, D. and Schachter, B. J., "Two Algorithms for Constructing a Delaunay Triangulation," *International Journal of Computer and Information Sciences*, vol. 9, no. 3, pp. 219–242, 1980.

[71] Maus, A., "Delaunay triangulation and the convex hull of n points in expected linear time," *BIT Journal*, vol. 24, pp. 151–163, 1984.

[72] Mindlin, R. D., "Solution of St. Venant's Torsion Problem by Power Series," *International Journal of Solids and Structures*, vol. 11, pp. 321–328, 1975.

[73] Morris, D. and Kanade, T., "Image-consistent surface triangulation," in *Proceedings IEEE on Computer Vision and Pattern Recognition*, pp. 332–338, 2000.

[74] Oblonsek, C. and Guid, N., "A fast surface-based procedure for object reconstruction from scattered points," *Computer Vision and Image Understanding:CVIU*, vol. 69, no. 2, pp. 185–195, 1998.

[75] Ohya, T., Iri, M., and Murota, K., "Improvements of the incremental method for the Voronoi diagram with computational comparison of various algorithm," *Journal of the Operations Research Society of Japan*, vol. 27, pp. 306–337, 1984.

[76] O'Rourke, J., *Computational Geometry in C*. New York: Cambridge University Press, 1994.

[77] Pagano, N. J., "Exact solutions for composite laminates in cylindrical bending," *Journal of Composite Materials*, vol. 3, pp. 398–411, July 1969.

[78] Pagano, N. J., "Exact solutions for rectangular bidirectional composites and sandwich plates," *Journal of Composite Structures*, vol. 4, no. 1, pp. 20–34, 1970.

[79] Petrov, E. and Geradin, M., "Finite element theory for curved and twisted beams based on exact solutions for three-dimensional solids: Part 1: Beam concept and geometrically exact nonlinear formulation," *Computer Methods in Applied Mechanics and Engineering*, vol. 165, pp. 43–92, 1998.

[80] Petrov, E. and Geradin, M., "Finite element theory for curved and twisted beams based on exact solutions for three-dimensional solids: Part 2: Anisotropic and advanced beam models," *Computer Methods in Applied Mechanics and Engineering*, vol. 165, pp. 93–127, 1998.

[81] Piegl, L. and Tiller, W., *The Nurbs Book*. Berlin, New Jersey: Springer-Verlag, second ed., 1997.

[82] Popescu, B., *Asymptotically Correct Refinements in Numerical Cross-Sectional Analysis of Composite Beams*. Atlanta, Georgia: PhD thesis, Aerospace Engineering, Georgia Institute of Technology, 1998.

[83] Popescu, B. and Hodges, D. H., "Asymptotic treatment of the trapeze effect in finite element cross-sectional analysis of composite beams," *International Journal of Non-Linear Mechanics*, vol. 34, no. 4, pp. 709–721, 1999.

[84] Popescu, B. and Hodges, D. H., "Asymptotic treatment of the trapeze effect in finite element cross-sectional analysis of composite beams," *International Journal of Non-Linear Mechanics*, vol. 34, no. 4, pp. 709–721, 1999.

[85] Popescu, B., Hodges, D. H., and Cesnik, C. E. S., "Obliqueness effects in asymptotic cross-sectional analysis of composite beams," *Computers and Structures*, vol. 76, no. 4, pp. 533–543, 2000.

[86] Rand, O., "On the importance of cross-sectional warping in solid composite beams," *Composite Structures*, vol. 49, pp. 393–397, 2000.

[87] Ren, J. G., "Exact solutions for laminated cylindrical shells in cylindrical bending," *Composite Science and Technology*, vol. 29, no. 3, pp. 169–187, 1987.

[88] Rineau, L. and Yvinec, M., "A generic software design for Delaunay refinement meshing," *Computational Geometry*, vol. 38, pp. 100–110, 2007.

[89] Ruppert, J., "A New and Simple Algorithm for Quality 2-Dimensional Mesh Generation," in *Proceedings of the Fourth Annual Symposium on Discrete Algorithms*, (Association for Computing Machinery), pp. 83–92, Jan. 1993.

[90] Sappa, A. D. and Garcia, M. A., "Coarse-to-fine approximation of range images with bounded error adaptive triangular meshes," *Journal of Electronic Imaging*, vol. 16, no. 2, pp. 023010:1–11, 2007.

[91] Shamos, M. I. and Hoey, D., "Closest-Point Problems," in *16th Annual Symposium on Foundations of Computer Science*, (IEEE Computer Society Press, Berkeley, California), pp. 151–162, Oct. 1975.

[92] Tanemura, M., Ogawa, T., and Ogita, N., "A new algorithm for three dimensional Voronoi tessellation," *Journal of Computational Physics*, vol. 51, pp. 191–207, 1983.

[93] Taufik, A., Barrau, J., and Lorin, F., "Composite beam analysis with arbitrary cross section," *Composite Structures*, vol. 44, pp. 189–194, 1999.

[94] Trabucho, L. and Viano, J., "Mathematical modeling of rods," in *P. Ciarlet and J. Lions, editors, Handbook of Numerical Analysis*, vol. IV, pp. 487–974, Elsevier, 1996.

[95] Volovoi, V. V., *On End Effects in Prismatic Beams*. Atlanta, Georgia: PhD thesis, Aerospace Engineering, Georgia Institute of Technology, Jan. 1997.

[96] Volovoi, V. V. and Hodges, D. H., "Theory of anisotropic thin-wailed beams," *Journal of Applied Mechanics*, vol. 67, pp. 453–459, Sept. 2000.

[97] Watson, D., "Computing the n-dimensional Delaunay tessellation with apphcation to Voronoi polytopes," *The Computer Journal*, vol. 24, no. 2, pp. 167–172, 1981.

[98] Yu, W., *On Timoshenko-Like Modeling of Initially Curved and Twisted Composite Beams*. Atlanta, Georgia: Master's thesis, Aerospace Engineering, Georgia Institute of Technology, Dec. 2000.

[99] Yu, W., *Variational Asymptotic Modeling of Composite Dimensionally Reducible Structures*. Atlanta, Georgia: PhD thesis, Aerospace Engineering, Georgia Institute of Technology, Apr. 2002.

[100] Yu, W., Volovoi, V. V., Hodges, D. H., and Hong, X., "Validation of the variational asymptotic beam sectional analysis," *AIAA Journal*, vol. 40, no. 10, pp. 2105–2112, 2002.

VITA

Uttam Kumar Chakravarty was born on November 07, 1975 in Bangladesh. He acquired B.S. in Mechanical Engineering degree on September 1999 from Bangladesh University of Engineering and Technology (BUET), and served as a lecturer (faculty member) at the department of Mechanical Engineering, BUET from November 1999 to July 2000. He came to USA with student visa for graduate studies at Tuskegee University on August 2000. He finished M.S. in Mechanical Engineering degree there and joined the School of Aerospace Engineering at Georgia Institute of Technology for further graduate studies on August 2003. In May 2005, he acquired his second M.S. degree. Upon finishing his M.S. degree, he continued his graduate studies at the Georgia Institute of Technology and acquired Ph.D. degree in Aerospace Engineering on April 2008.